SINTEF

OC2021 A-006 - Unrestricted

Report

Methane seeps

A desktop study

Author(s)
Tor Nordam, Anusha L. Dissanayake, Odd Gunnar Brakstad

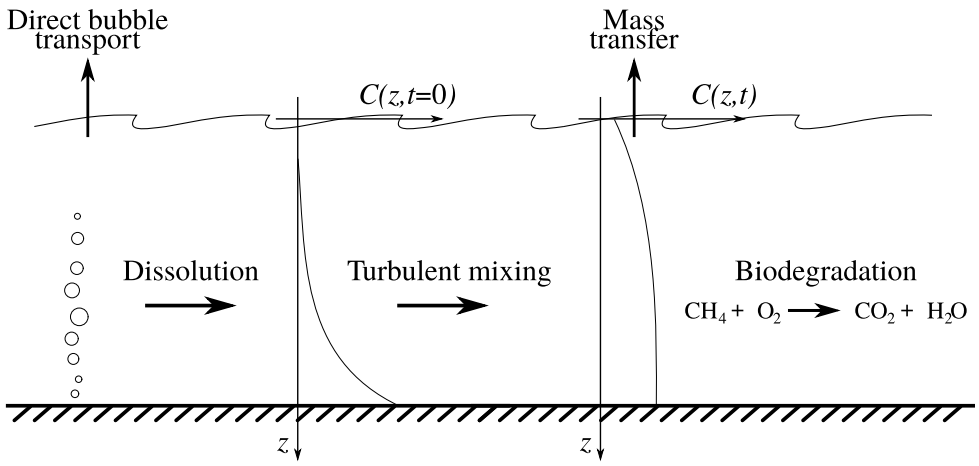

SINTEF Ocean
Climate and Environment
2021-02-19

SINTEF Ocean
SINTEF Ocean

Address:
P. O. box 4762 Torgard
NO-7465 Trondheim
NORWAY

www.sintef.no

Enterprise Number: NO 937 357 370 MVA

KEYWORDS:
Methane seeps, transport modelling, biodegradation, climate contribution

Report

Methane seeps

A desktop study

VERSION
4

DATE
2021-02-19

AUTHOR(S)
Tor Nordam, Anusha L. Dissanayake, Odd Gunnar Brakstad

CLIENT(S)
Norsk olje og gass

CLIENT'S REFERENCE
Trym Edvardsson

PROJECT
302005742

NUMBER OF PAGES AND ATTACHMENTS
59

ABSTRACT
We have conducted a literature review and a simplified one-dimensional modelling study on the fate of methane bubbles and dissolved methane in the water column originating from methane seeps.

From the literature review, we have found that the physical processes describing the rise and dissolution of methane bubbles are relatively well understood, and several studies use very similar modelling approaches. When it comes to biodegradation rates for dissolved methane in seawater, there is far more uncertainty, and published values span a range of six orders of magnitude. These rates may also depend on local conditions, and on methane concentrations, as higher concentrations allow methane-degrading bacteria to exist in larger numbers.

On the topic of how methane seeps contribute to the acidification of the ocean, we find that the amounts of methane released from seeps are probably too small to make a significant difference, compared to other sources of CO_2, such as the dissolution of atmospheric CO_2 into the ocean.

Modelling of seeps at three different depths (50 m, 120 m and 300 m) indicates that almost all of the methane released as bubbles will dissolve into the water column before the bubbles reach the surface. For the dissolved methane, we have used the diffusion-reaction equation to investigate how much biodegrades, and how much is released to the atmosphere via mass transfer across the sea surface. To reflect the uncertainty in published biodegradation rates, we conducted a parameter study, running simulations for biodegradation half-lives ranging from 10 to 1000 days. The model results indicate that for methane seeps at 50 m depth most of the methane will reach the atmosphere, for seeps at 120 m depth, more than half the methane will reach the atmosphere if the biodegradation half-life is longer than about 50 days, and for seeps at 300 m depth, more than half of the methane will reach the atmosphere if the half-life is longer than about 300 days. In these studies, we have assumed a relatively well-mixed water column during the winter season.

REPORT NUMBER
OC2021 A-006

ISBN
978-82-7174-408-3

CLASSIFICATION
Unrestricted

CLASSIFICATION THIS PAGE
Unrestricted

PREPARED BY	CHECKED BY	APPROVED BY
Tor Nordam	Jørgen Skancke	Atle Kleven

Document History

VERSION	DATE	VERSION DESCRIPTION
1	1.10.2020	First draft to client
2	21.12.2020	Second draft to client
3	29.1.2020	Final draft to client
4	19.2.2020	Final version of report

SINTEF

Contents

Summary

We have conducted a literature review and performed a simplified one-dimensional modelling study to investigate the fate of methane entering the ocean from small seeps at the seafloor. As the bubbles from a seep rise through the water column, some or all of the methane will dissolve into the water, and some may reach the atmosphere directly with bubbles that reach the sea surface. Dissolved methane will be redistributed in the water column due to vertical turbulent mixing. The two relevant fate processes for dissolved methane are biodegradation and escape to the atmosphere via evaporation at the surface. The different processes have been illustrated in the figure below.

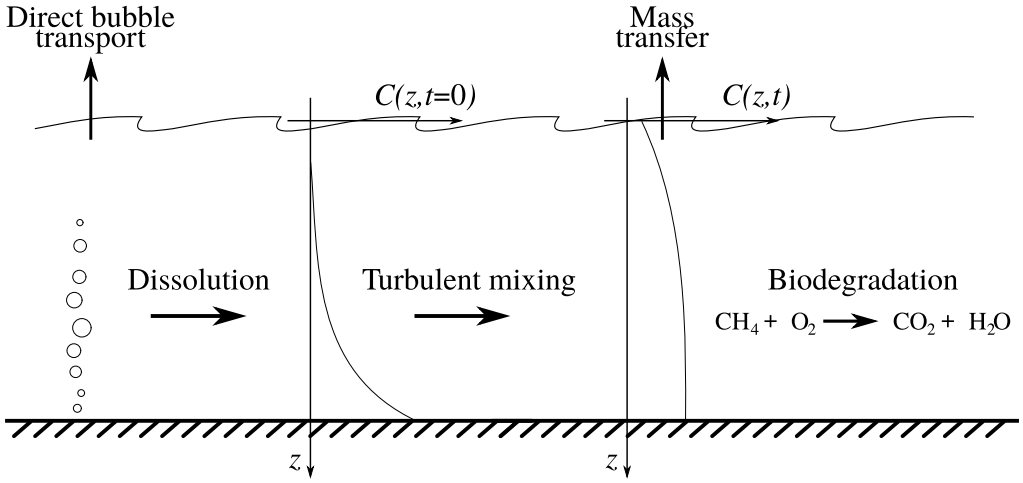

Illustration of the different processes that we have reviewed in the literature and accounted for in the modelling study.

Modelling, as well as published findings, indicates that the majority of the methane from a seep will be dissolved into the water column, with only a small fraction reaching the atmosphere via direct bubble transport. For the dissolved methane, its fate is decided by the balance between the biodegradation rate and the rate at which methane is mixed to the surface, from where it can evaporate to the atmosphere. To investigate the effect of different biodegradation rates, we conducted a parameter study, running simulations for biodegradation half-lives ranging from 10 to 1000 days. The model results indicate that for methane seeps at 50 m depth most of the methane will reach the atmosphere, for seeps at 120 m depth, more than half the methane will reach the atmosphere if the biodegradation half-life is longer than about 50 days, and for seeps at 300 m depth, more than half of the methane will reach the atmosphere if the half-life is longer than about 300 days. The reason is that the long half-life means that most of the methane will remain in the water column for a sufficiently long time to eventually escape to the atmosphere during winter when the vertical mixing in the water column is stronger than during summer. In these studies, we have assumed a relatively well-mixed water column during the winter season.

On the topic of acidification of the ocean due to methane seeps, there is theoretically a contribution when methane is transformed to CO_2 and water. However, we find that the contribution from methane released in seeps is relatively small and negligible compared to other sources of CO_2, such as dissolution of CO_2 from the atmosphere into the ocean.

Our conclusion from the literature review is that there are very large uncertainties in some important parameters. Most notably, there is a very large variation in the published biodegradation rates for methane in seawater. There is also some uncertainty in the intensity of vertical mixing throughout the year. The chosen one-dimensional approach also ignores horizontal transport and dilution, as well as the history of the methane concentration in a particular volume of water. However, even with these uncertainties, we can tentatively assume from the modelling study that more than half of the methane released in seeps will reach the atmosphere.

In order to constrain the large uncertainties we find both in the published biodegradation rates of methane, and in our fate modelling, further research is needed.

Sammendrag på norsk

Vi har gjennomført et litteraturstudie og et forenklet endimensjonalt modelleringstudie for å undersøke skjebnen til metan fra små utslipp på havbunnen. Når metanboblene stiger gjennom vannsøylen vil metanet helt eller delvis løses opp i det omliggende vannet, mens noe av metanen kan bli med boblene helt opp til overflaten og slippes direkte ut i atmosfæren. Metanen som løses i vannet vil bli blandet og omfordelt i vannkolonnen ved turbulent blanding. De to avgjørende prosessene for den endelige skjebnen til løst metan er bionedbrytning til vann og CO_2 og transport til atmosfæren ved fordamping gjennom havoverflaten. De relevante prosessene er illustrert i figuren under.

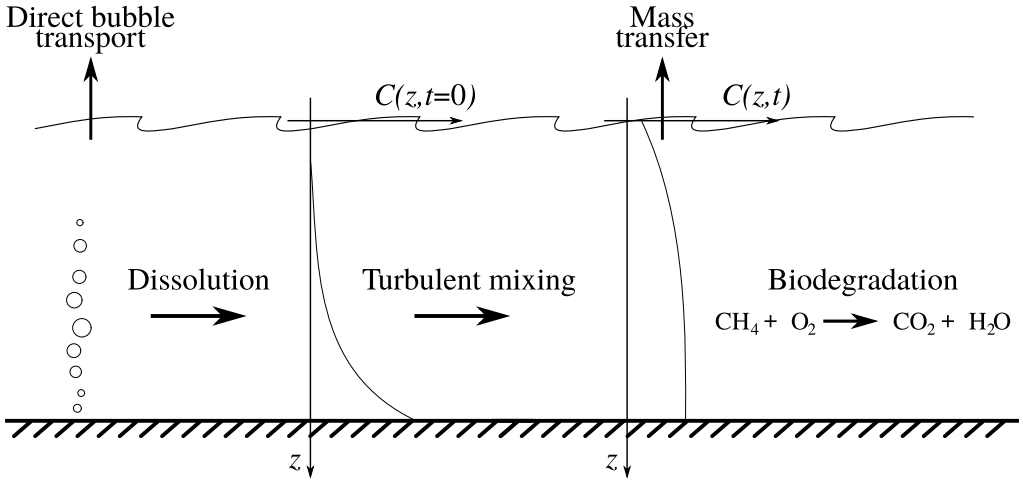

Illustrasjon av de ulike prosessene vi har sett på i litteraturstudien og tatt hensyn til i modelleringsarbeidet.

Modellering, samt publiserte resultater i litteraturen, indikerer at mesteparten av metanen fra et lite utslipp på havbunnen vil bli løst i vannkolonnen, med kun en begrenset andel som når atmosfæren via direkte transport med bobler. For den andelen som løses i vannkolonnen vil den videre skjebnen bli avgjort av forholdet mellom biodegraderingsraten, og den tiden det tar før løst metan blir blandet opp til overflaten og unnslipper til atmosfæren ved fordamping. For å undersøke effekten av ulike biodegraderingsrater har vi gjennomført et parameterstudie, med biodegraderingsrater tilsvarende halveringstider fra 10 til 1000 dager. Modellresultatene indikerer at for utslipp på 50 m dyp vil nesten all metanen nå atmosfæren, for utslipp på 120 m dyp vil mer enn halvparten av metanen nå atmosfæren hvis halveringstiden er omtrent 50 dager eller mer, og for utslipp på 300 m dyp vil mer enn halvparten nå atmosfæren hvis halveringstiden er omtrent 300 dager eller mer. Grunnen til det er at den relativt langsomme nedbrytingen gjør at metanen forblir i vannkolonnen lenge nok til å unslippe til atmosfæren om vinteren når den vertikale blandingen er sterkere. I disse studiene har vi antatt en relativt homogen vannkolonne i vintersesongen.

Når det gjelder havforsuring har små metanutslipp et teoretisk bidrag ved at metan brytes ned til CO_2 og vann. Imidlertid er mengdene relativt små, og vi finner at bidraget fra metan er utbetydelig sammenlignet med CO_2 fra andre kilder, slik som løsning av CO_2 fra atmosfæren til havet.

Fra litteraturstudiet konkluderer vi at det er stor usikkerhet i noen viktige parametere. Det mest påfallende er at det er en svært stor variasjon i publiserte biodegraderingsrater for metan i sjøvann. Det er også noe usikkerhet i hvordan den vertikale blandingen varierer gjennom året. Den valgte endimensjonale modelltilnærmingen tar heller ikke hensyn til horisontal transport og fortynning, eller historisk konsentrasjon av metan over tid i et bestemt volum sjøvann. Imidlertid finner vi at selv med disse usikkerhetene kan vi tentativt anta at mer enn halvparten av metanen som slippes ut fra små kilder på havbunnen vil nå atmosfæren.

For å avgrense de store usikkerhetene både i publiserte biodegraderingsrater, og i skjebnemodelleringen vår, er det nødvendig med videre forskning.

1 Introduction

Sources of methane (CH_4) in the ocean are mainly natural seeps, hydrothermal venting systems close to ocean ridges, underwater mud volcanoes, and releases from oil and gas fields (Etiope, 2015). Moreover, there is a potential for methane release to the ocean due to increase in temperature and ice retreat, thawing and unleashing the methane stored in hydrates or permafrost (Kroeger et al., 2011; Pohlman et al., 2017; Phrampus et al., 2014). The focus of this report is on seeps, which are continuous sources releasing methane at very low flow rates from the seafloor. Seeps can occur individually or in clusters, and can be naturally occurring, or related to human activities such as petroleum exploration and production. Seeps are identified as one of the sources of methane releases to the atmosphere, contributing to green house effects (Judd, 2004; Kvenvolden et al., 2001; Etiope, 2015; Liira et al., 2019; Sahling et al., 2014). Due to the high Global Warming Potential (GWP) of methane (see, e.g., Solomon et al., 2007, p. 33), the amount of methane reaching the atmosphere from seeps has received attention with regards to its contribution to climate change. Quantifying this amount is important to constrain the uncertainty in modelling studies of the earth's future climate. On the other hand, a recent study by Pohlman et al. (2017) indicates that methane emissions may increase biological uptake of carbon dioxide (CO_2) by stimulating CO_2 consumption by photosynthesizing phytoplankton in surface water. The study indicates that upwelling of cold, nutrient-rich water from near the seafloor carried by methane emissions have created high dissolved oxygen, high pH, and enrichment of ^{13}C in CO_2 in surface water enhancing primary production creating a sink for CO_2.

As methane bubbles are released at a seep source and rise through the water column, methane dissolves into the water, and other dissolved gases, mainly nitrogen and oxygen, may enter the bubble. If a seep is located in shallow water, such as on continental shelves, a significant fraction of methane may be transported directly with the bubble to the surface. In deeper waters, most or all of the methane will dissolve in the water column (Hovland and Judd, 1992; Hovland et al., 1993; McGinnis et al., 2006a). Note that even if the methane itself has dissolved, bubbles may still reach the surface, but in this case the bubble is almost entirely made up of nitrogen and oxygen (Olsen et al., 2017, Fig. 7).

Dissolved methane in the water column can be transferred to the atmosphere at the air-sea surface boundary if there is a sufficient concentration of methane in the surface mixed layer (Rehder et al., 1998; von Deimling et al., 2011; Mau et al., 2017). Methane in dissolved form can also biodegrade, i.e., it is oxidised by bacteria in the water column (Grant and Whiticar, 2002). If dissolved methane is present in large quantities, the biodegradation process may lead to oxygen depletion, although this is not relevant for the relatively low concentrations of methane from seeps.

There are several factors that control the fate of methane released from subsea seeps. The main factors for bubbles are the initial bubble size, the water depth at the release, ocean temperature and salinity, and concentration of dissolved gases (nitrogen, oxygen and methane) in the water column. Since dissolved methane does not significantly react or transform in the ocean, the ultimate fate of dissolved methane is decided by the balance between mixing and mass transfer to the surface, and biodegradation.

In this report we present results from a simplified one-dimensional modelling study to understand how much methane released from seeps will reach the atmosphere. The study focuses on selected locations on the Norwegian continental shelf (NCS), and investigates different values of the mentioned control parameters. Our focus will be on natural seep sources and the seeps originating from abandoned oil and gas fields. Other possible deep water sources of methane are not considered as they have a very small potential to contribute to the atmospheric methane, as found in previous studies Hovland et al. (1993).

The outline of the report is as follows. In Section 2, we present the literature review. We focus first on the literature describing seeps generally, and then seeps on the NCS. Next we review the literature on modelling bubbles rising from seeps, and modelling the transfer of dissolved methane from the sea surface to the atmosphere. We then review literature on the biodegradation of dissolved methane in the ocean, and finally we review ocean acidification.

In Section 3, we describe our chosen modelling approach. We first describe the modelling of methane rising as bubbles from the seafloor, and calculate the amount of methane that dissolves into the water column as a function of depth, and the amount that is transported directly to the surface and released into the atmosphere.

Next, we describe the mixing of dissolved methane in the water column, and the evaporation of dissolved methane across the sea surface and into the atmosphere, and the biodegradation of methane. We present and discuss the results of some selected scenarios, which are relevant for the Norwegian continental shelf.

Section 4 contains a discussion of our results, assumptions and the associated uncertainties. We also discuss the literature more broadly, and outline some suggestions for future research in order to constrain the uncertainties. Finally, we provide some concluding remarks.

2 Literature review

2.1 Methane seeps on the Norwegian continental shelf

Methane escaping from submarine seeps can originate from microbial degradation of organic matter in shallow sediments, called biogenic (microbial) methane, or thermogenic (petrogenic) methane formed as a part of the petroleum-generation processes under high pressure and temperature conditions in deep sedimentary layers in the crust (Judd, 2004; Hovland and Judd, 1988). Microorganisms produce almost pure methane, while thermogenic methane is often accompanied by appreciable amounts of ethane, propane and butane gases (Kennicutt, 2017). Isotopic analysis can to some degree be used to separate methane of different origins, as the carbon present in deep resevoirs is depleted in the unstable ^{14}C isotope. This has for example been used by Cain et al. (2017), who detected an atmospheric methane plume over the North Sea with possible origins from North Sea gas fields.

Several natural seep fields and oil and gas fields are present in and around the NCS within Norwegian geological boundaries. They are distributed at varying water depths and are the main source of methane that will be considered in the simulations of this study. Methane seeps may occur near oil and gas fields if wells are drilled through or near shallow gas reservoirs or pockets, creating pathways for gas to rise to the seafloor and escape into the water column (Böttner et al., 2020; Vielstädte et al., 2015). Rock type, local geology, and hydraulic connectivity in the strata are reported to play a role in this migration of gases. Moreover, gases may escape from faulty, damaged or cracked seals of abandoned wells (Moeinikia et al., 2018; Tveit et al., 2019) or even from actively used subsea installations if cracks or leaks are not detected. Further discussion of these scenarios are available for limited regions on the NCS (Böttner et al., 2020; Vielstädte et al., 2017; Crémière et al., 2016; Vielstädte et al., 2015). Additional reports of similar leaks are available for other parts of the North Sea in the UK and the Dutch sectors (von Deimling et al., 2011; Rehder et al., 1998; Römer et al., 2017) and from the USA. Abandoned wells are for example reported to be contributing about 4-7 % of the annual anthropogenic methane emissions in Pennsylvania (Kang et al., 2014; Townsend-Small et al., 2016).

Vielstädte et al. (2015); Vielstädte et al. (2017) studied three abandoned wells with seepages at 81 m to 93 m water depth in Utsira High in the Norwegian sector of the North Sea. The three wells (16/7-2, 15/9-13 and 16/4-2) are reported to have multiple single bubble streams released from small depressions on the seabed distributed in a $10\,m^2$ area around each well. The release rates were found to be highly variable depending on number of seeping vents per well. Observations include measurement of bubble sizes from video image analysis and direct measurement of gas flow rates at the releases. Based on these measurements, the estimated methane released at the seabed for each of the three wells were found to be 1, 4 and 19 tons per year. A summary of the results for the three wells are given in Table 1 (see Table S1 in the supplementary material of Vielstädte et al. (2017) for the original data). The methane released was identified to be biogenic, indicating its origin as gas pocket accumulations. The observed bubble diameters varied, with a mean bubble radius of 2.4 mm, 2.7 mm, and 5.7 mm respectively for the three wells. Using mass transport modelling, it was estimated that for the wells in question, around 4-5% of the released methane would be transported directly to the surface in the form of bubbles, while a larger fraction would dissolve in the top 50 m of the water column, where it may later transfer to the atmosphere. See Section 2.2.2 in the supplementary material of Vielstädte et al. (2017) for details.

Table 1: All numbers are taken from Table S1 in the supplementary material of Vielstädte et al. (2017). The annual mass released can be calculated by multiplying with the density of methane at standard temperature and pressure (STP, 25 °C and 1 bar), which is $0.657\,g\,L^{-1}$, and rounding to the nearest integer number of tons.

Well	Flow rate per seep [L/min] (STP)	Number of seeps	Annual amount [tons/year]
15/9-13	0.9	2	1
16/4-2	1.6	8	4
15/9-13	1.4	39	19

Based on regional seismic and water column imaging data in the North Sea, Böttner et al. (2020) has developed an approach to assess methane leakages from subsea decommissioned wells. Their study area covered an area of 200 000 km^2 with 1792 wells. They report that the presence of accumulations of gas in the crust within close proximity to decommissioned wells was found to be the most likely scenario for the formation of the seeps at the seafloor and noted that the leakages were highly variable. They estimated the methane released to the atmosphere from these sources in the North sea to 900–3700 tonnes per year, making that a major source for the regional methane budget. They also propose long term repeated water column monitoring surveys in the areas of abandoned wells to identify seepage activities.

The Norwegian Petroleum Directorate webpages[1] have details on oil and gas fields in Norwegian waters. As of August 2020, the area shown in 3 has 124 oil and gas fields with 1952 exploration wellbores, and 5034 development well bores. Information about wells that have been shut down is also available[2], and has been used to inform some of the choices of locations for the present modelling study. Details are given in Section 3.4.

Methane seeps are expected to continuously form in natural fields over long periods of time. However, the seepage from one specific location is not necessarily continuous, as it can be influenced by variations in the seep migration process in underlying strata, leading to variation in the release flow rate and composition (Hovland et al., 1993; DelSontro et al., 2015). This may be a result of seismic activities that disturb the flow path, lost connection to the supply source, or self sealing processes that are triggered by subsurface bacterial mats (Hovland, 2002). The seepage rates can vary from slow seepage to rapid venting. Fluxes from a single vent have been observed to vary by more than three orders of magnitude, from 3 mL/min to more than 10 L/min (von Deimling et al., 2011; Leifer and MacDonald, 2003).

2.1.1 Central North Sea

Hovland and Sommerville (1985); Hovland and Judd (1988); von Deimling et al. (2011) describe methane seepage present in the Norwegian part of the central North Sea, located in Norwegian block 1/9. There are many seepage locations within water depths of 65 m to 75 m (Hovland et al., 1993). Methane release volume rates from this area have been estimated by several authors. Hovland and Sommerville (1985) describe an ROV study of an area with a diameter of about 100 m, estimated to contain 120 seeps. 22 of those seeps were inspected more closely, where gas was found to escape from small circular vents in the sand, with both the vents and the bubbles having a diameter of about 10 mm. The volume flow rate measured at ambient pressure at 75 m depth was 24 m^3 d^{-1} (Hovland and Sommerville, 1985). The authors note that no bubbles were observed at the surface, leading them to assume that most of the gas dissolves in the water column. In a later study, Hovland et al. (1993) estimate the methane flow rate from this area of seeps to be 47 g m^{-2} yr^{-1}, over an area of about 120 000 m^2, for a total of 5.6 tonnes per year.

Von Deimling et al. (2010) used a custom, multibeam hydroacoustic device and observed 52 vents in the 2075 m^2 area covered by the device. From their data, they were able to observe variations in release rate apparently caused by the tides, where several seeps have reduced rates, or stop completely, during high tide. von Deimling et al. (2011) has again quantified seeps in the same location, and report that the main seepage area, with five methane ebullition areas, is found to be 21 times larger than previously thought. Their estimate of methane release is about 26 tonnes per year from the seepage area. They also measured methane concentrations, and found values up to 268 nM of dissolved methane in the vicinity of the seeps, which is reported to be about 100 times higher than background. The area of venting reported in von Deimling et al. (2011) is 0.14 km^2 with 550 vents with typical bubble diameters from 4.4 to 4.5 mm.

von Deimling et al. (2011) further report that modelling of bubble rise indicates that less than 4% of the released methane is transported directly to the surface. However, they hypothesise that almost all the dissolved methane in the water column may eventually be released into the atmosphere, in particular during autumn and winter when there is less stratification and strong vertical mixing due to high winds. They also noted that methane fluxes to the atmosphere in these areas may have been underestimated as many of the research cruises

[1] factpages.npd.no/en

[2] factpages.npd.no/en/field/pageview/shutdown

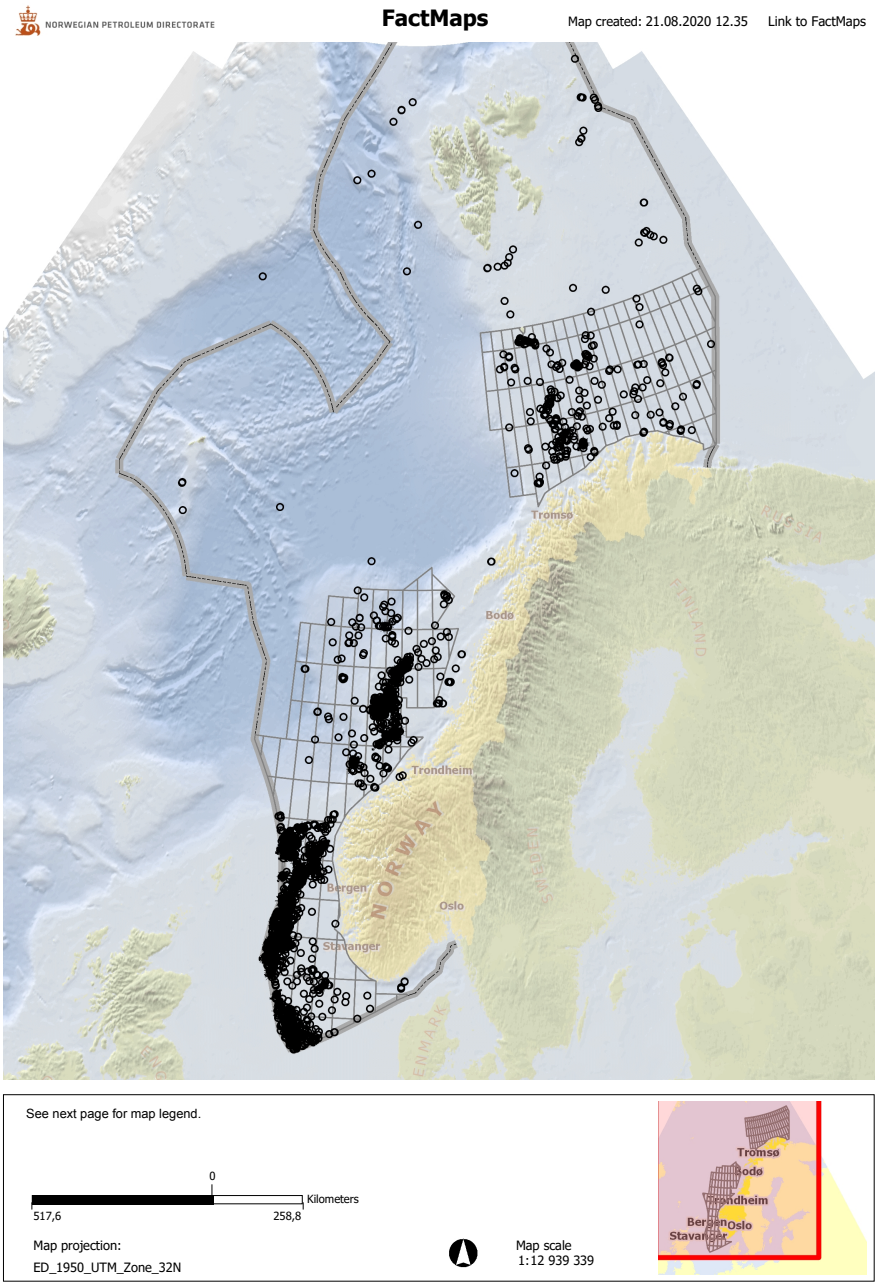

Figure 3: Oil and Gas Fields in Norwegian Continental Shelf and Svalbard. Source: `factpages.npd.no`

in the area are done in the summer season with calmer conditions.

2.1.2 Svalbard and the Barents Sea

Many observations of natural seeps are reported in the Arctic around Svalbard (Liira et al., 2019; Myhre et al., 2016; Panieri et al., 2017; Jansson et al., 2019; Pisso et al., 2016; Roy et al., 2019). Methane gas flares have been recorded in the water column south-west of Spitsbergen and on the west Spitsbergen continental margin, and in the Southern part of Nordfjorden (Roy et al., 2019; Gentz et al., 2014; Mau et al., 2017). Flares in this context refers to series of bubbles rising from the seafloor, which may or may not dissolve completely before they reach the surface.

The flares observed by Roy et al. (2019) in the southern part of Nordfjorden were found at depths between 152 and 226 m, rising to heights of 36 to 140 m above the seafloor, with an average rise distance of 80 m. The same study also reports a high density of pockmarks on the seafloor in the 300 km^2 large study area in Nordfjorden.

Mau et al. (2017) observed thousands of bubble emission sites over a distance of 630 km from Bjørnøya to Kongsfjordrenna along the continental margin off Svalbard. The bubble flares were observed in water depths from 33 m to 429 m with a median of 103 m. Moreover, 70% of the bubble emission sites they observed occurred at water depth of less than 120 m, having probability of direct release of methane to the atmosphere from bubbles reaching the surface. The dissolved methane plume generated by seeps and methane emission clusters was found to extend hundreds of kilometers along the Svalbard continental margin. Mau et al. (2017) estimate that the total amount of methane present in the plume at any given time is about 8400 tonnes. They further discuss the fate of this methane, and try to estimate the amount lost to biodegradation, and the amount lost to the atmosphere. Based on highly variable measurements of methane oxidation rates, Mau et al. (2017) estimate a daily degradation rate between 0.02% and 7.7% (median 1.8%) of the dissolved methane present in the plume. Rate of escape to the atmosphere is also quite uncertain, with estimates of 5.9% per day and 0.07% per day.

Sahling et al. (2014) observed widespread gas emissions at the continental margin west of Svalbard at water depths between 80 and 415 m. Intensive gas emissions were found to be present at 80 m to 90 m water depths in the main ridge of the Forlandet moraine complex. In this study, methane released as bubbles from the seafloor in a margin width of 14 km was estimated to be 53×10^6 mol (equal to 848 tonnes) per year.

Sauter et al. (2006) documented hydrate-coated methane bubble releases at the Haakon Mosby Mud Volcano, located at 1270 m water depth at the Bjørnøya slide scar on the south west Barents Sea. Methane plumes observed were extending from the seabed up to 750 m into the water column with estimated a gas flux of 0.2 (0.08–0.36) mol s^{-1} at the seafloor.

Liira et al. (2019) studied pockmarks and surrounding seabed in Isfjorden and Mohnbukta in western and eastern Spitsbergen and describe the geochemical characteristics of hydrocarbon gas from them. They report hydrocarbon venting systems with low methane concentration and similar seeping patterns in both areas, but with many pockmarks present in the Isfjorden area, while no pockmarks were observerd in Mohnbukta. This absence was explained as due to thinner sediment cover (1–2 m) in the area. Damm et al. (2005) measured methane concentration in the water column south west and east of Spitsbergen and found methane concentrations exceeding the atmospheric equilibrium concentration by up to two orders of magnitude (10–240 nM). The methane in the water column is reported to be created by submarine methane discharge at spread along the south west Spitsbergen shelf.

Gentz et al. (2014) found for the well-stratified water column in the West Spitsbergen continental margin during the summer, that the majority of methane from seeps dissolves into the water column below the pycnocline. This leads to high concentrations of dissolved methane in the lower water column which does not readily reach the atmosphere due to the stratification.

2.1.3 Other locations on the Norwegian Continental Shelf

Sauer et al. (2017) describe methane gas bubbling in Hola trough in the Northern NCS at a water depth of about 220 m in an area of about 2000 m^2 covered with methane derived authigenically (mineral or sedimentary rock deposit generated where it is found or observed[3]).

On the mid-Norway continental shelf Hovland and Judd (1992); Hovland (1990b,a) provide details of the presence of gas-associated mud diapirism in which seepages tend to occur and long chains of cold-water coral reefs that have evidently thrived on the venting light hydrocarbon sources.

Mau et al. (2017) estimated sea-air flux of dissolved methane for water sampled 3 m to 11 m below the sea-surface, in the surface mixed layer in along the continental margin west of Svalbard. The estimated fluxes ranged between 0.2 and 2.0 nmol m^{-2} s^{-1}, with a median of 0.021 nmol m^{-2} s^{-1}. Consequently, 73 % of all

[3] https://en.wikipedia.org/wiki/Authigenesis

estimated methane fluxes to the atmosphere range between 0 and 0.1 $\mathrm{nmol\,m^{-2}\,s^{-1}}$. They report that the fluxes were strongly affected by wind speed. Speeds between 0.3 and 12.6 $\mathrm{m\,s^{-1}}$ were prevalent during their survey, and they carried out 59 % of the sampling under low wind speeds less than $5\,\mathrm{m\,s^{-1}}$. Mau et al. (2017, 2015) also state that increased depth of the surface mixed layer may considerably increase the flux to the atmosphere.

2.2 Methane seeps in the Arctic sea and their fluxes to the atmosphere

In the Arctic sea, some field observations related to methane seeps are reported in the literature, including estimates of methane fluxes released to the atmosphere. These reports indicate as for elsewhere that the methane observed in the atmosphere mostly originates from the diffusive fluxes from the sea (mass transfer of dissolved methane from the ocean to the atmosphere), rather than from direct transport of methane in bubbles that reach the ocean surface unless the releases are from shallow depths Thornton et al. (2016); Shakhova et al. (2010); Shakirov et al. (2020); Li et al. (2017); Lorenson et al. (2016).

Large quantities of methane are stored in the Arctic as shallow water hydrates, and in the permafrost, making these deposits sensitive to a warming climate (James et al., 2016). From their review on methane emissions from seafloor sediments in the Arctic ocean, James et al. (2016) state that to fully understand and explain the effect of methane release from sediments on climate, we first need to understand anaerobic and aerobic oxidation of methane, bubble transport, and the effects of ice cover on how methane enters the atmosphere.

From remote sensing data, Bondur and Kuznetsova (2015) identified possible sources of natural hydrocarbon gas seeps in Arctic waters. They summarized gas sources in the Barent sea, the Norwegian sea, the Beaufort sea, the Laptev Sea and in the East Siberian sea. The sources were identified with the indications of dome-shaped gas emissions, gas plumes, surface temperature changes and local effects on sea ice, presence of bubbles in the water column and on the water surface, and anomalous phytoplankton production. With extensive at-sea observational data on concentration of dissolved methane in the East Siberian Arctic shelf area, Shakhova et al. (2010) find that more than 80% and 50% of bottom and surface waters respectively are supersaturated with methane relative to the atmosphere. They further find that the flux to the atmosphere is composed of both diffusive and ebullition components. They suggest the need for year-around detailed observations of atmospheric mixing ratios to monitor potential enhanced venting during fall due to breakdown stratification in water column and during break up of ice from May to July.

Thornton et al. (2016) carried out surface water and atmospheric measurement of methane in the Laptev Sea and the ice-free part of the western East Siberian Sea, and the average diffusive methane fluxes from the sea were found to be $2.99\,\mathrm{mg\,m^{-2}\,d^{-1}}$ and $3.80\,\mathrm{mg\,m^{-2}\,d^{-1}}$ respectively. These estimates were reported to integrate all local methane sources, and their findings suggest that the majority of the methane release happens through mass transfer of dissolved methane, with only a limited local effect of direct bubble transport.

Berchet et al. (2016) also studied methane emissions from the East Siberian Arctic Shelf. Based on a comprehensive statistical analysis of the atmospheric methane observations and of the simulations of high-resolution model representing Arctic atmospheric transport, they estimated the annual methane emissions in the region to range from 0.0 to $4.5\,\mathrm{Tg\,yr^{-1}}$, in contrast to previous estimates of 8 to $17\,\mathrm{Tg\,yr^{-1}}$. This difference is stated to be due to overestimation of methane leakage through sea ice in winter.

Shakirov et al. (2020) and Chand et al. (2012) observed occurrence of several gas flares and pockmarks along a segment of the Ringvassøy Loppa Fault Complex in Barents Sea, indicating open fractures and active fluid flow. The area was reported to be in the proximity of large oil fields, Skrugard and Havis, and north of the Snøhvit hydrocarbon field. They indicated the possible occurrence of more gas flares in the region, based on their observation of many flares along a comparatively small area, in a short segment of a regional fault complex.

Shakirov et al. (2020) also present a review of the literature on methane fluxes in the western and eastern Arctic and summarise that 32 to $112\,\mathrm{Tg\,yr^{-1}}$ is released to the atmosphere in the Arctic region, mainly due to the presence of wetlands in the region. However, they conclude that the estimates of methane sources and transport pathways in sediments and into the water column carry a large uncertainty due to the complexity of the formation process and different migration mechanisms. They suggest further integrated studies to asses the methane distribution, dynamics of oxidation patterns in the sediments and in the water column.

Berbesi et al. (2014) studied the potential methane contributions to the atmosphere from the Western Canada Sedimentary Basin and the Central Graben area of the North Sea, during the evolution of petroleum systems. They estimate maximum leakage rates in the order of 10^{-3} to $10^{-2}\,\mathrm{Tg\,yr^{-1}}$, for thermogenic methane and maximum biogenic methane generation rates of $10^{-2}\,\mathrm{Tg\,yr^{-1}}$ in the Western Canada Sedimentary Basin. Maximum estimates for thermogenic methane leakage rates were reported to be in the order in $10^{-2}\,\mathrm{Tg\,yr^{-1}}$ in the Central Garben area. They conclude that at geologic time scales, the thermal generation of methane, as a single process, would not be able to drive climate changes and stated the requirement of focused flow and sudden gas release from the reservoirs to exert a significant effect on Earth's climate. They have made this conclusions by the global scale extrapolation of estimated rates of thermogenic gas generation from above two study areas.

Li et al. (2017) measured dissolved methane at various depths in the western Arctic Ocean and found the surface waters in all the measuring stations were oversaturated with methane. They estimated the average sea to atmosphere flux to be $10.08\,\mu\mathrm{mol\,m^{-2}\,d^{-1}}$ in the Chukchi Sea shelf (CSS), and find that this accounts for 52% of the export of methane from the CSS, while oxidation of methane in the water columns accounts for 43 %.

2.3 Methane releases from sedimentary basins and river deltas

Kroeger et al. (2011) identify sedimentary basins rich with organic deposits both as containing very large amounts of organic carbon, and as a source for methane into the ocean and the atmosphere. Their study is focused on the possible contribution from variable methane fluxes from sedimentary basins, in driving the global climate both in time scales of millions of years, and over geologically short periods of time. Thus they state the importance of better understating the fluxes from various sedimentary basis, rates of migration to the surface and mechanisms by which methane leaking from sedimentary basins reach the atmosphere, to reduce the uncertainty in present day atmospheric methane budgets.

Kohnert et al. (2017) present a study on biogenic and geologic CH_4 emissions in the Mackenzie Delta region, Canada. They estimated that $0.038\,\mathrm{Tg\,yr^{-1}}$ are emitted in the study area, of which methane from geologic sources amounts to $0.0064\,\mathrm{Tg\,yr^{-1}}$. They further state that geologic sources of methane are found only in a small fraction of the total area surveyed, and that the individual geological sources were about 20 times stronger than typical biogenic sources. Thus, geological sources contribute a disproportionate amount, relative to their area, towards the total methane emissions in the region. Another study in the Beaufort Sea-Mackenzie Delta Basin, by Osadetz and Chen (2010), suggests that major Arctic deltas and continental shelves should be studied to estimate their potential contribution to the atmospheric methane budget. Their estimates for regional methane flux sequestered in gas hydrates is that it is certainly smaller than $4.2\,\mathrm{mg\,m^{-2}\,d^{-1}}$, and probably not greater than $0.12\,\mathrm{mg\,m^{-2}\,d^{-1}}$.

2.4 Uncertainty in estimates of methane released from seeps to the ocean and the atmosphere

The highly variable nature of both natural seeps, and seeps at abandoned oil and gas fields, in terms of their release flow rates and distribution (Vielstädte et al., 2015; Kennicutt, 2017; Sauer et al., 2017) has lead to challenges in detection, accurate field measurements, and detailed estimation of flow rates. Taken together, these factors make it difficult to estimate the net flux that will ultimately be released to the atmosphere (DelSontro et al., 2015). These estimation difficulties can clearly be seen in methane release estimate studies in different regions of the North sea, the Norwegian sea and the Arctic sea summarized in the previous sections and also pointed out by a study on methane releases in Dutch sea by Wilpshaar et al. (2019). Uncertainties are also present in separately identifying the natural and anthropogenic seeps of methane, as the natural seep sites are common grounds where the oil and gas fields are developed and wells are drilled for exploration and extracting of oil and gas (Wilpshaar et al., 2019).

Several obstacles are present during the detection phase of seeps in the field with acoustic instrumentation. Similar acoustic responses in shallow water make it hard to differentiate between low and high gas concentrations, causing difficulty in accurate quantification based on this method (Judd and Hovland, 1992; Roy et al., 2019). Hence, even though acoustic signals of many seep fields are available, quantification of releases are

limited. When flow rates are measured, they are either interpreted from the bubble sizes and numbers based on video or still images, or based on the flow rate measurements taken for a short period of time in the field. However, there is a possibility for the release flow rates to vary with time, e.g., due to the tides (Boles et al., 2001; Sultan et al., 2020), and at varying release locations in the same field. This variability may depend on location specific characteristics such as the capacity and depth of underlying gas accumulations, soil type, presence of seismic activities, etc. In case of leaking from abandoned wells, specific detailed information about the state of different wells such as the integrity of the well sealing and the connectivity of the wells to possible underlying gas reservoirs is limited. Methods and tools are still being developed to estimate this information for databases of existing wells and seismic characterisations (Böttner et al., 2020; Vielstädte et al., 2015; Vielstädte et al., 2017).

Based on the available limited data on seep fields, overall methane releases have been estimated for larger regions, using extrapolation under certain assumptions for each of the above parameters. These extrapolated estimates vary over a large range, with no clear consensus on the different assumptions among different stakeholders and studies (Wilpshaar et al., 2019). A majority of the studies are stressing the need for further research on the above aspects, in order to get an accurate estimation of methane releases to the ocean and to the atmosphere.

2.5 Microbial methane oxidation

Microbial methane metabolism includes both methane formation and degradation. While methane formation is a strict anaerobic process, appearing only in the absence of oxygen, methane may be degraded by microbes in the marine environment by both anaerobic and aerobic processes. While the anaerobic processes are limited to the anoxic strata of marine sediments, only aerobic methane degradation will be relevant for the marine water column in a non-stagnant ocean, and no methane formation is therefore expected by microbial processes in the water column. In the water column methane degradation will be confined to dissolved methane, while methane in rapidly rising bubbles will be unaffected by microbial processes until dissolved in the water column, as the time scale for methane bubble rise and dissolution is much shorter than for degradation.

Since the topic of this report will be the fate methane in the marine water column, we will only focus on the aerobic microbial processes of methane metabolism, i.e. methane degradation of dissolved gas.

2.5.1 Oxidation process

The typical methane processes in the marine environment are illustrated in Fig. 4. In the deep sediment methanogenic zone, methane may be formed by thermogenic processes and released to the marine environment from cold seeps. Organic material deposited on the seafloor is mineralized to CO_2 in the aerobic zone of the sediments, while fermented to hydrogen and CO_2 and smaller organic compounds (e.g. acetate) in the anaerobic sulphate zone of the sediments. In the deeper methanogenic zone, buried organic matter will be transformed to methane and CO_2 by anoxic methanogenic processes, and CO_2 may also be further reduced to methane (Fuchs, 1987). Methane diffusing to the aerobic upper zone and to the seawater will be oxidized by methanotrophic processes.

Microbial degradation of methane is a one-step process, in which methane is directly transformed to carbon dioxide, without any intermediate metabolite products.

$$CH_4 + 2\,O_2 \rightarrow CO_2 + 2\,H_2O \tag{1}$$

Aerobic oxidation of methane in seawater is performed by so-called *methanotrophic* microbes, contrary to *methanogenic* microbes, which are responsible for anaerobic methane formation. Methanotrophic microbes include typical 1-carbon utilizing bacteria within a wide range of bacterial and archaeal genera, including *Methylomarinum*, *Methylobacter*, *Methylococcus*, *Methylomicrobium*, *Methylomonas*, *Methylocaldum*, *Methylocystis*, *Methylosinus*, *Methylocella*, *Methyloacidophilum*, *Methylothermus*, *Methylocapsa*, *Methylophaga*, and *Methylosarcina* (Abdallah et al., 2014; Gutierrez and Aitken, 2014). Most of the methanotrophic microbes possess a methane monooxygenase gene responsible for methane oxidation (*pmoA*) (McDonald and

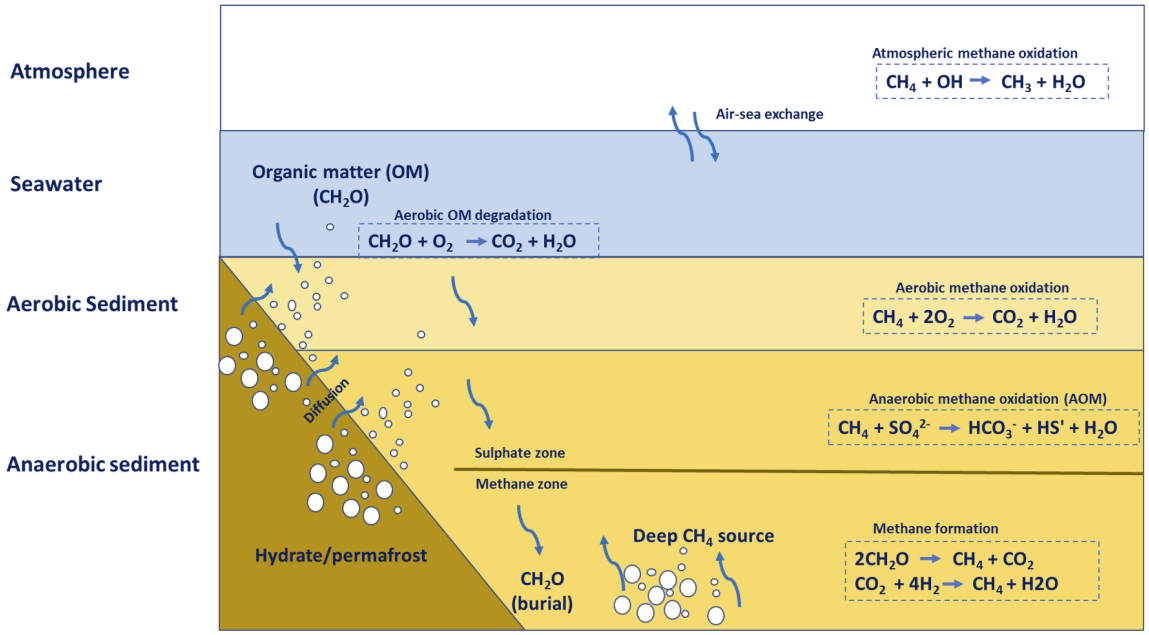

Figure 4: Methane processes in the marine environment. Based on a similar figure by Bui (2018).

Murrell, 1997). Interestingly, several microbes may also perform anaerobic oxidation of methane, also using a methane monooxygenase gene for oxidation (Luesken et al., 2011). Several of these anaerobic methane oxidizers are prevalent in marine sediments, using sulphate or nitrate/nitrite as electron acceptors instead of oxygen (Niewöhner et al., 1998; Haroon et al., 2013).

$$CH_4 + SO_4^{2-} \rightarrow HCO_3^- + HS^- + H_2O \tag{2}$$

$$CH_4 + 4NO_3^- \rightarrow CO_2 + 4NO_2^- + 2H_2O \tag{3}$$

$$3CH_4 + 8NO_2^- \rightarrow 3CO_2 + 4N_2 + 2H_2O + 8OH^- \tag{4}$$

The anaerobic methane oxidation processes involve different types of microbes, like consortia of anaerobic methanotrophic archaea (ANME) and sulphate-reducing bacteria (SRB), or ANME coupled with nitrate- or nitrate-reducing bacteria (Nauhaus et al., 2005; Haroon et al., 2013). However, since the anaerobic processes appear exclusively in sediments, these are not the topic of this report focusing on the processes in the water column, and the rest of this chapter will therefore focus entirely on the aerobic methane oxidation processes.

2.5.2 Calculating methane oxidation rates in a static system

Methane oxidation rates are determined by simple first-order rate kinetics, according to the following equation:

$$R_{ox} = k \cdot [CH_4], \tag{5}$$

where R_{ox} is the oxidation rate of methane, k is a rate coefficient, and $[CH_4]$ is the methane concentration. The half-life (T_{50}) may be derived directly from the first-order rate coefficient k:

$$T_{50} = \ln(2)/k, \tag{6}$$

where $\ln(2) \approx 0.693$ is the natural logarithm of 2.

2.5.3 Methane oxidation rates in seawater

A review of publicly available research papers describing methane oxidation rates in natural seawater revealed large differences between oxidation rates, illustrated by half-lives ranging from 1 day close to an Atlantic gas

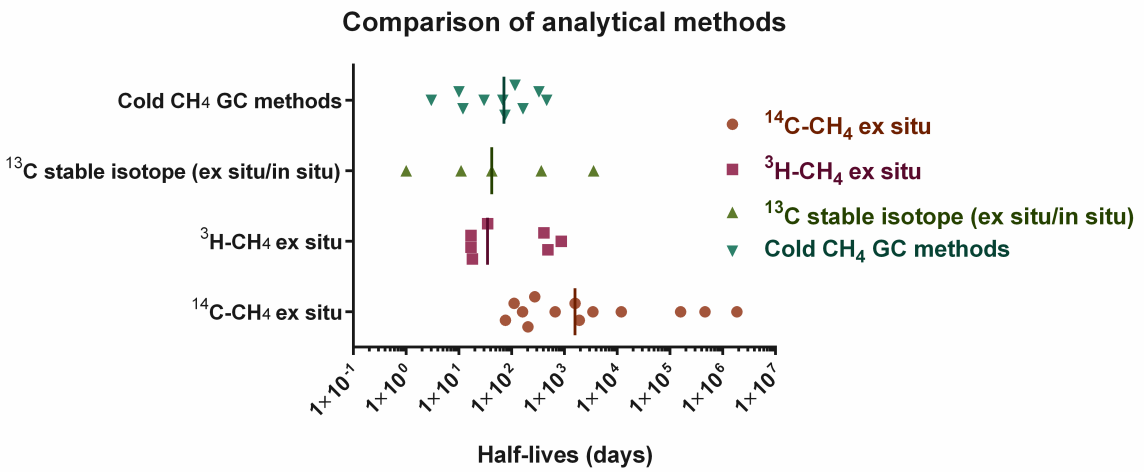

Figure 5: Comparison of methane oxidation half lives from multiple studies related to the analytical methods used.

seep (Leonte et al., 2017) to close infinitely in oxic water of a stratified Pacific fjord (Ward et al., 1989). The determination of methane oxidation rates may depend on several factors, like bacterial community organization and size, method of measurement, temperature, water depth, and methane concentrations.

Analytical methods

Methane is measured either by ex situ or in situ methods. The ex situ methods include the use of "cold" or radiolabelled material, the latter using ^{3}H- or ^{14}C-labelled methane. The use of "cold" material requires high methane concentrations compared to realistic environmental concentrations, except close to gas seeps or in plumes of subsurface spills like the Macondo spill in 2010 (Camilli et al., 2010; Kessler et al., 2011). Gas chromatographic analyses of "cold" methane will have a detection limit of 0.01-0.1 mg/L, corresponding to approximately 1 µmol/L. However, methane concentrations in natural seawater are usually described in nmol/L ranges, so radiolabelled methane is instead used in most studies to determine oxidation rates at realistic concentrations. Some studies have indicated the use of ^{3}H-labeled CH_4 to generate faster oxidation rates than with ^{14}C-labeled CH_4 (Mau et al., 2013; Pack et al., 2015), and the ^{3}H method has therefore been used in other oxidation studies (Valentine et al., 2001, 2010).

In situ methods include the analysis of ^{13}C stable isotope, as applied in several studies ((Valentine et al., 2001; Weinstein et al., 2016; Leonte et al., 2017). Here, an amount of $^{13}CH_4$ is injected into the water sample, and if the compound is biodegraded, it is converted to $^{13}CO_2$ which leads to changes of the $^{13}C/^{12}C$ carbon isotope ratios of the total CO_2 and the carbonate system. Such a change of the stable isotope ratio therefore indicates the mineralization of the substrate, which can be used to calculate biodegradation rates. Typically, the use of stable isotope methods resulted in generally faster oxidation (half-lives ranging from 1 to 42 days; median 11 days) than ex situ methods with ^{3}H-labeled CH_4 or ^{14}C-labled CH_4 (half-lives ranging from 17 days to infinitively; median 460 days) (Ward et al., 1989; de Angelis et al., 1991; Valentine et al., 2001, 2010; Mau et al., 2013; Pack et al., 2015; Weinstein et al., 2016; Leonte et al., 2017). The differences in oxidation half-lives from several studies, also illustrating the difference between the different analytical methods, are shown as half-lives in Fig. 5.

Methane oxidation rates may also differ over time if water samples used for oxidation studies are sampled during different time periods, reflecting potential changes in microbial communities and sea water composition and characteristics. In a study performed with seawater collected in summer (August 2016), methane oxidation rates in an artificial natural gas (methane, ethane and propane) resulted in a half-life of 12-30 days, depending on initial methane concentration (Brakstad et al., 2017). However, in a later study with methane as part of artificial natural gas, and with seawater collected in winter (February 2019), rate determinations resulted in

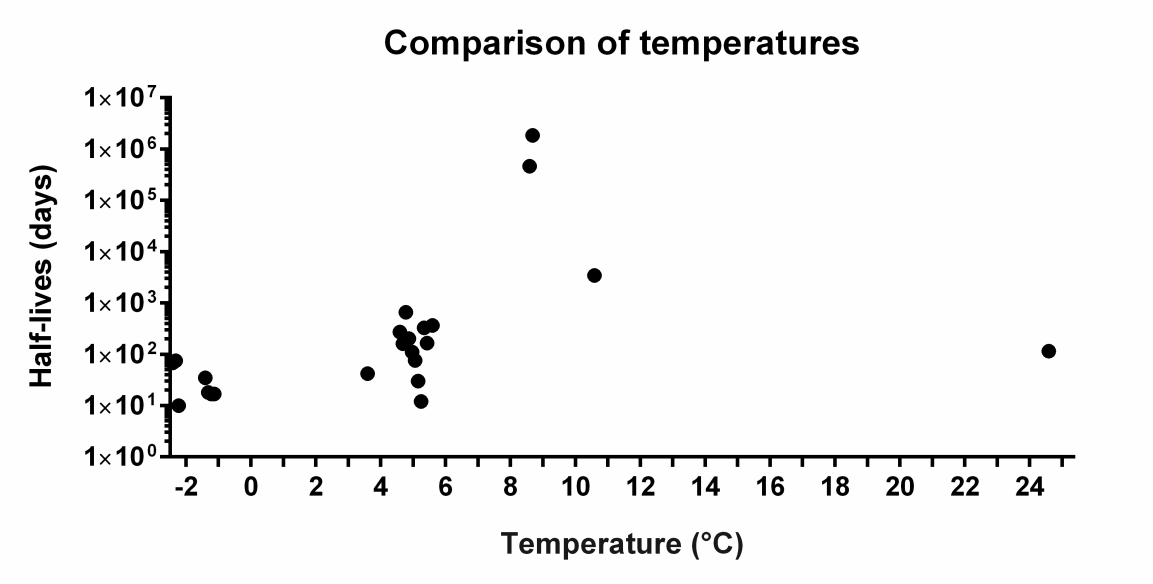

Figure 6: Comparison of methane oxidation half lives as a function of seawater temperature.

a half-life of approximately 330 days (manuscript in preparation). These experiments were performed in the presence of water-soluble oil compounds, but this did not seem to affect the methane oxidation rates (Brakstad et al., 2017).

Temperature

Methane oxidation rates have been determined both ex situ and in situ in seawater at different temperatures, ranging from shallow water at high temperatures above 20 °C, to Arctic water with sub-zero temperatures. The Arrhenius curve describes a temperature dependency of reactions, and biodegradation rates of soluble compounds have often been explained by the Q_{10} approach, suggesting a rate coefficient reduction by a constant factor (often around 2) when temperatures are decreased by 10 °C (Bagi et al., 2013; Nordam et al., 2020). However, rapid methane oxidation rates were measured in Arctic seawater from the Beaufort Sea and Svalbard ((Mau et al., 2013; Uhlig et al., 2018), with oxidation half-lives ranging from 10 to 75 days (median value 18 days). On the other hand, at a temperature of 25 °C, an oxidation half-life of 116 days was measured at Cape Cook Lookout Bight in North Carolina (Sansone and Martens, 1978). The lack of consistency between temperature and oxidation half-lives are illustrated in Fig. 6 for studies where oxidation temperatures were documented. Temperature alone is therefore not a sufficient quantity to predict half-life values.

Water depth

Water depths are important for gas solubility. In deep waters, both pressure and low temperatures will result in increased solubility from gas bubbles (Johansen, 2003).

Several studies have investigated vertical methane oxidation profiles in the water column. In a study of seawater collected from the Bering Sea (Bristol Bay) with seawater collected from the near surface (5 m depth) and from near seabed (30-300 m depths) in January, August and May, the oxidation rates were generally faster in the near-bottom (average half-lives of 147 days) than near-surface samples (average half-lives 349 days), as determined by ex-situ analyses with ^{14}C-labelled methane. The faster oxidation rates in the near-bottom samples corresponded to higher methane concentrations measured in the near-bottom samples than the near-surface samples ((Griffiths et al., 1982)).

In a study of with seawater collected from surface to 200 m depths in the Summer period from the Saanich Inlet fjord in British Columbia (Canada), the highest methane oxidation rates occurred in a typical stratification depth at 140 m with an oxic-anoxic interface, although the highest methane concentration was in the bottom

water. However, oxygen levels were low in the bottom water emphasizing that low oxygen saturation may affect methane oxidation (Ward et al., 1989).

In a study of stratified tropical Pacific seawater, the combined impacts of methane and dissolved oxygen concentrations on the methane oxidation rates were also described. Oxygen minimal zones typically occurred around 400 m depths, resulting in methane peak concentrations (9-20 nmol/L), while surface and deep-water concentrations ranged from 5 to 8 nmol/L and less than 1 nmol/L, respectively. Typically, the methane oxidation rates were highest in the upper water column with oxygen saturation, lowest in the oxygen minimal zone, enabling lateral methane transport within this zone. However, the oxidation rates determined in these samples were extremely slow with half-lives ranging from 400 to more than 800 days (Pack et al., 2015).

The same methane oxidation trends as described above were also measured in a stratified Arctic fjord (Storfjorden, Svalbard), with ice melt water in the upper 60 m, Arctic water between 60 m and 100 m, and brine-enriched shelf water between 100 m and 140 m depth. The highest methane concentrations were associated with the ice melt and Arctic water at 40-100 m depth (20-70 nmol/L), compared to the concentrations above 40 m (10-30 nmol/L) and below 100 m (5-10 nmol/L). Once again, the highest methane oxidation rates were determined where methane concentrations were at its highest (40-100 m depth), with rates of 1-2.5 nmol/L/day, compared to <0.1-0.5 nmol/L/d above 40 m, and 0.2-0.8 nmol/L/d below 100 m depth, using ex situ ^{3}CH4 oxidation analysis (Mau et al., 2013).

Depth-related oxidation rates determined in non-stratified Pacific seawater (Eel river Basin offshore California) showed increased methane concentrations and oxidation rates in near-bottom water. The oxygen concentrations deceased gradually from approximately 250 µM (8 mg/L) in surface water, to approximately 50 µM (1.6 mg/L) in the bottom water at 550 m depth. This resulted in increased methane concentrations and oxidation rates in the near-bottom water (deeper than 400 m). While methane concentrations differed between 20 and 300 nmol/L in the deeper water (> 400 m), they were low (3-10 nmol/L) in the upper water column (< 400m). Methane oxidation rates were very low both in the deeper and upper water column, but with faster half-lives in the deeper column with high methane concentrations (approximately 1 year) compared to upper water column (close to 10 years) (Valentine et al., 2001).

Oxygen

As shown above (Eq. (1)) methane oxidation is primarily an aerobic process, with 2 moles of molecular oxygen required to oxidize one mole of methane. The typical oxygen saturation curve related to temperature is shown in Fig. 7 (OECD, 1992). The molecular oxygen saturation level in seawater at 5 °C is close to 0.3 mmol/L (10 mg/L) and 0.25 mmol/L (8 mg/L) at 5 °C, which theoretically enables the oxidation of 0.15 mmol/L (2.4 mg/L) and 0.12 mmol/L (1.9 mg/L) dissolved methane until complete oxygen deficiency occurs.

In stratified water, oxygen deficiencies may occur in deeper water layers, as also described above with Pacific waters (Ward et al., 1989; Pack et al., 2015). In these waters, oxygen may become a limiting factor for methane oxidation, although anaerobic processes may also be appear in the oxygen-depleted zones of the water column (Wakeham et al., 2007). Some of these areas with deep-water oxygen depletion are shown in Fig. 8, showing that particularly Pacific, southern Atlantic and Indian Ocean areas, besides the Black and Caspian Seas, are subject to oxygen deficiencies.

However, in well oxygenated water, oxygen is not a limiting factor, since methane concentrations will not be higher than the oxidation capacity of the seawater. In hotspot areas like gas seepages, pockmarks and hydrate destabilization zones, the local concentrations of methane may reach levels of 200-600 nmol/L (von Deimling et al., 2011; Graves et al., 2015)), and even concentrations of 30 µmol/L in sediment porewater (Krämer et al., 2017). Even these hotspot local concentrations will not result in serious oxygen deficiencies in well oxygenated seawater. In addition, dissolved methane will be rapidly diluted when released from local point sources. This may be exemplified with the Macondo oil spill in the Gulf of Mexico in 2010. During this spill, methane was the most abundant hydrocarbon released, expected to be between 9.14×10^9 and 1.25×10^{10} moles (Kessler et al., 2011), and with concentrations as high as 180 µmol/L close to the leaking well (Valentine et al., 2010). A persistent methane plume (more than 500 nmol/L) was measured at 1000 m to 1200 m depth at least for 6 km in the location southwest of the spill site, resulting in a small oxygen anomaly of up to 30 µmol/L (approximately

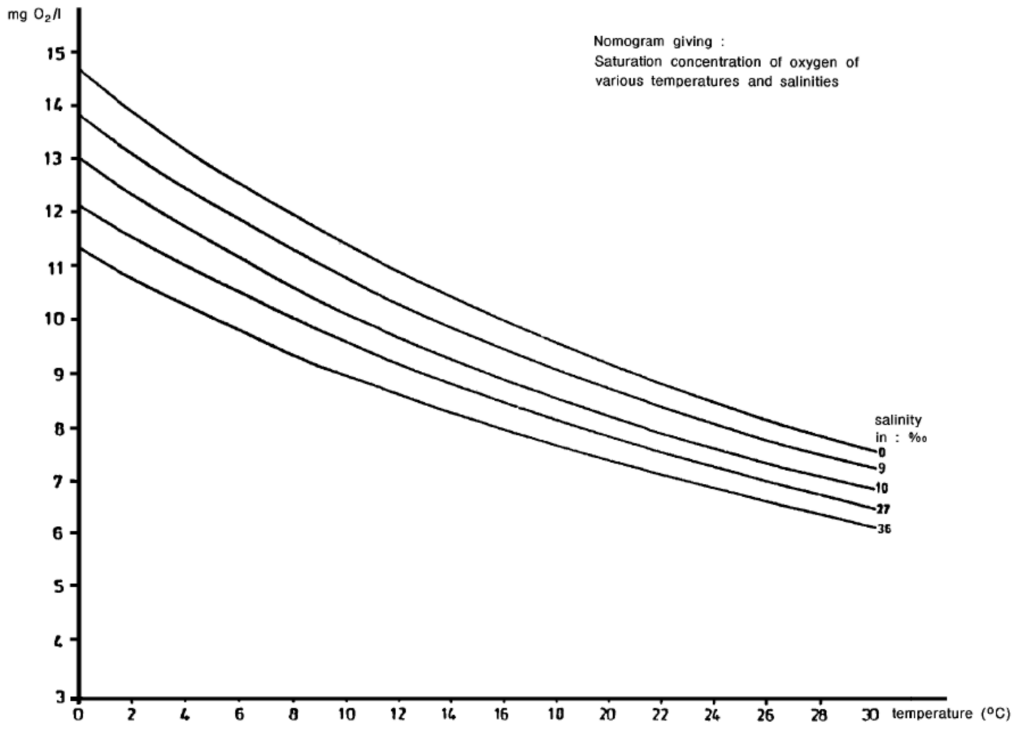

Figure 7: Saturation concentrations of oxygen at various temperatures and salinities (OECD, 1992).

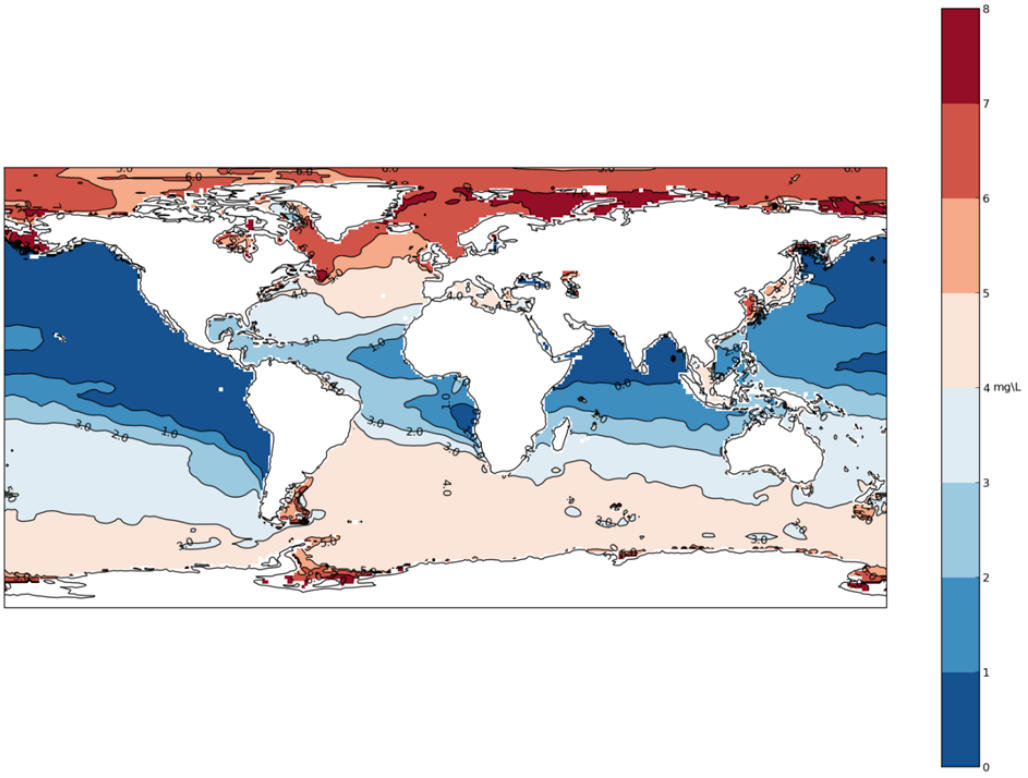

Figure 8: Global dissolved oxygen concentrations in the winter in the water column at 500 m depeth. Source: `www.nodc.noaa.gov`

1 mg/L) at the highest (Valentine et al., 2010). The data also showed that the released methane was mainly consumed by microbial oxidation during the spill period, resulting in a peak oxidation rate of 5 mmol/L/d (Kessler et al., 2011). The oxygen anomaly in the deep sea water column is shown in combination with the occurrences of methane and soluble hydrocarbons methane concentration in respectively Kessler et al. (2011, Fig. 1C) and Camilli et al. (2010, Fig. 1).

Methane concentrations

Based on the reviewed literature methane concentrations are important for the oxidation rates. However, this requires oxygenated environments, since oxygen-depleted water with high methane concentrations may show low oxidation rates, as shown in stratified waters (Ward et al., 1989). We should therefore compare methane concentration and oxidation rates in well-oxygenated non-stratified water, or in the oxygenated zones of stratified water. In this comparison it is necessary to consider the analytical methods used in the studies, since we have seen above that the choice of method impacts the oxidation rates, and cross-study comparisons therefore become difficult. We have therefore compared data within the same studies, and in environments without oxygen limitations.

In a study with seawater holding 5 °C, we measured oxidation rates for methane, starting with concentrations of 1720 µM and 24.1 µM), resulting in faster oxidation rate coefficients by a factor of 2.4 at the highest concentration (Brakstad et al., 2017). However, the highest methane concentration was unrealistically high compared to environmental concentrations.

A study with seawater from the Pacific Ocean (Eel river Basin offshore California), showed that oxidation rate coefficients were approximately 10 times higher in seawater with 7.6 mmol/L than with 2 mmol/L methane (Valentine et al., 2001). Studies with Arctic seawater from Svalbard showed increased oxidation rate coefficients by a factor of 1.9 at 40 nmol/L methane when compared to 10 nmol/L ((Mau et al., 2013)).

However, the best comparisons are probably data from the Macondo spill, although discharges of other gases (ethane, propane and butane) as well as other hydrocarbons may have impacted the degradation rates. During the spill, large amounts of samples were collected over extended periods of time. One of the studies measured a relation between rates and concentrations of propane, following a linear relationship up to 5000 nmol/L, and then reaching a saturation peak level, where rates became independent of propane concentrations (Valentine et al., 2010). Correspondingly, a relation between methane concentrations and oxidation rates were determined, as shown in (Kessler et al., 2011, Fig. 3), describing the relation by a one-dimensional model.

Following the spill from the start in April 2010 until September, the model describes an initially low methane oxidation rate for a pre-spill situation, with a low rate coefficient, exemplified as 0.0015. The initial low oxidation rate was related to low abundances of methanotrophic microbes, in line with data even from Pacific methane seeps, showing rate coefficients up to 0.0019 (Valentine et al., 2001). However, as methanotroph abundances increase, the oxidation rate coefficients increases dramatically, up to 0.2, resulting in a larger oxidation than accumulation, and in September, after closing the well, the methane oxidation coefficient declined to 0.0015 (Kessler et al., 2011). These differences in rate coefficients resulted in estimated half-lives ranging from 3 days at peak levels (25 µmol/L methane in late June-early July) to > 450 days at low methane concentrations (less than 2 nmol/L in September).

2.5.4 Oxidation rates relevant for the Norwegian Continental Shelf

As mentioned, dissolved methane concentrations may be of importance for estimations of oxidation rates. As described above, estimated oxidation rates varied from 0.2 d^{-1} triggered by average dissolved methane concentrations of 25 000 nM (average of 73 measurements) to 0.0015 d^{-1} at average concentrations of 1.4 nM (average of 671 measurements) during the Macondo oil spill (Kessler et al., 2011). It was further estimated during the Macondo spill that gas oxidation rates were linearly associated with concentration, as shown for propane (Fig. 9, left panel). In this figure, it is shown that propane oxidation rates were expected to follow a concentration-related first-order rate approach up to a saturation level of 5000 nM propane, while higher

concentrations resulted in concentration-independent zero-order rates (Valentine et al., 2010). Following this approach also for methane oxidation rates, one may assume a first-order rate approach between the concentrations of 1–4 nM to 25 000 nM, with zero-order rates at higher concentrations (Fig. 9, right panel).

A few studies have been reported on methane oxidation rates which may be relevant for the Norwegian Continental Shelf, including studies of natural gas seeps or abandoned wells leaking gas. Measurements of methane concentrations close to natural seepages in the central North Sea showed concentrations of 5–200 nM in the seawater close to the emission and below the thermocline, while concentrations of 4–8 nM were measured close to the sea surface (von Deimling et al., 2011). However, no oxidation rates were reported. In a study of abandoned North Sea wells, methane concentrations close to the wells varied from 100 to 200 nM below the thermocline, to 40–100 nM above the thermocline. Two water samples collected above one of the wells showed very low rates of $0.19 \pm 0.07\,\mathrm{nM\,d^{-1}}$ and $1.40 \pm 0.83\,\mathrm{nM\,d^{-1}}$ (Vielstädte et al., 2017). Assuming methane concentrations of 100 nM, this would result in rate coefficients of 0.0019–0.014 $\mathrm{d^{-1}}$ (half-lives of 50–360 days). However, the dissolved methane concentrations in these samples were not reported.

In two studies of the abandoned North Sea well 22/4b, nearfield methane concentrations ranged from 500 nM to more than 60 000 nM in the bottom water close to the well at 60–85 m depth, 40–13 000 nM in the thermocline (40–60 m depth) and from less than 5 nM 20 nM above the thermocline, while farfield concentrations showed median concentrations of 200 nM below and 20 nM above thermocline (von Deimling et al., 2015; Steinle et al., 2016). The average methane oxidation rate coefficient were estimated to be $0.005 \pm 0.007\,\mathrm{d^{-1}}$, $0.011 \pm 0.013\,\mathrm{d^{-1}}$, and $0.0004 \pm 0.06\,\mathrm{d^{-1}}$, in the bottom, thermocline and surface waters, respectively, corresponding to half-lives ranging from 66 days to more than one year (Steinle et al., 2016).

Measurements of seepages along the continental margin off Svalbard to Bjørnøya showed methane concentration ranging from less than 10 nM to 100 nM, and with measured methane rate coefficients ranging from approximately 0.02–0.08 $\mathrm{d^{-1}}$, which corresponds to half-lives of 9–35 days (Mau et al., 2017). In another study with Arctic seawater (Storfjorden, Svalbard), maximum oxidation rate coefficients were estimated to be 0.03 $\mathrm{d^{-1}}$ (half-life 23 days) at high methane concentrations (72 nM), and decreasing (not reported) with lower methane concentrations (Mau et al., 2013). These data therefore indicate faster methane oxidation rates in the Arctic than in the North Sea water samples.

In order to select for relevant methane oxidation rates, two approaches are described here. The first approach is based on the model described in Fig. 9. In this model, oxidation rates may be related to different concentrations of dissolved methane. Discharged gases are rapidly diluted in the water column, and oxidation rates are slow processes. We may therefore expect considerable methane dissolutions before significant oxidation may become evident. Most of the studies relevant for the Norwegian Continental Shelf are performed in shallow water (less than 200 m depth), and we may expect rapid dilutions to concentrations measured in the water columns above the thermocline. Typically, concentrations from less than 5 nM up to 100 nM (von Deimling et al., 2011, 2015; Steinle et al., 2016; Mau et al., 2017; Vielstädte et al., 2017). If concentrations of 10–20 nM are relevant to use, the oxidation rates of 0.04675–0.0608 $\mathrm{d^{-1}}$ (half-lives 11-15 days) are given by the linear model show in the right panel of Fig. 9. However, concentrations of 1–2 nM (close to typical methane background levels) will result in an oxidation rate of 0.00468–0.006 08 $\mathrm{d^{-1}}$ (half-lives of 113-148 days).

Another approach may be to identify the oxidation rates at low methane concentrations from experimental studies, mainly those relevant for the Norwegian Continental Shelf, for instance 20 nM (Table 2) or 10 nM or lower (Table 3). In Table 2 we have selected oxidation rates described at dissolved methane concentrations close to 20 nM in some of the literature used in this report. These data have been collected irrespective of seawater temperature, location or methane concentration methods. However, first-order rates are assumed during the determinations of rate coefficients and half-lives. The data in Table 2 showed rate coefficients from 0.0014 $\mathrm{d^{-1}}$ to 0.1 $\mathrm{d^{-1}}$, resulting in half-lives from 7 to 495 days. Of the selected studies, we only included one study with relevance for the North Sea, and with data from three water samples, a bottom water at 85 m depth, a sample from the thermocline at 42 m depth, and a mixed layer sample from 11 m depth (Steinle et al., 2016). The oxidation test with the North Sea water was performed as a 2-day test with ^{14}C-labelled methane, and the average rate coefficients varied significantly, from $0.041 \times 10^{-2}\,\mathrm{d^{-1}}$ to $1.1 \times 10^{-2}\,\mathrm{d^{-1}}$ for the water samples (Steinle et al., 2016). The rate coefficient marked with † in Table 2 is an estimated maximum rate coefficient,

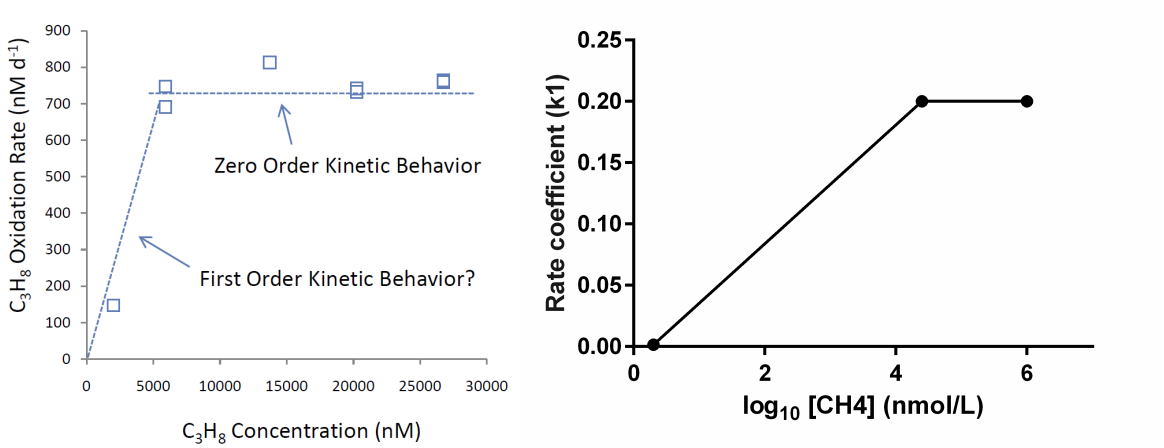

Figure 9: A possible relation between methane oxidation rate coefficient and methane concentrations (left panel) (Valentine et al., 2010), based on a combination of concentration-dependent first-order rates, followed by concentration-independent zero-order rates, as shown for propane respiration (right panel) (Kessler et al., 2011).

indicating low degradation rates for the seawater in vicinity to an abandoned North Sea well.

Some of the same studies also included rate data for lower methane concentrations (Table 3). Two of these studies showed that reduced concentrations decreased oxidation rates significantly (Pack et al., 2015; Uhlig et al., 2018), while one study showed the opposite trend (Weinstein et al., 2016). Thus, it seems that the uncertainties related to the oxidation rates were particularly evident for the lower methane concentrations.

Table 2: Methane concentrations, oxidation rate coefficients and half-lives determined in selected studies with methane concentrations close to 20 nM in natural seawater. A dash (-) means the information is not given in the reference. †Rate coefficient based on maximum oxidation rate.

Conc [nM]	Rate coeff. [d^{-1}]	Half-life [days]	Temp. [°C]	Water source	Depth	Reference
16	0.009	75	-1.8	Beaufort Sea	Shallow	Uhlig et al. (2018)
10	0.008	87	10–12	Pacific	Oxycline	Ward et al. (1989)
17	0.06	12	-	Pacific	0–100 m	Pack et al. (2015)
21	0.08	8	-	US Atlantic	400–500 m	Weinstein et al. (2016)
22	0.10	7	-	Us Atlantic	400–500 m	Leonte et al. (2017)
20	0.05	14	-	Svalbard	-	Mau et al. (2017)
20	0.0014†	495	10	North Sea	40 m	Steinle et al. (2016)

Table 3: Methane concentrations, oxidation rate coefficients and half-lives determined in selected studies with methane concentrations 10 nM or lower in natural seawater. A dash (-) means the information is not given in the reference.

Conc [nM]	Rate coeff. [d^{-1}]	Half-life [days]	Temp. [°C]	Water source	Depth	Reference
4.4	negative	-	-1.8	Beaufort Sea	Shallow	Uhlig et al. (2018)
5	0.001	690	-	Pacific	0–100 m	Pack et al. (2015)
9.7	0.4594	1.7	-	US Atlantic	400–500 m	Weinstein et al. (2016)

2.5.5 Conclusions

The reviewed data on methane oxidation showed high variability in the results, with oxidation half-lives derived from rate coefficients and methane concentrations varying from a few days to several years. Some of the large difference could be related to the different experimental and analytical methods used, others to the studies in

stratified water, with very low oxidation in samples with oxygen deficiencies (hypoxia) and high methane concentrations. In non-stratified water without oxygen limitations, oxidation is related to methane concentrations, with high methane concentrations stimulating the propagation of methanotrophic microbes. During the Macondo oil spill, methane concentrations increased dramatically, from a background of 10 to 20 nM (Valentine et al., 2010) up to 25 µM (a 1000-fold increase in concentration).

We specifically sought to identify methane oxidation rates for the Norwegian Continental Shelf and the Barents/Arctic Sea. Only one relevant study was identified, performing methane oxidation experiments with waters close to abandoned wells, and showing variable oxidation rates (Steinle et al., 2016). We describe two approaches for determination of oxidation rates. A conservative approach could be to use a low rate coefficient in water with low methane concentrations (e.g. $0.0015\,d^{-1}$), which may increase gradually by increased methane concentrations up to 0.2 (Kessler et al., 2011), describing the concentration-dependent effects of methane on the propagation of methanotrophic microbes (Fig 9, left panel).

The other approach was based on calculated oxidation rates at selected low methane concentrations (e.g. 20 nM or lower). The results of these studies are shown in Tables 2 and 3, and we see that there are very large variations in the results.

There are still large uncertainties related to the oxidation rates of methane in seawater. Since both selection of analytical methods and concentrations seem to be of significant importance for the oxidation rates, it could be of importance to perform a systematic comparison of these. Particularly at low methane concentrations (from 20 nM down to less than 10 nM), the rates seem to vary significantly, and some studies have even reported negative rates at these concentrations, i.e., methane concentrations rise instead of decrease during degradation studies (Uhlig et al., 2018).

2.6 Ocean acidification

Ocean acidification is the result of pH reductions in the ocean mainly caused by increased concentrations of dissolved CO_2 in the water. Acidification has several ecological impacts, and among the most deleterious are the impacts on shell-forming marine organisms such as plankton, benthic molluscs, echinoderms, and corals. Although the oceans cover 70 % of the earth's surface and can accumulate and buffer CO_2, increasing atmospheric CO_2-concentrations will reduce the buffering capacity of seawater as CO_2 accumulates (Pörtner, 2008; Doney et al., 2009). Future scenarios have suggested that the seawater pH in the world's oceans may decrease by more than 0.3 pH-units by the end of the century, if the global seawater surface temperatures increases by more than 2 °C in the same timeframe (Gattuso et al., 2015). Since the ocean is a CO_2 sink, a main source of oceanic CO_2 is accumulation from the atmosphere, including anthropogenic sources. Other sources are internal emissions from destabilized gas hydrates, CO_2 vents and hydrocarbon seeps. Gas hydrates and hydrocarbon seeps involve methane releases, with oxidation of methane to CO_2.

2.6.1 The Ocean carbonate system and implications

Dissolved CO_2 in the ocean is part of the carbonate systems, which is governed by a number of chemical reactions (Doney et al., 2009):

$$CO_{2(atmos)} \leftrightarrow CO_{2(aq)} + H_2O \leftrightarrow H_2CO_3 \leftrightarrow H^+ + HCO_3{}^- \leftrightarrow 2H^+ + CO_3{}^{2-} \tag{7}$$

At a seawater temperature of 8.1 °C, nearly 90% of the inorganic carbon is in the form of bicarbonate ($HCO_3{}^-$), 9 % as carbonate ($CO_3{}^{2-}$), while only 1 % is dissolved CO_2. Adding CO_2 to seawater, increases aqueous CO_2, bicarbonate and hydrogen ions (H+), and the latter lowers the pH. Carbonate ion concentrations declines because of increasing H+ concentrations, and the suggested 0.3-0-4 pH drop is equivalent to approximately a 150 % increase in H+ and 50% decrease in carbonate concentrations (Orr et al., 2005; Doney et al., 2009). Over the longer timescale, the ocean's abilities of absorb CO_2 depends on the extent of $CaCO_3$ dissolution in the water column and in the sediments:

$$CaCO_3 \leftrightarrow CO_3{}^{2-} + Ca2+ \tag{8}$$

Calcium carbonate is derived from shells and skeletons of e.g. plankton, corals, coral organisms and will be dissolved or become stored in shallow or deep-sea sediments (Feely et al., 2004; Berelson et al., 2007)). $CaCO_3$ formation and dissolution vary with saturation state, Ω, defined as the products of calcium and carbonate ion concentrations, where K_{sp} is the stoichiometric solubility constant:

$$\Omega = \frac{[Ca^{2+}][{CO_3}^{2-}]}{K_{sp}} \tag{9}$$

Shell and skeleton formation occurs when $\Omega > 1$, while dissolution appears when $\Omega < 1$ (Doney et al., 2009). The solubility product, K_{sp} depends in particular on the mineral phase, and $CaCO_3$ form aragonite is more soluble than calcite (Mucci, 1983), with different saturation states (Feely et al., 2010):

$$\Omega_{arg} = \frac{[Ca^{2+}][{CO_3}^{2-}]}{K_{sp,cal}} \tag{10}$$

$$\Omega_{arg} = \frac{[Ca^{2+}][{CO_3}^{2-}]}{K_{sp,arg}} \tag{11}$$

An example of the relations between salinity, oxygen, and aragonite saturation states were shown for inlet water from the Pacific Ocean to the Puget Sound in 2008. In summertime, seawater undersaturated with oxygen (less than 100 µmol/L) entered the deeper water in the Sound, with low pH (< 7.75), high salinity (> 31.0), and low aragonite saturation state ($\Omega_{arg} \approx 0.9$) (Feely et al., 2010). Another example is show from the Mauna Loa Ocean Station in the subtropical North Pacific Ocean (Doney et al., 2009). These data showed a correspondingly increased atmospheric and seawater increase in CO_2 records over a 17 year time period, and with reductions in pH, as well as calcite and aragonite saturation states over this period.

Based on projected average ocean temperature increases by either 1 °C or 2 °C, estimated CO_2 pressure (pCO_2) could increase from 380 µatm, to 560 µatm and 840 µatm, respectively. This could result in ocean pH reductions from 2001-levels of 8.05, to 7.91 and 7.76, respectively. The calcite and aragonite saturation (Ω_{cal} and Ω_{arg}) would then be reduced by 21% and 38% compared to 2001 saturation levels (Houghton et al., 2001; Guinotte and Fabry, 2008).

The altered carbonate chemistry caused by acidification may also affect primary production, for instance through coastal eutrophication. When nutrients are transported into coastal areas like estuaries, bacterial consumption of organic matter increases the CO_2-production, which favours primary production. However, if acidification reduces the calcite and aragonite saturation, this may negatively impact primary production and calcification of numerous marine organisms. Weakened primary production will further increase CO_2 accumulation and acidification (Borges and Gypens, 2010).

2.6.2 Sources

The main sources for increased CO_2 levels in the oceans are accumulation of atmospheric CO_2 from increased anthropogenic activities, increased organic input to the oceans and mineralization of this matter, emissions from CO_2 and hydrocarbon vents, and destabilized methane hydrates. Also biologically produced methane from organic matter may constitute a considerable source. While atmospheric accumulations and emissions from CO_2 vents may have direct impact on pH, emissions from methane sources will depend on the oxidation capacities and conversion rates to CO_2, before potentially affecting pH and acidification. It has been estimated the oceans have absorbed close to 50% of all anthropogenic CO_2 emissions to the atmosphere, amounting for more than 440 Gt CO_2 (Sabine et al., 2004). At present, the oceans take up about 2 of the 6 Gt C per annum from human activity (Pörtner, 2008).

Local high-emission CO_2 sources include CO_2 vents. One example is a shallow (2-3 m depth) Mediterranean volcanic CO_2 vent off Ischia island, close to Naples in Italy. The seawater is here acidified by gas comprising 90-95 % CO_2 and less than 1 % methane. The pH levels were reduced from 8.1-8.3 at reference stations (250-500 m away from the vents) to 7.8-6.6 close to the vents, while CO_2 concentrations increased

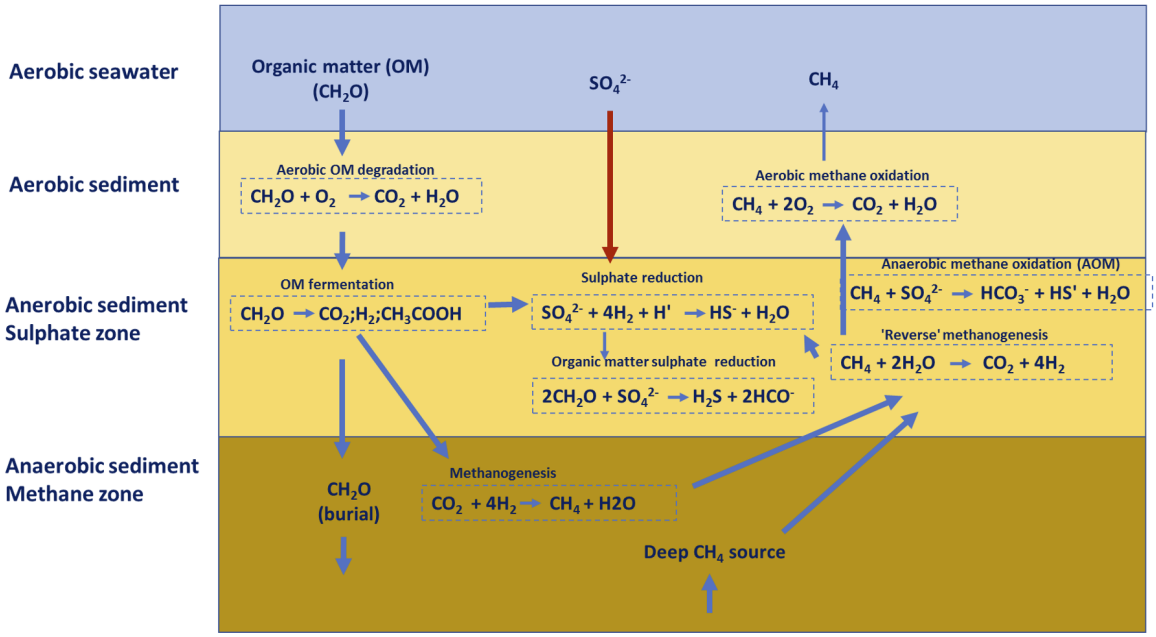

Figure 10: Biogenic methane formation in marine sediments, originating from combined processes of aerobic degradation, fermentation, sulphate reduction and methanogenesis, and involving sedimentation and burial of organic matter (CH_2O), sulphate from seawater, and thermogenic methane. The net emission of methane to seawater is based on methane formation and oxidation by anaerobic and aerobic oxidation of methane. Based on a similar figure by Pohlman et al. (2013).

from 4.6 µmol/L at the reference stations to 40 to 60 µmol/L close to the vent. The calcite and aragonite saturations stages were reduced from 9.2 and (Ω_{cal}) and 6.0 (Ω_{arg}) to 1.6 (Ω_{cal}) and 1.0 (Ω_{arg}) close to the vent (Hall-Spencer et al., 2008; Kerrison et al., 2011).

The current main methane source is probably hydrocarbon seeps. These are located mainly along tectonic plate boundaries (Judd, 2003).

Annual production of methane from freshwater and marine sources have been estimated to 85 Tg per year (Reeburgh, 2007), with marine seeps potentially accounting for approximately 20 Tg methane per year, i.e. 4 % of the global emissions, to the atmospheric methane (Etiope et al., 2008). Methane emissions from thermogenic sources are further supplemented by biogenic methanogenesis (Pohlman et al., 2013), as shown in Fig. 10.

Methane released to the water column may then be oxidized to CO_2 by aerobic processes. The oxidation rates may depend on methane concentrations, and oxidation rate coefficients may vary between 0.2 in areas with high methane concentrations and high abundances of methane-oxidizers and 0.001 in water with low concentration and low abundances of oxidizing microbes (Valentine et al., 2001; Kessler et al., 2011; Ruppel and Kessler, 2017). However, in deep water regions with low oxygen concentrations (hypoxia), CO_2 oxidation may be limited, if not formed by anaerobic processes in completely oxygen-free waters. Hypoxic seawater for the Caspian Sea has for instance similar hydrocarbon biodegradation rates under anoxic and oxic conditions (Miller et al., 2019).

A future potential methane source is destabilized methane hydrate. Methane is by far the most predominant gas within natural gas hydrates, and 1 m^3 of gas hydrate sequesters a maximum of 180 m^3 of methane as measured at standard temperature and pressure (Ruppel and Kessler, 2017). An approximate amount of 1800 Gt methane is expected to be trapped in gas hydrates in terrestrial (permafrost) and marine environments, with 99 % of these in marine sediments (expected range 500-10 000 Gt) (Boswell and Collett, 2011; Pohlman et al., 2011; Ruppel and Kessler, 2017). Higher ocean temperatures due to global warming will result in decreased hydrate stability and hereby increased methane emissions from gas hydrates. A model prediction assumed 50 % of the hydrate methane in the Arctic Ocean dissolved into the sediment porewater oxidized to CO_2, and changes

in seawater carbonate chemistry were calculated by adding the microbially produced CO_2 to the background dissolved inorganic carbon. This resulted in some areas of the Arctic Ocean having pH values decreased by up to 0.25 units within the next 100 years (Biastoch et al., 2011). This model implies that most of the methane remains in the ocean and is subject to oxidation processes and is not released to the atmosphere.

While deep sea methane releases to the water column is mostly consumed by methanotrophic microbes and oxidized to CO_2, methane generated in coastal shallow water is to a larger extent emitted to the air. Studies from the Belgian North Sea coast showed average flux intensities one order of magnitude higher than values characteristic of continental shelves and three orders of magnitude higher than values characteristic of the open ocean, and concentrations of up to 1128 nmol/L, with averages of 139 nmol/L, which was approximately 6 times higher than in the off-shore area (24 nmol/L) (Borges et al., 2016).

2.6.3 Eutrophication

Increased nutrient loading into estuaries causes the accumulation of algal biomass, and microbial degradation of this organic matter decreases oxygen levels and contributes towards hypoxia. Microbial degradation of organic matter may increase CO_2 production, and reduce pH in local environments. Studies from the northeast US coast have shown seawater with pH values from close to 8.0 to less than 7.4 during summer and fall months, respectively, concurrent with the decline in dissolved oxygen concentrations close to hypoxic levels, and with Ω_{arg} reaching levels close to 1 or less (Wallace et al., 2014).

As mentioned above, eutrophication may also negatively affect primary production and calcification of marine organisms by local acidification, weakened primary production causing further increase in CO_2 accumulation and acidification (Borges and Gypens, 2010).

2.6.4 Contribution of methane to potential ocean acidification

So what will the contribution of methane to ocean acidification be? To perform such estimates, we have not accounted for possible future scenarios with global warming and increased seawater temperatures, that may result in increased instability of marine gas hydrates, particularly in shallow arctic waters.

The upper layers of the oceans have low methane concentrations. Oceanic North Sea concentrations averaged 24 nmol/L (Borges et al., 2016) while typical CO_2 concentrations at the upper layers of normal seawater pH (pH=8) will be approximately 15 µmol/L (Garcia-Tigreros and Kessler, 2018). We further assume that the low methane concentrations will result in slow oxidation, e.g. with a rate coefficient of 0.001 because of low abundances of methanogenic microbes (Valentine et al., 2001; Kessler et al., 2011; Ruppel and Kessler, 2017). Since oceanic methane sources are mainly formed in deep-sea sediments, slow transport and dilution result in low concentrations reaching the upper water column. It is also expected that transport of methane as bubbles from the deeper ocean is limited, since most of the methane will dissolve and diffuse in the water column, or methane in the bubbles will be replaced by other gases like nitrogen and oxygen (McGinnis et al., 2006b; Vielstädte et al., 2015). We therefore assume that potential impact to upper water increased column acidification will come from absorbance of atmospheric CO_2 from anthropogenic sources.

In deep sea water near the sources of methane formation, and with poor water mixture, the situation will be different. This may be exemplified by a study from the US Atlantic coast. The Hudson Canyon is located on the northern Atlantic Margin and contain several gas seeps. From a release of methane at 700 m depth methane accumulated at a depth of 400-450 m, concurrent with increased CO_2 concentrations and reduced pH, with 150 nmol/L methane concentrations, and an estimated oxidation rate of 15 nmol/L/day. The CO_2 concentrations at the same depth were approximately 25 µmol/L (close to 1 µmol/L higher than in a reference area outside the canyon), and the pH was 7.9 (0.05 units lower than in the reference area). It was concluded from these results that in the area of elevated CH_4 concentrations and aerobic oxidation rates, aerobic CH_4 oxidation to CO_2 was only responsible for 0.3 ± 0.2 % of the observed change in dissolved inorganic carbon (DOC) (Garcia-Tigreros and Kessler, 2018). Based on data from methane seep areas, global estimates of potential methane-derived DOC flux was 0.2 to 20.3 Tg C/year (Pohlman et al., 2011), corresponding to 3×10^{-5} to 3×10^{-3}% of the marine DOC, estimated to be 0.60×10^{18} gC (Hedges et al., 1992).

High methane concentrations were also determined in coastal areas, from methanogenic activities in anoxic sediments, with methane concentrations of up to 1128 nmol/L, and with averages of 139 nmol/L (Borges et al., 2016). Assuming all of the methane is oxidized (no atmospheric emissions), and at fast oxidation dates at these high concentrations of 0.2 d^{-1} (Kessler et al., 2011), since methanotrophic microbes are continuously stimulated, this would result in an average formation of 25 nmol/L CO_2/day, corresponding to approximately 1 µg/L/day CO_2. Compared to modelled anthropogenic input of CO_2 in Atlantic seawater, expected to be higher than 40 µmol/L in the upper 100 m water column (Doney et al., 2009), these "hot-spot" areas contribute with insignificant levels of increased CO_2 concentrations (and potential contributions to ocean acidification). Even at the peak level of 1128 nmol/L CH_4 (Borges et al., 2016), a maximum of 200 µmol/L CO_2/day would be formed. Depending on local current conditions, the seawater with potential elevated CO_2 concentrations will be "diluted" by transport and mixing with deeper water.

2.6.5 Conclusion

Ocean acidification is caused by increased levels of CO_2 in the seawater, resulting in reduced ocean pH, with impacts on the carbonate system and the solubility of $CaCO_3$, which again is crucial for the calcification of numerous marine organisms, including phytoplankton. Sources of increased CO_2-input to the oceans include atmospheric CO_2 from anthropogenic sources, increased organic input to the oceans and mineralization of this matter, emissions from CO_2 and hydrocarbon vents, and destabilized methane hydrates. Methane is released to the ocean's water column from both hydrocarbon vents and biogenic processes, like methanogenesis in anoxic sediments and in hypoxic seawater. However, dissolved methane in sediment pore water and in the seawater column is oxidized by methanotrophic microbes, with assumed oxidation rates depending on the local methane concentrations. Compared to the CO_2 concentrations in seawater, as well as the estimated input of CO_2 from the atmosphere (including anthropogenic sources), current contribution of methane releases to the marine water column are anticipated to have small or insignificant impacts on potential ocean acidification, even at "hot-spot" areas in coastal areas. However, future predictions describing global warming and massive destabilization of methane hydrates, particularly in shallow Arctic areas, suggest impacts of released methane and subsequent oxidation processes to local or regional ocean acidification, although these processes are anticipated occur over long periods of time.

2.7 Modelling of Seeps

A numerical model developed for the fate of methane originating from seeps needs to account for the physical, chemical and biological processes associated with methane bubbles. When a bubble is released under water, it will rise vertically due to positive buoyancy as the density of gases are lower than ambient sea water. As a bubble rises, its size and shape evolves as it expands due to reduced pressure and exchanges mass due to dissolution of methane and uptake of gases from the water column Leifer and Judd (2002). This causes changes in bulk properties such as density, viscosity, interfacial tension, and in chemical properties such as solubility of different chemical components in the gas mixture in the bubble. The bubbles move in water from a combination of their terminal velocity and ambient currents. Terminal velocity depends on the size and shape of the bubbles, their density, viscosity and interfacial tension and the difference in density between the bubble and the ambient water. Thus, to predict an accurate fate behavior all these inter-related processes need to be taken into account. Existing models developed to simulate the fate of bubbles from methane seeps include those of Leifer and Patro (2002); McGinnis et al. (2006b); Jun (2018); Vielstädte et al. (2015).

Seeps release bubbles of varying size, but generally in a 1-10 mm size range. The initial bubble size plays an important role in the methane flux to the atmosphere DelSontro et al. (2015). When the release flow rates are low these bubbles have a tendency to rise as individual bubbles, but if the seep has a strong flow the bubbles may form a weak plume with upwelling ambient water. Wang et al. (2019) proposed a set of non-dimensional scaling parameters to describe plume spreading, liquid volume flux and kinematic momentum flux of weak bubble plumes. Models for seeps tend to focus on tracking individual bubbles rather than considering weak plumes, as the physical understanding of these weak plumes are limited. For example, Wang et al. (2020)

observed a seep field in the Gulf of Mexico with 1.0 ± 0.2 L/min of gas release with bubble sizes varying from 1-10 mm with an average size of 5.1 mm and showed that buoyancy induced upwelling was negligible for the bubble stream and a coherent plume is not formed confirming the laboratory observations presented in Wang et al. (2019).

The composition of seep bubbles is in general a mixture of natural gases with light hydrocarbons (methane, ethane, propane, butane) and smaller amounts of carbon dioxide, nitrogen, and occasionally hydrogen sulphide Kennicutt (2017); Leifer et al. (2000). However, the major component of the gas is methane. Bubble dissolution is driven by the difference between the solubility of different gas components in a bubble and the concentration of that component in water. The solubility of each gas component is different in a mixture than it is considered individually and depends on the mass fractions of the individual components in the mixture of gases in the bubble.

The rise velocity of bubbles varies according to their size and shape and bubble properties such as viscosity and interfacial tension. Bubbles can have spherical, spherical-cap or ellipsoidal shape depending on their size and this can vary from one size to the other as bubble expand/shrink as they rise and dissolve. The non-dimensional numbers Reynolds number ($Re = \frac{du_s}{\mu}$), Morton number ($M = \frac{g\mu^4(\Delta\rho)}{\rho\sigma^3}$), and Eötvös number ($E_o = \frac{g\Delta\rho d^2}{\sigma}$) based on Clift et al. (1978) are often used to define the the shape variations in the models Zheng and Yapa (2000); Jun (2018). In these formulations d is bubble diameter, μ and σ are the dynamic viscosity and the interfacial tension of water, and $\Delta\rho$ is the density difference of the ambient water and the bubble. Terminal velocities are calculated for these different size regimes. Additionally, the mass transfer coefficient across the bubble-water interface, which controls the dissolution, also varies with the size regime Clift et al. (1978); Johnson et al. (1969); Zheng and Yapa (2002); Jun (2018). The mass transfer coefficient accounts for the diffusive transport mechanism across the interface between the bubble and the ambient at which the mass transfer occurs Leifer and Patro (2002); Olsen et al. (2017). The mass transfer coefficient also dependents on the films of surfactants on the bubbles and these films act as barriers and hinder mass transfer. Surfactant free bubbles are refereed to as 'clean' and as 'dirty' otherwise. Surfactants on bubbles reduce the interfacial tension and cause resistance to motion at the interface leading to reduced mass transfer Clift et al. (1978). Hence in a system, defining the status of a bubble is important when mass transfer is estimated.

For individual bubbles Olsen et al. (2017, 2019) present a detailed investigation of mass transfer correlations for bubbles based on laboratory experiments and a field experiments carried out in Trondheimsfjord, Norway. They define that transition in mass transfer behavior between dirty and clean bubbles occur with sizes 3.5 and 4.5 mm. For bubbles smaller than 3.5 mm an expression for contaminated or dirty conditions are suggested to be used while for bubbles larger than 4.5 mm clean conditions are suggested. Olsen et al. (2017, 2019) study was carried out under non-hydrate formation conditions.

Mass transfer is hindered by the formation of gas hydrates on bubbles. Gas hydrates of methane may occur in high pressure and cold ambient conditions below about 600 m water depth of gas hydrate stability zone. Hydrate shells have been observed to form on methane bubbles in natural seeps in the field McGinnis et al. (2006b); Sauter et al. (2006); Wang et al. (2016, 2020) as well during both laboratory Warzinski et al. (2014) and field experimentsRehder et al. (2002, 2009). Models account for mass transfer reduction in bubbles from seeps due to hydrate formation by considering the transfer of bubble surface from mobile to immobile partially or completely McGinnis et al. (2006a); Rehder et al. (2002, 2009); Leifer and Patro (2002); Jun (2018); Wang et al. (2020).

2.8 Modelling evaporation of dissolved methane to the atmosphere

Methane dissolved in seawater can escape to the atmosphere through evaporation at the air-ocean boundary and is one of the two fate processes for methane in our model, the other being biodegradation. For methane dissolved in the lower water column, turbulent vertical mixing can bring it to the ocean surface. Gas exchange between the atmosphere and the ocean is a widely studied topic. For example, understanding how the ocean absorbs CO_2 from the atmosphere is an essential component in climate modelling. Mass transfer at the surface is a function of concentration on both sides of the boundary, and also depends in a non-trivial way on the sea

state, and thus the wind. The expression for the flux through the boundary (positive flux upwards) is

$$j = k\,(C_0 - C_{eq})\,, \tag{12}$$

where k is the mass transfer coefficient, and C_0 is the concentration of methane in the water near the surface. The concentration of methane in the atmosphere is represented by C_{eq}, which is the concentration of methane in seawater at equilibrium with the atmosphere (Happell et al., 1995). This equilibrium concentration can be calculated by Henry's law, taking the pressure, temperature and salinity into account.

The mass transfer coefficient, also called the mass transfer velocity due to having units of length per time, is given by (Garbe et al., 2014, p. 56)

$$k = u_* \beta \mathrm{Sc}^n, \tag{13}$$

where u_* is the friction velocity, $\mathrm{Sc} = \nu/D$ is the Schmidt number, giving the ratio of viscosity and diffusivity, and both β and n depend on conditions at the surface. In modelling mass transfer, we assume that the concentration of methane remains constant in the bulk near the surface, due to turbulent mixing, but that a gradient exists in a thin boundary layer on either side of the surface, where mass transfer is controlled by molecular diffusion. This is illustrated in Fig. 11, which shows concentration profiles and boundary layers near the interface. From Fick's law,

$$j = -D\frac{\partial C}{\partial z}, \tag{14}$$

where D is now the molecular diffusivity, we see that a constant gradient in concentration gives rise to a constant flux through the boundary layer. Assuming steady-state, this must be the case, as the concentration would otherwise grow or decay indefinitely at some point near the surface. Note that since the diffusivity is different in air and water, so is the concentration gradient.

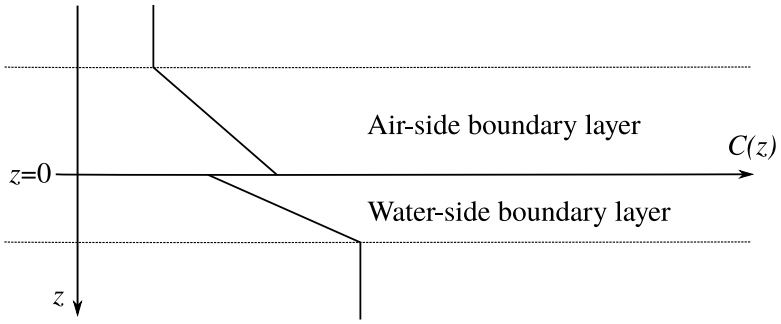

Figure 11: Illustration of concentration profiles and boundary layers near the air-water interface. The thickness on the boundary layers depend on conditions, but will be quite thin, less than 1 mm, with the water-side boundary layer being thinner than the air-side.

In our case, for methane dissolved in water, the water-side boundary layer will be the rate-limiting step, due to the viscosity and the lower molecular diffusivity in water Garbe et al. (2014). For this reason, we need only the water-side mass transfer coefficient. This coefficient depends on conditions at the surface, including wind, waves, rain, and potentially sea ice, as well as on the viscosity of sea water, and on the molecular diffusivity of methane in sea water (Garbe et al., 2014). Different parameterisations exist, taking different effects into account.

For the purposes of this study, we will use a relationship where the water-side transfer coefficient is related to the square of the wind speed (Wanninkhof, 1992). In particular, we use a parameterisation of the mass transfer coefficient given by (Najjar and Orr, 1998)

$$k_w = a(U^2 + v)\left(\frac{\mathrm{Sc}}{660}\right)^{-1/2}, \tag{15}$$

where $a \approx 0.336\,\mathrm{cm\,h^{-1}\,s^2\,m^{-2}}$ is an empirical parameter that has been fitted to data, U is the wind speed at 10 m height, and v is the variance of the wind speed. This relationship is widely used (Garbe et al., 2014, p. 97). The Schmidt number for methane in sea water depends, as mentioned, on the relationship between the kinematic viscosity of sea water, and the molecular diffusivity of dissolved methane in sea water:

$$\mathrm{Sc} = \frac{\nu}{D}. \tag{16}$$

3 Modelling study

In this section, we describe our chosen one-dimensional modelling approach for considering the transport of methane from seeps at the seafloor to the atmosphere. We assume that once methane has been released as a bubble from the seafloor, there are only two possible outcomes, or fates: Either, the methane reaches the atmosphere (via direct bubble transport, or dissolution and subsequent mass-transfer at the surface), or the methane dissolves, and then biodegrades to CO_2 and H_2O in the water column. The goal of the modelling study is to estimate the fraction of released methane that reaches the atmosphere, and the fraction that biodegrades, for a set of representative scenarios.

The modelling approach treats bubbles and dissolved methane as two separate steps, each with several processes that must be taken into account:

- For rising bubbles, calculate:
  - Rise speed.
  - Dissolution of methane into the water column, as a function of depth.
  - Dissolution of other gases (nitrogen and oxygen) from the water column into the bubble.
  - Fraction of released methane which is transported directly to the atmosphere with the bubbles.
- For the methane that dissolves from the rising bubbles, calculate:
  - Vertical mixing in the water column.
  - Biodegradation in the water column.
  - Escape to the atmosphere via mass transfer across the sea surface.

In the subsections that follow, we first present the model for rising bubbles, then we present the model for the fate of dissolved methane, followed by a presentation of the modelling results for some representative cases on the Norwegian Continental shelf.

3.1 Single Bubble Model

The Single Bubble Model (SBM) of the Texas A&M Oil-spill (outfall) Calculator (TAMOC) is used for the simulations of methane seeps in this study. The TAMOC modeling suite is an open source model[4] which simulates underwater petroleum liquid and/or gas releases as individual particles or multi-phase plumes, and predicts their behavior in three dimensional space in stratified, still and sheared environments (Socolofsky et al., 2015; Dissanayake et al., 2018; Gros et al., 2017; Jun, 2018). In this study, we use the SBM to track a single bubble in the water column, and its evolution while taking into account non-ideal behavior, mass and heat exchange with the ambient environment. The model estimates individual bubble properties, namely the density, shape, size, diameter, slip velocity, and interfacial tension, as well as the fugacity, solubility, and dynamic viscosity of methane at different ambient conditions while rising in the water column.

3.1.1 Governing equations

TAMOC uses the Peng-Robinson equation-of-state (Peng and Robinson, 1976) to predict the real-fluid behavior of different petroleum compounds under high pressure conditions following the procedure of Michelsen and Mollerup (2004) (see also McCain, 1990; Gros et al., 2016)) along with volume translation (Lin and Duan, 2005; Péneloux et al., 1982). This is used to estimate the dispersed-phase particle densities accurately and to simulate the behavior of live petroleum fluid mixtures (also defined as the equilibrium state of gas and liquid phase) (Socolofsky et al., 2015; Gros et al., 2016). Terminal velocities and mass transfer coefficients of the dispersed-phase particles are calculated based on Clift et al. (1978), Kumar and Hartland (1999) and Johnson et al. (1969). The aqueous solubility of each component in a dispersed-phase particle is calculated using the modified Henry's law and mixture fugacities (King and Danckwerts, 1969; Krichevsky and Kasarnovsky, 1935; Zheng and Yapa, 2002; McGinnis et al., 2006a; Gros et al., 2016).

[4]The model is available from `github.com/socolofs/tamoc`

The mass transfer rate of a chemical component is taken to be a function of the mass transfer coefficient, β, as mentioned above and the solubility, C, of the chemical component, calculated as follows:

$$\frac{\mathrm{d}m}{\mathrm{d}t} = -A\beta(C - C_a)\,, \tag{17}$$

where $\mathrm{d}m/\mathrm{d}t$ is the rate of dissolution of the component, C_a is the ambient concentration of the dissolving component, and A is the surface area of the particle.

The heat exchange of a bubble with the surroundings is calculated as follows.

$$\frac{\mathrm{d}T_p}{\mathrm{d}t} = -A\beta_T C_p(T_p - T_a)\,, \tag{18}$$

where $\mathrm{d}T_p/\mathrm{d}t$ is the rate of change in particle temperature, β_T is the heat transfer coefficient; C_p is the heat capacity of the particle, and T_p and T_a are the particle and ambient temperatures, respectively. Advection of bubbles in three-dimensional space takes the ambient velocity and bubble terminal velocity, w_s, into account and can be stated as

$$\frac{\mathrm{d}x}{\mathrm{d}t} = u_a \tag{19a}$$

$$\frac{\mathrm{d}y}{\mathrm{d}t} = v_a \tag{19b}$$

$$\frac{\mathrm{d}z}{\mathrm{d}t} = w_a + w_s, \tag{19c}$$

where x, y are the horizontal position components, and z is the depth in the water column, and u_a, v_a and w_a are the ambient current velocities in the x, y and z directions. For the purposes of this study, we consider vertical transport only, and we assume that the vertical current component is zero.

The equations above, together with a model for the bubble rise velocity, make up a set of coupled ordinary differential equations, which must be solved to find how the position and composition of a bubble changes with time. In TAMOC, these equations are solved with `integrate.ode` from the SciPy library (Virtanen et al., 2020), specifically using the VODE linear multistep integrator with a backwards differentiation formula (Brown et al., 1989), which is an implicit method suited for stiff equations.

3.1.2 Model validation studies

Jun (2018) presents extensive validation of the SBM from TAMOC with experimental data for individual bubble and droplet properties and its application to natural hydrocarbon seeps and methane bubble experiments in high pressure environment (Gros et al., 2020). Further, the TAMOC SBM has been used to simulate natural seeps in the Gulf of Mexico (Mahdi et al., 2020; Leonte et al., 2018; Römer et al., 2019) and CO_2 seeps in Panarea Island (Gros et al., 2019).

3.2 Diffusion-reaction model

With the SMB (see Section 3.1), we calculate the path of individual bubbles to the surface, under different initial and ambient conditions. The output from this model includes the fraction of methane that is transported directly to the surface with the bubble, and the fraction that is dissolved, as a function of depth. In order to calculate how much of the dissolved methane eventually makes it into the atmosphere, we model the fate of the dissolved methane with the diffusion-reaction equation. This models escape through the surface to the atmosphere, and biodegradation, as two competing fate processes for the dissolved methane. The depth and the ambient conditions will influence the fraction that goes to the atmosphere, and the fraction that biodegrades.

The diffusion-reaction equation is a partial differential equation that describes how the concentration of some substance, $C(z,t)$, changes with time and position (see, e.g., Hundsdorfer and Verwer (2003)). In one

spatial dimension, it reads

$$\frac{\partial C(z,t)}{\partial t} = \frac{\partial}{\partial z}\left(K(z)\frac{\partial C(z,t)}{\partial z}\right) + R(z), \tag{20}$$

where $K(z)$ is the diffusivity, and $R(z)$ is a reaction term. In our case, $C(z,t)$ describes the concentration of methane at different depths and times, $K(z)$ is the eddy diffusivity describing turbulent mixing in the ocean, and the reaction term $R(z)$ describes the biodegradation of methane. The diffusivity, $K(z)$, will depend on ambient conditions, and must be chosen in a suitable way for each location, as well as the relevant season. The initial conditions for the diffusion-reaction model consist of concentration profiles of dissolved methane, obtained from the single bubble model.

3.2.1 Eddy diffusivity

The eddy diffusivity, $K(z)$ in Eq. (20), represents vertical mixing caused by turbulent eddies in the ocean. While the eddy diffusivity is related to the dissipation of turbulent kinetic energy, it is not a directly measurable physical quantity, but rather a parameterisation of the combined effect of turbulent stirring and molecular diffusion along concentration gradients (see, e.g., (Thorpe, 2005, pp. 19–23)). Available techniques for obtaining estimates of eddy diffusivity include different experimental approaches combined with theoretical expressions (Thorpe, 2005, pp. 180–183), as well as pure analytical and numerical models taking ambient conditions into account in different ways (Burchard and Bolding, 2001; Umlauf et al., 2003).

Values of the vertical eddy diffusivity span several orders of magnitude. In the deep ocean (deeper than about 1500 m), Walter Munk obtained an average value of $1.3 \times 10^{-4}\,\mathrm{m}^2/\mathrm{s}$ based on an elegant argument related to maintaining observed steady-state temperature profiles (Munk, 1966; Thorpe, 2005, p. 38). Similar values have been found in, e.g., long-term tracer diffusion studies (Rye et al., 2012). Near the surface or the seafloor, or in shallower waters, vertical mixing can be far higher. The eddy diffusivity is driven by sources of kinetic energy, such as breaking waves, wind stress, and friction against the seafloor. During winter, cooling surface water may become denser than the underlying water, leading to overturning. Conversely, heating of surface waters in summer gives rise to a stable stratification, which may inhibit vertical mixing.

Density profiles inferred from CTD (conductivity, temperature, depth) measurements do not directly give quantitative information about the eddy diffusivity, but can give qualitative information about the degree to which the water column is mixed. In Fig. 12, some examples of density profiles are shown. These profiles are measured at different positions as shown in the left panel of Fig. 12, and taken during the months of February and August in the years between 1995 and 2016. They illustrate that the layer of constant density near the surface, called the surface mixed layer, can be a few meters, or some tens of meters, but we can also have a situation where the density is nearly constant down to 200 m or more.

3.2.2 Reaction term for biodegradation

We model biodegradation of dissolved methane as a first-order decay process,

$$\frac{\mathrm{d}Q}{\mathrm{d}t} = -kQ \tag{21}$$

where Q is the amount of dissolved methane, and k is a rate parameter. The solution to Eq. (21) is that the amount of dissolved methane will decay exponentially,

$$Q(t) = Q_0 \mathrm{e}^{-kt}. \tag{22}$$

As seen in Section 2.5.3, published values of the degradation rate parameter vary across a very wide range, meaning there is very large uncertainty in how to choose this parameter. The degradation rate will almost certainly depend in a non-trivial way on methane concentration, and also (but to a lesser degree) on other local factors as well as temperature.

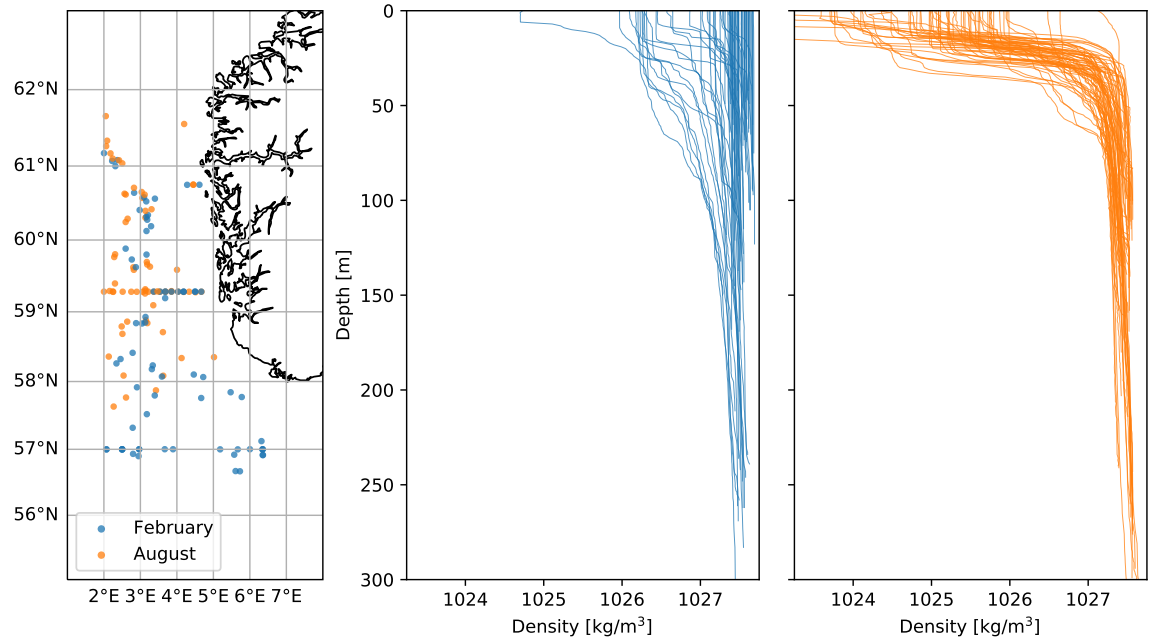

Figure 12: Density inferred from CTD profile data. These density profiles were taken either in the month of February (blue) or in August (yellow) at different positions, and in different years betwene 1995 and 2016. The purpose is to illustrate that the thickness of the surface mixed layer can be just a few meters, or there can be nearly constant density for 200 meters or more. This has a large impact on the vertical mixing. The CTD profiles have been downloaded from the Norwegian Marine Data Center (`https://nmdc.no/`) operated by the Institute of Marine Research, and density was calculated according to Millero and Poisson (1981).

3.2.3 Boundary conditions

The boundary conditions of the diffusion-reaction model describe what happens to dissolved methane at the boundaries of the domain, i.e., at the seafloor and at the surface. At the seafloor, we simply assume a no-flux boundary condition in the diffusion model. At the surface, the flux of methane is determined by mass transfer. As previously mentioned, the expression for the flux through the boundary is

$$j = k_w \left(C - C_{eq}\right), \tag{23}$$

where C is the concentration of dissolved methane in the water near the surface, C_{eq} is the concentration of dissolved methane corresponding to equilibrium with the methane concentration in the atmosphere, and k_w is the water-sided transfer velocity. For our case, the air-sided transfer is not the rate-limiting step, therefore we can ignore the air-sided transfer velocity and approximate k_w as shown in Eq. (15) (see Section 2.8 for details).

To model the flux across the air-sea interface, we use a Neumann boundary condition that specifies the flux. The diffusive flux is given by

$$j_D = -K(z)\frac{\partial C(z,t)}{\partial z} \tag{24}$$

and hence we can use the prescribed flux to determine the value of the derivative at the boundary. See below and Appendix A for further details.

3.2.4 Numerical solution method

We solve the diffusion-reaction equation numerically using a finite difference scheme. The spatial discretisation uses a central second-order finite difference. First, we multiply out the right-hand side of Eq. (20), to obtain

$$\frac{\partial C(z,t)}{\partial t} = \left(\frac{\partial}{\partial z}K(z)\right)\left(\frac{\partial C(z,t)}{\partial z}\right) + K(z)\frac{\partial^2 C(z,t)}{\partial z^2} + R(z), \tag{25}$$

We then discretize the z-axis to a grid of points, $z_n = z_0 + n\Delta z$, and approximate the spatial derivatives with central finite differences, obtaining the following semi-discretised equation:

$$\begin{aligned}\frac{\partial C(z,t)}{\partial t} \approx \frac{1}{\Delta z^2}\Bigg[&\frac{1}{4}\big(K(z_{n+1}) - K(z_{n-1})\big)\big(C(z_{n+1},t) - C(z_{n-1},t)\big) \\ &+ K(z_n)\big(C(z_{n+1},t) - 2C(z_n,t) + C(z_{n-1},t)\big)\Bigg] + R(z_n).\end{aligned} \tag{26}$$

At the sea-floor boundary, we prescribe a no-flux boundary condition, using the finite-difference approximation of Eq. (24) to obtain

$$j_D(z_0) = 0 \approx -K(z_0)\frac{C(z_1,t) - C(z_{-1},t)}{2\Delta z} \Rightarrow C(z_1,t) = C(z_{-1},t), \tag{27}$$

which we can use to eliminate the "ghost point" z_{-1}, which is outside the boundary. Similarly, at the surface, we obtain

$$j_D(z_N) = k_w(C(z_N) - C_{eq}) \approx -K(z_N)\frac{C(z_{N+1},t) - C(z_{N-1},t)}{2\Delta z} \tag{28a}$$

$$\Rightarrow C(z_{N+1},t) = C(z_{N-1},t) - \frac{2\Delta z}{K(z_N)}k_w(C(z_N) - C_{eq}), \tag{28b}$$

again allowing us to eliminate the point z_{N+1}, which is outside the boundary.

To solve Eq. (26) numerically, we introduce a timestep Δt, such that $t_n = t_0 + n\Delta t$, and we discretise the equation using the implicit trapezoid method, also known as the Crank-Nicolson method, which is second-order accurate in time, and has unconditional stability. With this method, obtain

$$C(z_n, t_{n+1}) = C(z_n, t_n) + \frac{\Delta t}{2}\big[F(t_n) + F(t_{n+1})\big], \tag{29}$$

where $F(t_n)$ is the right-hand side of Eq. (26), with boundary conditions as described by Eqs. (27) and (28a). Writing everything out, we obtain a linear system of equations that must be solved at each timestep. The full matrix expression is shown in Appendix A.

In the implementation used to carry out the simulations presented in this report, we made use of the features for sparse linear algebra found in `scipy.sparse`. Specifically, the tri-diagonal matrices (see Eq. (36)) are stored as `scipy.sparse.dia_matrix`, and the linear system of equations is solved with the bi-conjugate gradient stabilised method (BiCGStab) using `scipy.sparse.linalg.bicgstab`, automatically switching to the generalised minimal residual (GMRES) method using `scipy.sparse.linalg.gmres` for those rare occasions where BiCGStab fails to converge.

3.3 Selected scenarios and parameter estimation

We have selected three different locations on the Norwegian Continental Shelf as case studies. In what follows, we first describe how we obtained the different input parameters to the modelling, before we go through one set of results for each of the three cases in detail. Next, we consider variations of some of the input parameters, in order to highlight what are the major uncertainties in the predictions. An overview of the simulation parameters is given in Table 4.

3.3.1 Location, depth, bubble size and ambient conditions

The three different locations were chosen based on their depths, which are 50 m, 120 m, and 300 m. The intention is to highlight how the fate of the methane released in a seep differs from shallow to deeper waters, and depths ranging from 50 m to 300 m are typical for the Norwegian Continental Shelf. The initial bubble size, 5 mm, was selected from among a range of observation-based values found in the literature. Temperature and salinity profiles, which are used to model dissolution in the single bubble model, were taken from NOAA's World Ocean Atlas, using data for the winter or summer seasons. Dissolved oxygen profiles, which determine how much oxygen will enter the bubble from the water column, were also taken from the World Ocean Atlas. Dissolved nitrogen is not available in the World Ocean Atlas. This has been estimated by assuming that the water column is in equilibrium with the atmosphere. Taking pressure into account, this gives a profile of dissolved nitrogen that depends on depth.

3.3.2 Biodegradation rates

Biodegradation rates are perhaps the largest source of uncertainty in the modelling. From the data presented in Fig. 5, we see that half-lives for methane oxidation presented in the literature span across six orders of magnitude, from about one day to about one million days, with the majority of the data found in the range from 10 days to 10 000 days. We present some results with a relatively low value of 100 days, and later use a half-life of 500 days which may be more representative for water volumes with low methane concentration. We will also discuss the estimation of biodegradation rates in more detail later.

3.3.3 Eddy diffusivity profiles

Eddy diffusivity is among the more difficult parameters to estimate. As discussed in Section 3.2.1, this is not a property that can be measured directly, but rather a parameterisation of the effective vertical mixing caused by turbulence in the water column. Vertical mixing will change with the time of year, but also with local conditions, wind, etc. Due to the large uncertainty, and the limited scope of this study, we have chosen to use some simple, idealised profiles.

During summer, a stable density stratification will typically form, where the upper part of the water column is warmer and may have lower salinity than the lower part. The transition between the upper and lower water column, where the density gradient is largest, is called the pycnocline. This can be seen in the right panel of Fig. 12, showing density profiles at different locations taken during the month of August. Qualitatively, it is well known that vertical mixing across the pycnocline is inhibited by the stable stratification, due to the energy required to lift the underlaying dense waters (Thorpe, 2005, pp 8–12). Vertical mixing above the pycnocline (in the surface mixed layer) and below the pycnocline may be much higher.

In winter, the water column tends to be more uniform, which allows relatively unhindered vertical mixing throughout more of the water column. In the middle panel of Fig. 12, density profiles taken in the month of February are shown. Some of these show virtually constant density to depths of 100 m or more, indicating that the water column is well mixed. For a further illustrative example of the difference between summer and winter conditions, see Bolding et al. (2002, Fig. 4), which shows modelled temperature profiles across one year for a location in the Northern North Sea, supported by measurements.

These qualitative differences between the mixing conditions during summer and winter are relevant to the question of the fate of dissolved methane, as mentioned by, e.g., von Deimling et al. (2011):

> *"Modeling indicates that less than ∼4% of the gas initially released at the seafloor is transported via bubbles into the mixed layer and, ultimately, to the atmosphere. However, because of the strong seasonality of mixing in the North Sea, this flux is expected to increase as mixing increases, and almost all of the methane released at the seafloor could be transferred into the atmosphere in the stormy fall and winter time."*
>
> Quoted from the abstract of von Deimling et al. (2011)

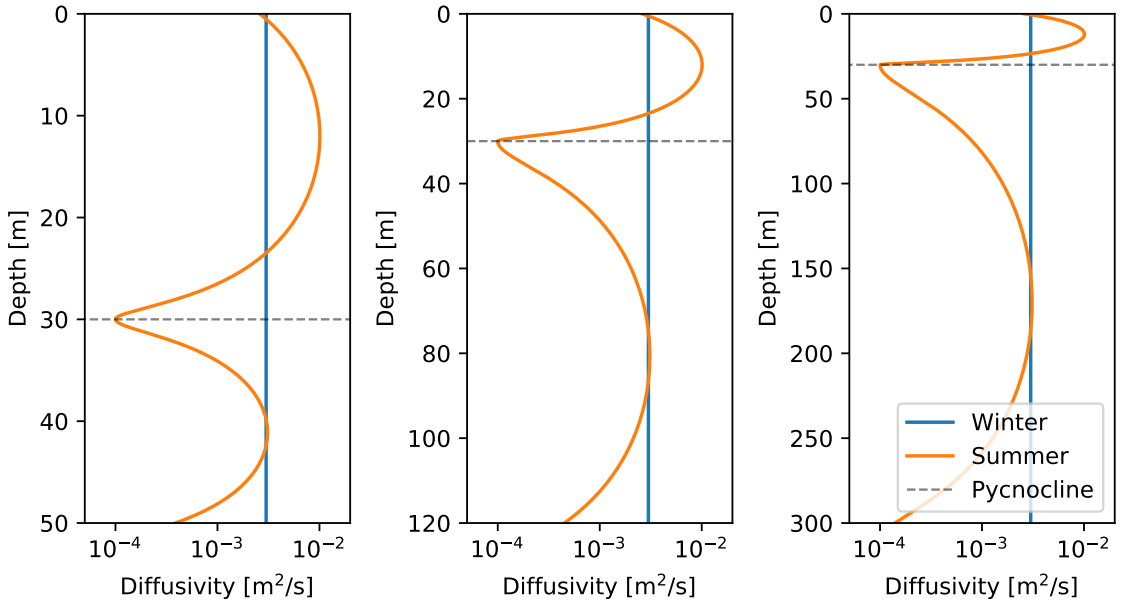

Figure 13: Diffusivity profiles designed to investigate the difference between summer and winter mixing conditions.

To investigate this question, we have chosen two different diffusivity profiles, which are qualitatively meant to represent the different mixing conditions during summer and winter. For summer conditions, we have created a variable diffusivity profile which is qualitatively based on Bolding et al. (2002, Fig. 6). It features a minimum in the diffusivity of $10^{-4}\,\mathrm{m}^2/\mathrm{s}$ at a depth of 30 m, consistent with a pycnocline at this depth, and has maxima in the diffusivity in the interior of the mixed layers, as well as diffusivity that decreases towards the surface and the seafloor, as expected from the law of the wall.

For winter conditions, we have simply assumed a constant diffusivity of $3 \times 10^{-3}\,\mathrm{m}^2/\mathrm{s}$, which is equal to the maximum used below the pycnocline for the summer conditions. The constant value is meant to represent a water column that has almost constant density throughout.

We stress that these diffusivity profiles are only simplifications that are meant to capture some of the differences between summer and winter conditions. In reality, the intensity of the vertical mixing will change continuously throughout the year, driven by factors such as the wind, tides, and air temperature. The depth of the pycnocline will also change throughout the summer season.

3.3.4 Mass transfer coefficient

Finally, we need to estimate the mass transfer coefficient for the transport of methane across the interface between the ocean and the atmosphere. This has been calculated from

$$k_w = a(U^2 + v)\left(\frac{\mathrm{Sc}}{660}\right)^{-1/2}. \tag{30}$$

See Section 2.8 for details. Wind speed squared, U^2, and variance, v, were assumed to be constant, and obtained by taking averages over one year of observations of wind speed from the platforms at Heimdal and Gullfaks C. The average wind speed squared was $\langle U^2 \rangle = 81\,\mathrm{m}^2/\mathrm{s}^2$, and the variance was $v = 18\,\mathrm{m}^2/\mathrm{s}^2$. The wind data used are shown in Fig. 14. We use a Schmidt number of 677 for methane in seawater (Wanninkhof et al., 2009), which in turn gives a mass transfer coefficient of $k_w = 9.2 \times 10^{-5}\,\mathrm{m/s}$.

For the flux through the surface, we also need the air-side concentration of methane. However, assuming that methane concentration in the water is far higher than the equilibrium concentration with the atmosphere,

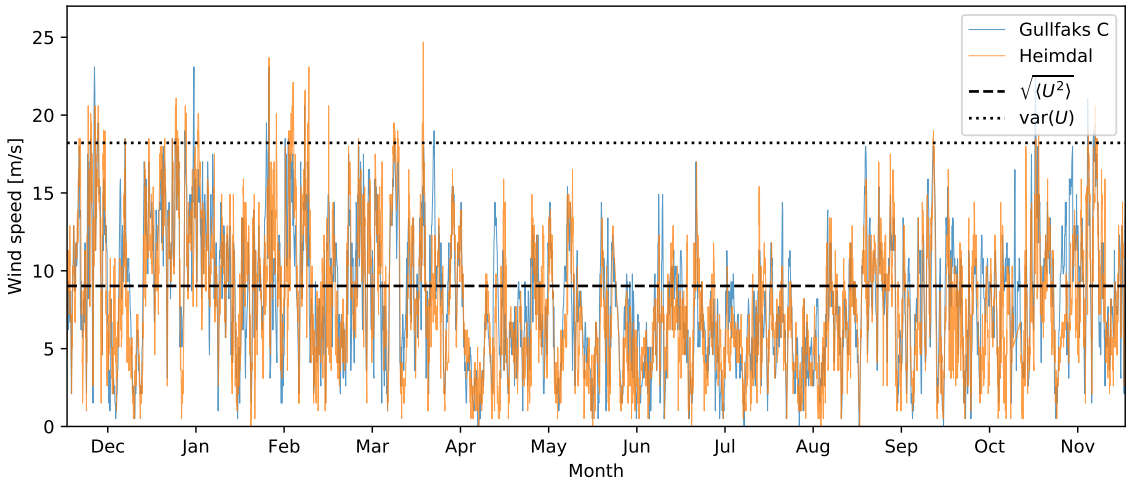

Figure 14: One year of wind speed measurements, from December 1, 2019 to December 1, 2020, at the platforms Heimdal and Gullfaks C. The data were downloaded from Norsk Klimaservicesenter (`https://klimaservicesenter.no/observations/`).

we set $C_{eq} = 0$. This means that we assume the concentration of methane in the air is too low to influence the mass transfer.

3.3.5 Overview of case studies

Table 4 contains an overview of the parameters we have chosen for the set of three case studies.

Table 4: Input parameters for example simulations. †The dissolved nitrogen profiles have been estimated by assuming the water column nitrogen concentration to be en equilibrium with the atmosphere. ‡The eddy diffusivities are idealised profiles, as shown in Fig. 13.

	Case 1	Case 2	Case 3
Position (lat, lon)	(56.5 N, 4.5 E)	(59.5 N, 2.5 E)	(64.5 N, 6.5 E)
Water depth	50 m	120 m	300 m
Initial bubble size	5 mm	5 mm	5 mm
Temperature and salinity	World ocean atlas	World ocean atlas	World ocean atlas
Dissolved oxygen	World ocean atlas	World ocean atlas	World ocean atlas
Dissolved nitrogen†	Equilibrium	Equilibrium	Equilibrium
Eddy diffusivity‡	Details in text	Details in text	Details in text
Biodegradation half-life	100 days	100 days	100 days
Mass transfer coefficient	0.0091 m/s	0.0091 m/s	0.0091 m/s

3.4 Results

Here, we present the results of the modelling study. First, we present and describe in detail results for all three cases, both winter and summer seasons. We show both how the concentration of dissolved methane in the water column develops, as well as the mass balance showing the fractions of the released methane that biodegrades, and ends up in the atmosphere. This is meant to introduce the model results, and explain the different features of summer and winter mixing conditions.

3.4.1 Example results for all three cases and both seasons

In Figs. 15 and 15, we show model results for all three cases, and for summer and winter mixing conditions, as defined by the diffusivity profiles shown in Fig. 13.

Comparing first the three cases under summer mixing conditions (Fig. 15), the first thing to note is that only in Case 1 (release depth 50 m) is there any direct bubble transport of methane to the surface. Approximately 10% of the methane is brought to the surface with the bubble in this case, while the remaining 90% dissolves in the water column, giving rise to the initial concentration labeled "0 days".

For Case 2, which is in a water depth of 120 m, essentially all the methane has dissolved from the bubble by the time the bubble reaches a depth of 40 m. Hence, none of the methane is directly transported to the atmosphere, and the bulk of the methane is dissolved at a depth greater than 80 m. In case 3, which is even deeper at 300 m, all the methane dissolves below about 220 m depth.

The distribution of dissolved methane, with larger concentration at greater depths, is due to a combination of effects. First, as the bubble rises, dissolved nitrogen and oxygen from the water column will dissolve into the bubble, thus diluting the methane in the bubble. Second, the bubble expands as the pressure drops, and hence it rises faster, dissolving less methane per meter of the water column it passes through.

The next thing to note is that we can clearly see the effect of the reduced mixing at the pycnocline (at 30 m depth) for all three cases, although it is most pronounced for Case 2. Below the pycnocline, the dissolved methane quickly becomes evenly distributed, while the slow passage across the pycnocline is the limiting step that controls the rate at which the methane reaches the atmosphere.

To better understand the difference between the three cases, we consider the right-hand column in Fig. 15 which shows how the mass balance develops in time. For Case 1, we see that about 9% has been directly transported to the surface, and in short order, the majority of the rest of the methane also reaches the atmosphere through mass transfer at the surface (evaporation). For Cases 2 and 3, we see that all the methane is initially dissolved, and we also see that it takes a few days before the methane starts to escape to the surface in Case 2, and even longer in Case 3. This is because the methane is initially dissolved at some depth, and before it can escape, it must reach the surface through vertical mixing. We also observe that a larger fraction of methane biodegrades in Cases 2 and 3, although the biodegradation half-life is 100 days in all three cases. This is simply because the escape to the atmosphere takes longer in the deeper cases, thus giving methane degrading bacteria more time to work on the dissolved methane.

Moving on to the winter mixing conditions, in Fig. 16, we again observe that only in Case 1 is there any direct bubble transport to the surface. Next, we note that the absence of a pycnocline means that the dissolved methane is mixed throughout the water column faster than for the summer mixing conditions. Hence, there is also more escape to the atmosphere in these cases, as expected. Comparing for example Case 2, for summer and winter conditions, we see that there is substantially less biodegradation during winter. As the biodegradation half-life is still 100 days, this is solely due to dissolved methane reaching the surface and escaping to the atmosphere at a faster rate, due to the lack of a minimum in the diffusivity at the pycnocline.

3.4.2 Varying input parameters

From the results thus far presented, we see that under the given assumptions, the fraction of methane that eventually makes it into the atmosphere is very much dependent on the release depth. However, the depth dependence is not necessarily the same for other input parameters. Of the input parameters presented in Table 4, the biodegradation half-life is almost certainly the most difficult to estimate, followed by the eddy diffusivity, and the balance between these two determines the fate of the methane to a large degree. In order to explore the dependency on these parameters, we present below some variations on the above scenarios.

The biodegradation rate we have considered so far, equivalent to a half-life of 100 days, is high compared to relevant rates found from the literature. As described in Section 2.5.3, reported rates in the literature vary by many orders of magnitude, with the majority of the data indicating half-lives between 10 days and 10 000 days. The half-life of 100 days considered so far is in the lower half of this range. We now consider a value of 500 days, which is roughly consistent with some other relevant studies such as Valentine et al. (2001) (half-life of

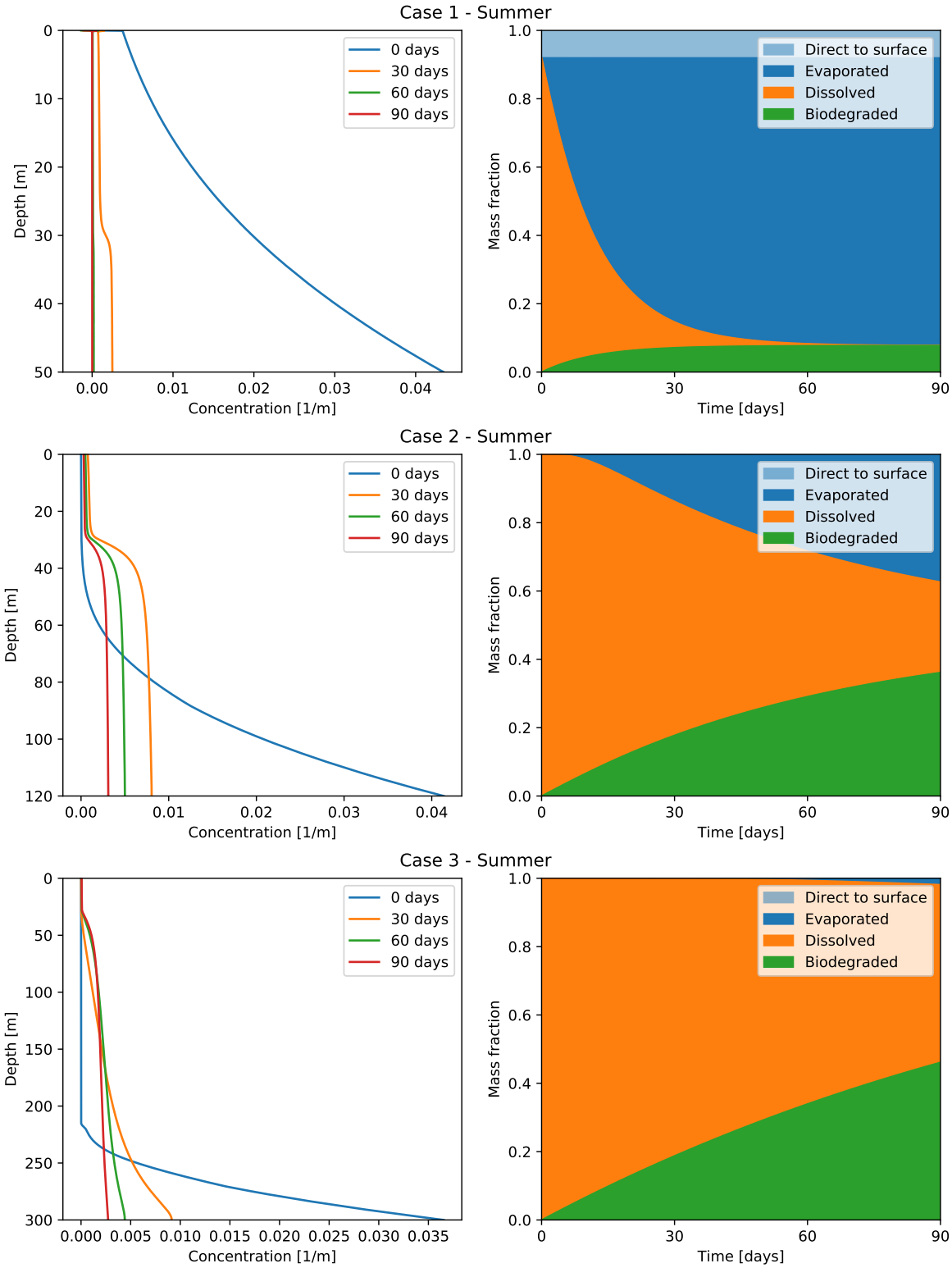

Figure 15: Modelling results for all three cases, for summer mixing conditions (see diffusivity profiles in Fig. 13). The plots in the left column show the concentration of dissolved methane at different times, and the plots in the right column show how the mass balance develops over time.

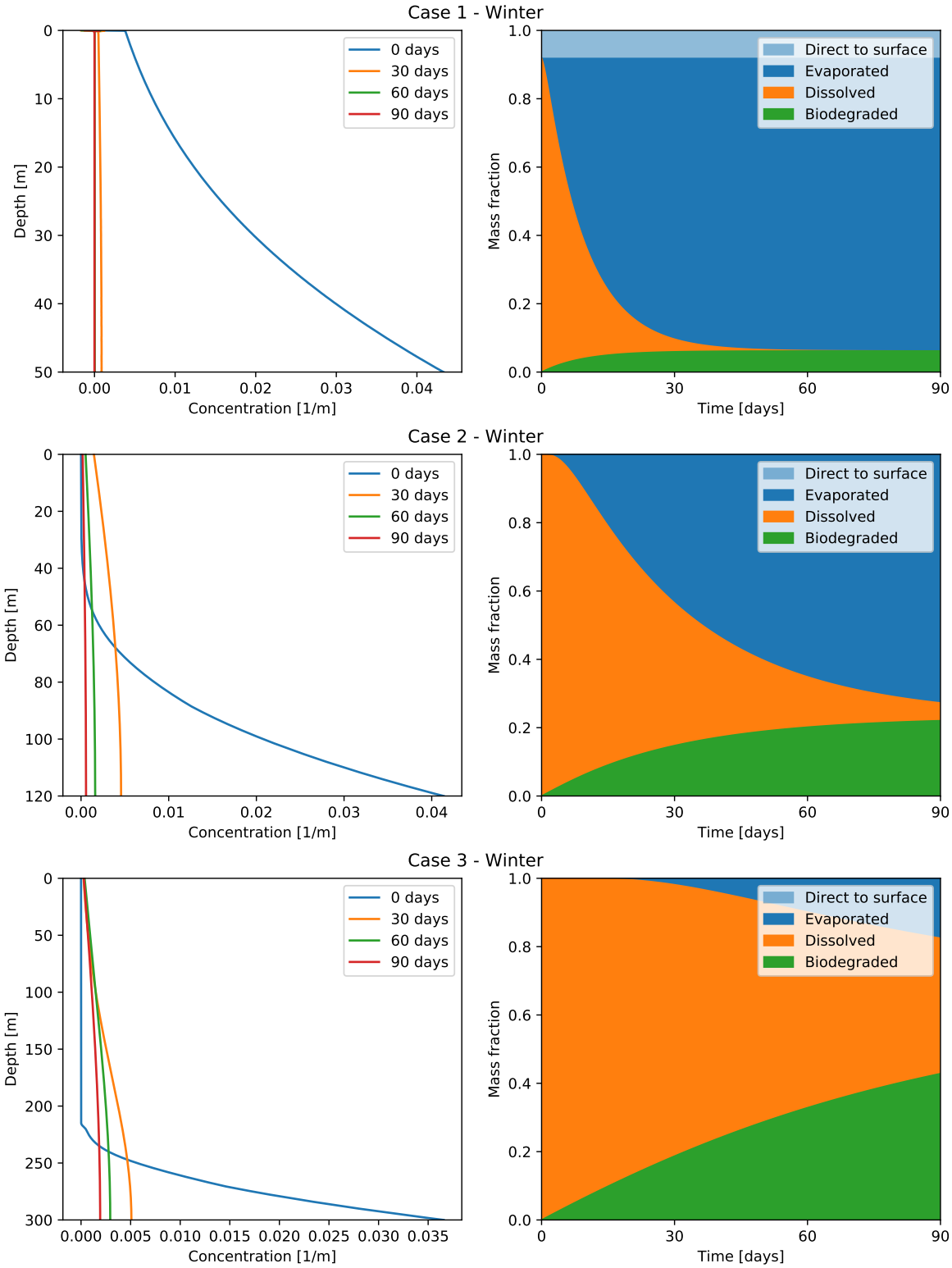

Figure 16: Modelling results for all three cases in winter mixing conditions (see diffusivity profiles in Fig. 13). The plots in the left column show the concentration of dissolved methane at different times, and the plots in the right column show how the mass balance develops over time.

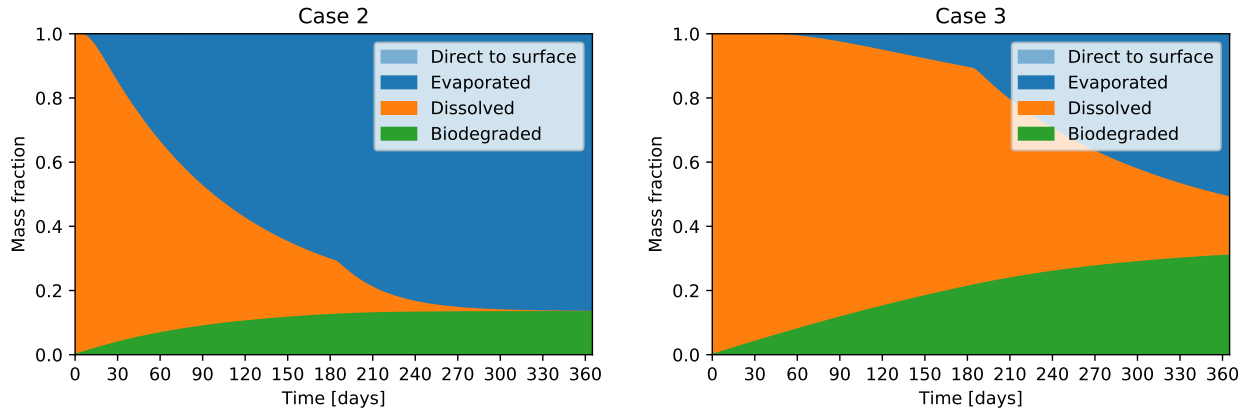

Figure 17: Mass balance as a function of time, for Cases 2 (120 m release depth) and 3 (300 meter release depth). The simulations have been run first for 182 days with vertical mixing corresponding to summer conditions, and then for 183 days with winter conditions. See Fig. 13 for the diffusivity profiles. In both cases, the biodegradation half-life was 500 days.

365 days), Kessler et al. (2011) (half-life of 462 days), and Ruppel and Kessler (2017) (half-life of 693 days).

Due to the slower biodegradation rate, it is necessary to run the simulations for longer time periods to see the difference in behaviour. Therefore, we also have to switch between summer and winter conditions. As an illustrative example, we have chosen to start simulations at the start of "summer", run for 182 days, then switch to winter mixing conditions, and run for another 183 days, making up one year.

In Fig. 17, we present the results for Cases 2 and 3. Case 1 has been omitted, since the almost all the methane escapes to the atmosphere during the first 30 days in this Case. We observe that even for Case 3 (Fig. 17, right panel), where the bubbles are released at a depth of 300 m, a little over half of the methane will reach the atmosphere after about one year. The release is slow at first, during summer mixing conditions, due to the low mixing across the pycnocline (see Fig. 13). However, when we transition to wintertime mixing conditions, with a high, uniform diffusivity throughout the water column, the methane starts escaping to the atmosphere at a higher rate.

3.4.3 Parameter study for biodegradation rate

The results presented in Fig. 17 suggests that methane released during summer may reach the atmosphere during winter, when the water column is mixed more strongly. However, this does of course depend on the biodegradation rate. If the lifetime of the methane in the water column is much less than half a year, then whatever methane is released during summer may largely be oxidised into CO_2 in the water column before it has time to reach the atmosphere.

To investigate this, we have conducted a parameter study where we have run simulations for a range of biodegradation half-lives from 10 days to 1000 days. For each case, and for each value of the half-life, we ran 4 simulations of one year each, starting at different times of the year. Winter and summer mixing conditions were applied for half a year each, as described in Section 3.4.2. The mass balances at the end of each of the 4 simulations were then averaged.

The results are shown in Fig. 18. For Case 1, where the bubbles are released at 50 m depth, we find that essentially all the methane will reach the atmosphere, unless the biodegradation half-life is extremely short. For Case 2, we find that a significant fraction of the methane may biodegrade if the half-life is 100 days or less. For Case 3, at 300 m release depth, we find that more than half of the methane will biodegrade, unless the biodegradation rate is longer than about 200 days. We note that these results depend on the assumptions of vertical mixing as outlined in Section 3.3.3.

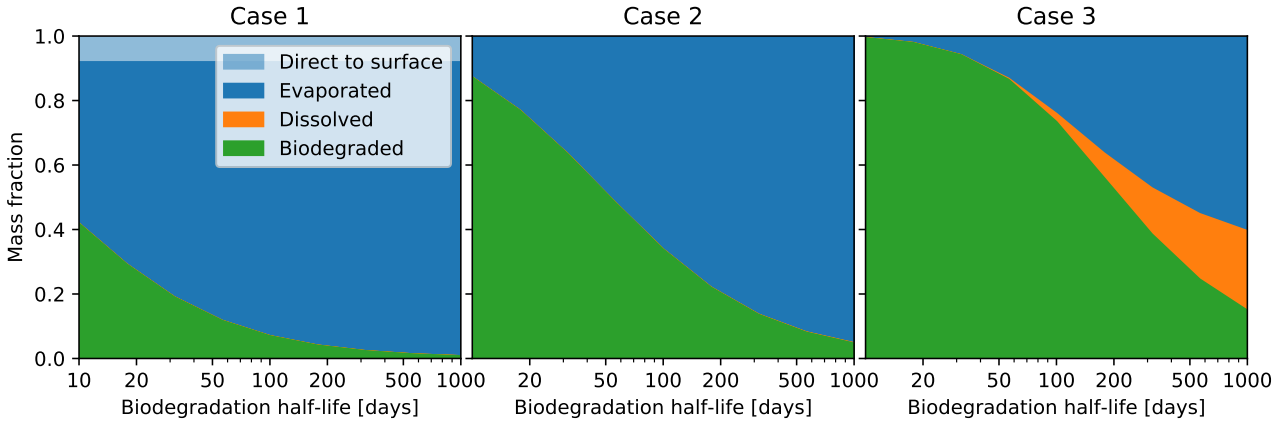

Figure 18: Mass balance after 365 days, averaged over 4 simulations starting at different times of the year, presented as a function of biodegradation half-life.

3.5 Summary of model results

It should be stressed that a large number of assumptions have gone into this modelling study. This is by necessity, due both to a lack of data, and the limited scope of this study. In our opinion, the two most uncertain parameters are the biodegradation rate and the vertical eddy diffusivity. In comparison, the parameters and equations of the bubble rise model, the diffusion-reaction scheme itself, and the mass transfer coefficient, may be considered relatively well understood, and any uncertainties will have smaller impacts on the results. One exception to this could be the dissolution rate of methane, which depends on assumptions of "clean" vs. "dirty" bubbles.

Another major uncertainty is to what degree a one-dimensional model is representative for real conditions in the ocean. In reality, horizontal transport and mixing will dilute the dissolved methane, which may impact both the biodegradation rate, and the mass transfer to the atmosphere. While the limited scope of the current study did not allow for a more comprehensive modelling study, it is clear that a more complete investigation should include three-dimensional modelling.

Nevertheless, we believe that the relatively simple model studies presented here are useful for discussing different scenarios and outcomes, and making some approximate estimates. By conducting parameter studies, like the one shown in Fig. 18, we can for example state with some certainty that with the assumed eddy diffusivity profiles, almost all the methane released in a seep at 50 m depth will reach the atmosphere, regardless of the biodegradation rate. For the deeper cases, however, it makes a significant difference if the biodegradation half-life is, e.g., 50 days, or 500 days.

4 Discussion and Conclusion

From our review of the literature, we find a relatively coherent picture of the fate of methane bubbles from seeps. Most studies report initial bubble sizes of a few millimeters, and most studies seem to indicate that a majority of the released methane dissolves in the water column before the bubbles reach the surface. This is found both by modelling studies, which calculate the methane dissolution as the bubble rises, and by measurement studies, for example observing methane bubbles (flares) by sonar.

There is some uncertainty in the modelling of rising gas bubbles, mainly related to the mass transfer coefficient between the bubble and the water. In particular, the difference between a so-called "clean bubble" mass transfer, and a "dirty bubble" can make a significant difference to the amount of direct transport of methane to the atmosphere. This has not been explored in our modelling study. All in all, however, we conclude that direct transport of methane from seeps to the atmosphere is only relevant for the most shallow locations.

When it comes to the fate of methane that dissolves in the water column, there is far less consensus. As we have attempted to illustrate by modelling selected cases, the ultimate fate of the dissolved methane depends to a large degree on:

- Biodegradation rate,
- Vertical mixing,
- Release depth.

Of these parameters the biodegradation rate is the most uncertain. Values reported in the literature span a range of six orders of magnitude, and vary with both concentration and experimental method. In our modelling study, we have considered two different biodegradation rates, corresponding to half-lives of 100 days and 500 days, and we see that this can make a significant difference, particularly in the case of deep releases.

We also conducted a parameter study where we have modelled a range of biodegradation half-lives from 10 to 1000 days (results shown in Fig. 18). For the shallowest case considered, with a release depth of 50 m, we find that most of the methane reaches the atmosphere regardless of the biodegradation rate, while for the two deeper cases (120 m and 300 m) the results are highly dependent on the biodegradation rate. If the half-life is much less than half a year, then we see that inhibited mixing due to stable stratification of the water column during summer can prevent the methane from reaching the atmosphere, giving it time to biodegrade. On the other hand, if the half-life is much more than half a year, then the methane will likely be mixed throughout the water column during winter, and eventually escape to the atmosphere.

The second most uncertain parameter is probably the vertical eddy diffusivity. As mentioned previously, this is not an physically observable parameter that can be measured directly, but rather a parameterisation of the mixing caused by turbulence in the water column. Different approaches to estimating the eddy diffusivity exist, including different modelling approaches, as well as turbulence measurements from which the eddy diffusivity may be inferred based on different assumptions. There are two key points that are important to get right in this context: First, when is the water column stably stratified, what is the depth of the pycnocline, and to how large a degree does it inhibit vertical mixing, and second, how uniform is the water column density during winter. Here, we have used even mixing throughout the water column in winter. CTD data indicates that some stratification may be present with a transition happening from 100 m to 150 m (Fig.12), but it is not straight forward to create a diffusivity profile from this data.

The last parameter, the release depth, is of course not uncertain as such, since it can be measured with high accuracy or easily obtained from nautical maps. However, at what depths seeps are distributed is uncertain, since there exists no complete survey of all seeps in Norwegian waters. If the majority of methane from seeps are released at depths of around 300 m, the total mass balance will look quite different compared to if the majority is released at shallower depths of for example 50 m.

4.1 Discussion of the chosen modelling approach

When it comes to the model itself, we have here used a relatively simple approach which takes into account bubble rise and direct transport to the atmosphere, as well as the fate of dissolved methane, including vertical

mixing, biodegradation, and escape to the atmosphere via mass transfer at the surface. However, we have used a one-dimensional model, and we have ignored horizontal transport, as well as any explicit dependence on concentration, working instead in fractions of the released methane. Working with a one-dimensional model is a very useful simplification; however, for the longer simulations of one year, such as those presented in Figs. 17 and 18, horizontal transport and dilution are certainly likely to play a role.

In reality, the biodegradation rate will depend on methane concentrations, as high concentrations will tend to lead to growth in number of methane-oxidising bacteria, thus leading to faster degradation rates with higher concentrations. Moreover, biodegradation rates will not only depend on the instantaneous concentration, but also on the history of the concentration in a particular volume of water. This cannot be accounted for in a one-dimensional model.

Horizontal mixing and dilution are also not included in a one-dimensional model. In particular, the horizontal mixing in the ocean is usually much faster than the vertical mixing, which will serve to reduce the concentrations of dissolved methane downstream of a seep area. This will impact the biodegradation rate, if we assume that to be dependent on concentration. Reduced concentration may also impact the mass transfer to the atmosphere, since the mass transfer rate depends on the difference between the concentration in the surface water, and the concentration at which the surface water is in equilibrium with the atmosphere.

Finally, the impact of horizontal advection with currents is of course not included in a one-dimensional model. The transport of dissolved methane with the currents may be of less importance. Assuming that the only two fate processes for dissolved methane are biodegradation and mass transfer to the atmosphere, then any horizontal displacement will not impact the fate of the methane. However, one relevant effect of horizontal currents is that biodegrading bacteria cannot develop and remain stationary in active seep areas, as there is always a continuous supply of fresh water from upstream. Also, horizontal advection may transport water exposed by one seep area over to another seep area, bringing with it higher concentrations of methane oxidizing bacteria than would be transported from areas without methane seeps.

4.2 Conclusion on acidification

Ocean acidification is caused by increased levels of CO_2 in the seawater. Methane released in seeps may be a source of CO_2, as methane biodegrades into CO_2 and water. Other sources of increased CO_2-input to the oceans include atmospheric CO_2 from anthropogenic sources, increased organic input to the oceans and mineralization of this matter, emissions from CO_2 and hydrocarbon vents, and destabilized methane hydrates. Compared to the CO_2 concentrations in seawater, as well as the estimated input of CO_2 from the atmosphere (including anthropogenic sources), the current contributions from methane seeps are anticipated to have small or insignificant impacts on potential ocean acidification, even at “hot-spot” areas in coastal waters.

However, future predictions describing global warming and massive destabilization of methane hydrates, particularly in shallow Arctic areas, suggest impacts of released methane and subsequent oxidation processes to local or regional ocean acidification, although these processes are anticipated to occur over long periods of time.

4.3 Conclusion on methane release to the atmosphere

Our first conclusion from the literature review is that there appears to be a consensus on understanding the immediate fate of methane bubbles released in seeps. Release rates and bubble sizes can be measured relatively accurately with, e.g., ROVs. The physics of bubbles rising through the water column, and the dissolution of methane from these bubbles, is relatively well understood, and models for these processes have been validated against experiments.

To model the fate of dissolved methane in the water column, we have numerically solved the diffusion-reaction equation, which is a well-known and standard approach. To represent the vertical mixing intensity, we designed idealised eddy diffusivity profiles representing summer and winter conditions. These are only estimates, but they qualitatively reproduce the fact that there is reduced mixing across the pycnocline in summer, and more complete mixing throughout the water column in winter.

When it comes to biodegradation rates for dissolved methane in the water column, there is a very large variation in published data. In our modelling studies, we have considered the effect of two different rates, corresponding to half-lives of 100 days and 500 days. Of these, 500 days is nearer the majority of the published data, and is of course also the more conservative estimate. Assuming a value of 500 days, we note that this is longer than one year, which means that methane initially dissolved at large depths will have some opportunity to be mixed to the surface during winter when vertical mixing is stronger.

We also conducted a parameter study, running the model for a range of different biodegradation half-lives from 10 to 1000 days. For the shallowest case considered (50 m release), we find that almost all the methane will reach the atmosphere, regardless of the biodegradation rate. For the two deeper cases (120 m and 300 m), there is more of a dependence on the biodegradation rate.

Putting all these points together, we find that even for methane released at the relatively large depth of 300 m, a large fraction of the released methane is likely to reach the atmosphere. Given the generally shallow NCS, we conclude that it seems likely that more than half of the methane released from seeps on the NCS will reach the atmosphere. To quantify the fractions and amounts with better accuracy, further research is needed.

4.4 Suggested future work

In order to constrain the large uncertainties we see both in the literature and our model results, further research can be undertaken. We would propose three main points:

- A survey of Norwegian waters, to determine where, and at what depths, methane seeps are distributed.
- Experimental work to measure biodegradation rates at a range of relevant concentrations and temperatures.
- A comprehensive modelling study, where a full three-dimensional ocean model is used to simulate active seep areas on the Norwegian sector, coupled to a model for growth of methane-degrading bacteria.

Appendix

A Full numerical scheme for the diffusion-reaction equation

Here, we write out in detail the numerical scheme for calculating the concentration at time t_{i+1}, given the values at time t_i. We use the implicit Crank-Nicolson scheme, which means that we get a linear system of equations, one equation for each position, z_n, and these equations must be solved at every timestep. We introduce the following shorthand notation:

$$C_n^i = C(z_n, t_i), \quad K_n = K(z_n), \quad K'_n = K(z_{n+1}) - K(z_{n-1}), \quad \alpha = \frac{1}{2}\frac{\Delta t}{\Delta z^2}, \quad \beta = \frac{\Delta t}{2}. \tag{31}$$

With this notation, the equation that must be solved to find C_n^{i+1} is

$$\begin{aligned} &C_{n-1}^{i+1}\left(\frac{\alpha}{4}K'_n - \alpha K_n\right) + C_n^{i+1}\left(1 + 2\alpha K_n + \beta q_n\right) + C_{n+1}^{i+1}\left(-\frac{\alpha}{4}K'_n - \alpha K_n\right) \\ &= C_{n-1}^{i}\left(-\frac{\alpha}{4}K'_n + \alpha K_n\right) + C_n^{i}\left(1 - 2\alpha K_n - \beta q_n\right) + C_{n+1}^{i}\left(\frac{\alpha}{4}K'_n + \alpha K_n\right). \end{aligned} \tag{32}$$

At the boundary points, z_0 and z_N, we have to modify this equation in order to eliminate the neighbouring "ghost points" that are outside the domain. Starting at the seafloor, at $z_0 = 0$, we use the no-flux boundary condition (see Eq. (27)) and change to a one-sided finite-difference $K'(z_0) = 2(K(z_1) - K(z_0))$, and obtain $C_{N+1}^i = C_{N-1}^i$, which yields

$$C_0^{i+1}\left(1 + 2\alpha K_n + \beta q_n\right) + C_1^{i+1}\left(-2\alpha K_n\right) = C_0^i\left(1 - 2\alpha K_n - \beta q_n\right) + C_1^i\left(2\alpha K_n\right). \tag{33}$$

Similarly, at the surface, z_N, we use the flux given by the mass transfer to prescribe the value of the derivative of the concentration at the boundary, again allowing us to eliminate the point z_{N+1} from the equations:

$$\begin{aligned} &C_{N-1}^{i+1}\left(-2\alpha K_N\right) + C_N^{i+1}\left(1 + 2\alpha K_N + \beta q_N + 2\Delta z k_w\left(\frac{\alpha}{2}\frac{K_N - K_{N-1}}{K_N} - \alpha\right)\right) \\ &= C_{N-1}^{i}\left(2\alpha K_n\right) + C_N^{i}\left(1 - 2\alpha K_n - \beta q_n - 2\Delta z k_w\left(\frac{\alpha}{2}\frac{K_N - K_{N-1}}{K_N} - \alpha\right)\right) + 4\Delta z k_w\left(\frac{\alpha}{2}\frac{K_N - K_{N-1}}{K_N} - \alpha\right) C_{eq}. \end{aligned} \tag{34}$$

Here, we introduce a further shorthand variable, given by

$$\Gamma = 2\alpha k_w \Delta z\left(1 - \frac{K_N - K_{N-1}}{2K_N}\right). \tag{35}$$

We can now proceed to present the full numerical scheme in the form of a (tri-diagonal) matrix equation:

$$\begin{bmatrix} 1+2\alpha K_0+\beta k q_0 & -2\alpha K_0 & 0 & & & 0 & 0 \\ \frac{\alpha}{4}K'_1 - \alpha K_1 & 1+2\alpha K_1+\beta q_1 & -\frac{\alpha}{4}K'_1 - \alpha K_1 & 0 & & & 0 \\ 0 & \ddots & \ddots & \ddots & 0 & & \\ & 0 & \frac{\alpha}{4}K'_n - \alpha K_n & 1+2\alpha K_n+\beta q_n & -\frac{\alpha}{4}K'_n - \alpha K_n & 0 & \\ & & 0 & \ddots & \ddots & \ddots & 0 \\ 0 & & & 0 & \frac{\alpha}{4}K'_{N-1} - \alpha K_{N-1} & 1+2\alpha K_{N-1}+\beta q_{N-1} & -\frac{\alpha}{4}K'_{N-1} - \alpha K_{N-1} \\ 0 & 0 & & & 0 & -2\alpha K_N & 1+2\alpha K_N+\beta q_n - \Gamma \end{bmatrix} \begin{bmatrix} C_0^{i+1} \\ C_1^{i+1} \\ C_2^{i+1} \\ \vdots \\ C_{n-1}^{i+1} \\ C_n^{i+1} \\ C_{n+1}^{i+1} \\ \vdots \\ C_{N-2}^{i+1} \\ C_{N-1}^{i+1} \\ C_N^{i+1} \end{bmatrix} = \tag{36}$$

$$\begin{bmatrix} 1-2\alpha K_0-\beta k_0 & 2\alpha K_0 & 0 & & & 0 & 0 \\ \frac{-\alpha}{4}K'_1 + \alpha K_1 & 1-2\alpha K_1-\beta q_1 & \frac{\alpha}{4}K'_1 + \alpha K_1 & 0 & & & 0 \\ 0 & \ddots & \ddots & \ddots & 0 & & \\ & 0 & -\frac{\alpha}{4}K'_n + \alpha K_n & 1-2\alpha K_n-\beta q_n & \frac{\alpha}{4}K'_n + \alpha K_n & 0 & \\ & & 0 & \ddots & \ddots & \ddots & 0 \\ 0 & & & 0 & -\frac{\alpha}{4}K'_{N-1} + \alpha K_{N-1} & 1-2\alpha K_{N-1}-\beta q_{N-1} & \frac{\alpha}{4}K'_{N-1} + \alpha K_{N-1} \\ 0 & 0 & & & 0 & 2\alpha K_N & 1-2\alpha K_N-\beta q_n+\Gamma_N \end{bmatrix} \begin{bmatrix} C_0^{i} \\ C_1^{i} \\ C_2^{i} \\ \vdots \\ C_{n-1}^{i} \\ C_n^{i} \\ C_{n+1}^{i} \\ \vdots \\ C_{N-2}^{i} \\ C_{N-1}^{i} \\ C_N^{i} \end{bmatrix} + \begin{bmatrix} 0 \\ 0 \\ 0 \\ \vdots \\ 0 \\ 0 \\ 0 \\ \vdots \\ 0 \\ 0 \\ 2\Gamma C_{eq} \end{bmatrix}. \tag{36}$$

References

R. Z. Abdallah, M. Adel, A. Ouf, A. Sayed, M. A. Ghazy, I. Alam, M. Essack, F. F. Lafi, V. B. Bajic, H. El-Dorry, et al. Aerobic methanotrophic communities at the red sea brine-seawater interface. *Frontiers in microbiology*, 5:487, 2014.

A. Bagi, D. M. Pampanin, O. G. Brakstad, and R. Kommedal. Estimation of hydrocarbon biodegradation rates in marine environments: a critical review of the q10 approach. *Marine environmental research*, 89:83–90, 2013.

L. Berbesi, R. di Primio, Z. Anka, B. Horsfield, and H. Wilkes. Methane leakage from evolving petroleum systems: Masses, rates and inferences for climate feedback. *Earth and Planetary Science Letters*, 387: 219–228, 2014.

A. Berchet, P. Bousquet, I. Pison, R. Locatelli, F. Chevallier, J.-D. Paris, E. J. Dlugokencky, T. Laurila, J. Hatakka, Y. Viisanen, et al. Atmospheric constraints on the methane emissions from the east siberian shelf. *Atmospheric Chemistry and Physics*, 16(6):4147–4157, 2016.

W. Berelson, W. Balch, R. Najjar, R. Feely, C. Sabine, and K. Lee. Relating estimates of caco3 production, export, and dissolution in the water column to measurements of caco3 rain into sediment traps and dissolution on the sea floor: A revised global carbonate budget. *Global Biogeochemical Cycles*, 21(1), 2007.

A. Biastoch, T. Treude, L. H. Rüpke, U. Riebesell, C. Roth, E. B. Burwicz, W. Park, M. Latif, C. W. Böning, G. Madec, et al. Rising arctic ocean temperatures cause gas hydrate destabilization and ocean acidification. *Geophysical Research Letters*, 38(8), 2011.

K. Bolding, H. Burchard, T. Pohlmann, and A. Stips. Turbulent mixing in the northern north sea: a numerical model study. *Continental shelf research*, 22(18-19):2707–2724, 2002.

J. Boles, J. Clark, I. Leifer, and L. Washburn. Temporal variation in natural methane seep rate due to tides, Coal Oil Point area, California. *Journal of Geophysical Research: Oceans*, 106(C11):27077–27086, 2001.

V. Bondur and T. Kuznetsova. Detecting gas seeps in arctic water areas using remote sensing data. *Izvestiya, Atmospheric and Oceanic Physics*, 51(9):1060–1072, 2015.

A. V. Borges and N. Gypens. Carbonate chemistry in the coastal zone responds more strongly to eutrophication than ocean acidification. *Limnology and Oceanography*, 55(1):346–353, 2010.

A. V. Borges, W. Champenois, N. Gypens, B. Delille, and J. Harlay. Massive marine methane emissions from near-shore shallow coastal areas. *Scientific reports*, 6:27908, 2016.

R. Boswell and T. S. Collett. Current perspectives on gas hydrate resources. *Energy & environmental science*, 4(4):1206–1215, 2011.

C. Böttner, M. Haeckel, M. Schmidt, C. Berndt, L. Vielstädte, J. A. Kutsch, J. Karstens, and T. Weiß. Greenhouse gas emissions from marine decommissioned hydrocarbon wells: leakage detection, monitoring and mitigation strategies. *International Journal of Greenhouse Gas Control*, 100:103119, 2020.

O. G. Brakstad, I. K. Almås, and D. F. Krause. Biotransformation of natural gas and oil compounds associated with marine oil discharges. *Chemosphere*, 182:555–558, 2017.

P. N. Brown, G. D. Byrne, and A. C. Hindmarsh. Vode: A variable-coefficient ode solver. *SIAM journal on scientific and statistical computing*, 10(5):1038–1051, 1989.

T. N. O. Bui. *Dissolved methane distribution in seawater and its controlling factors in the polar regions*. PhD thesis, Hokkaido University, 2018. http://hdl.handle.net/2115/71944.

H. Burchard and K. Bolding. Comparative analysis of four second-moment turbulence closure models for the oceanic mixed layer. *Journal of Physical Oceanography*, 31(8):1943–1968, 2001.

M. Cain, N. Warwick, R. Fisher, D. Lowry, M. Lanoisellé, E. Nisbet, J. France, J. Pitt, S. O'Shea, K. Bower, et al. A cautionary tale: A study of a methane enhancement over the north sea. *Journal of Geophysical Research: Atmospheres*, 122(14):7630–7645, 2017.

R. Camilli, C. M. Reddy, D. R. Yoerger, B. A. Van Mooy, M. V. Jakuba, J. C. Kinsey, C. P. McIntyre, S. P. Sylva, and J. V. Maloney. Tracking hydrocarbon plume transport and biodegradation at deepwater horizon. *Science*, 330(6001):201–204, 2010.

S. Chand, T. Thorsnes, L. Rise, H. Brunstad, D. Stoddart, R. Bøe, P. Lågstad, and T. Svolsbru. Multiple episodes of fluid flow in the sw barents sea (loppa high) evidenced by gas flares, pockmarks and gas hydrate accumulation. *Earth and Planetary Science Letters*, 331:305–314, 2012.

R. Clift, J. R. Grace, and M. E. Weber. *Bubbles, Drops, and Particles*. Academic Press, New York, NY, 1978.

A. Crémière, A. Lepland, S. Chand, D. Sahy, K. Kirsimäe, M. Bau, M. J. Whitehouse, S. R. Noble, T. Martma, T. Thorsnes, et al. Fluid source and methane-related diagenetic processes recorded in cold seep carbonates from the alvheim channel, central north sea. *Chemical Geology*, 432:16–33, 2016.

E. Damm, A. Mackensen, G. Budéus, E. Faber, and C. Hanfland. Pathways of methane in seawater: Plume spreading in an arctic shelf environment (sw-spitsbergen). *Continental Shelf Research*, 25(12-13):1453–1472, 2005.

M. A. de Angelis, J. A. Baross, and M. D. Lilley. Enhanced microbial methane oxidation in water from a deep-sea hydrothermal vent field at simulated in situ hydrostatic pressures. *Limnology and oceanography*, 36(3):565–570, 1991.

T. DelSontro, D. F. McGinnis, B. Wehrli, and I. Ostrovsky. Size does matter: Importance of large bubbles and small-scale hot spots for methane transport. *Environmental science & technology*, 49(3):1268–1276, 2015.

A. L. Dissanayake, J. Gros, and S. A. Socolofsky. Integral models for bubble, droplet, and multiphase plume dynamics in stratification and crossflow. *Environmental Fluid Mechanics*, 18(5):1167–1202, 2018.

S. C. Doney, V. J. Fabry, R. A. Feely, and J. A. Kleypas. Ocean acidification: The other CO_2 problem. *Annual Review of Marine Science*, 1(1):169–192, 2009. doi: 10.1146/annurev.marine.010908.163834.

G. Etiope. Natural gas seepage. *The Earth's Hydrocarbon Degassing, Springer*, 640, 2015.

G. Etiope, K. R. Lassey, R. W. Klusman, and E. Boschi. Reappraisal of the fossil methane budget and related emission from geologic sources. *Geophysical Research Letters*, 35(9), 2008.

R. A. Feely, C. L. Sabine, K. Lee, W. Berelson, J. Kleypas, V. J. Fabry, and F. J. Millero. Impact of anthropogenic CO_2 on the $CaCO_3$ system in the oceans. *Science*, 305(5682):362–366, 2004.

R. A. Feely, S. R. Alin, J. Newton, C. L. Sabine, M. Warner, A. Devol, C. Krembs, and C. Maloy. The combined effects of ocean acidification, mixing, and respiration on ph and carbonate saturation in an urbanized estuary. *Estuarine, Coastal and Shelf Science*, 88(4):442–449, 2010.

G. Fuchs. *Carbon Dioxide Reduction by Anaerobic Bacteria*, pages 263–273. Springer Netherlands, Dordrecht, 1987. doi: 10.1007/978-94-009-3923-3_14.

C. S. Garbe, A. Rutgersson, J. Boutin, G. de Leeuw, B. Delille, C. W. Fairall, N. Gruber, J. Hare, D. T. Ho, M. T. Johnson, P. D. Nightingale, H. Pettersson, J. Piskozub, E. Sahlée, W.-t. Tsai, B. Ward, D. K. Woolf, and C. J. Zappa. Transfer across the air-sea interface. In P. S. Liss and M. T. Johnson, editors,

Ocean-Atmosphere Interactions of Gases and Particles, pages 55–112. Springer Berlin Heidelberg, Berlin, Heidelberg, 2014. ISBN 978-3-642-25643-1. doi: 10.1007/978-3-642-25643-1_2. URL https://doi.org/10.1007/978-3-642-25643-1_2.

F. Garcia-Tigreros and J. D. Kessler. Limited acute influence of aerobic methane oxidation on ocean carbon dioxide and ph in hudson canyon, northern us atlantic margin. *Journal of Geophysical Research: Biogeosciences*, 123(7):2135–2144, 2018.

J.-P. Gattuso, A. Magnan, R. Billé, W. W. Cheung, E. L. Howes, F. Joos, D. Allemand, L. Bopp, S. R. Cooley, C. M. Eakin, et al. Contrasting futures for ocean and society from different anthropogenic co2 emissions scenarios. *Science*, 349(6243), 2015.

T. Gentz, E. Damm, J. S. von Deimling, S. Mau, D. F. McGinnis, and M. Schlüter. A water column study of methane around gas flares located at the west spitsbergen continental margin. *Continental Shelf Research*, 72:107–118, 2014.

N. J. Grant and M. J. Whiticar. Stable carbon isotopic evidence for methane oxidation in plumes above hydrate ridge, cascadia oregon margin. *Global Biogeochemical Cycles*, 16(4):71–1, 2002.

C. A. Graves, L. Steinle, G. Rehder, H. Niemann, D. P. Connelly, D. Lowry, R. E. Fisher, A. W. Stott, H. Sahling, and R. H. James. Fluxes and fate of dissolved methane released at the seafloor at the landward limit of the gas hydrate stability zone offshore western svalbard. *Journal of Geophysical Research: Oceans*, 120(9): 6185–6201, 2015.

R. P. Griffiths, B. A. Caldwell, J. D. Cline, W. A. Broich, and R. Y. Morita. Field observations of methane concentrations and oxidation rates in the southeastern bering sea. *Applied and environmental microbiology*, 44(2):435–446, 1982.

J. Gros, C. M. Reddy, R. K. Nelson, S. A. Socolofsky, and J. S. Arey. Simulating gas–liquid- water partitioning and fluid properties of petroleum under pressure: implications for deep-sea blowouts. *Environmental science & technology*, 50(14):7397–7408, 2016.

J. Gros, S. A. Socolofsky, A. L. Dissanayake, I. Jun, L. Zhao, M. C. Boufadel, C. M. Reddy, and J. S. Arey. Petroleum dynamics in the sea and influence of subsea dispersant injection during deepwater horizon. *Proceedings of the National Academy of Sciences*, 114(38):10065–10070, 2017.

J. Gros, M. Schmidt, A. W. Dale, P. Linke, L. Vielstädte, N. Bigalke, M. Haeckel, K. Wallmann, and S. Sommer. Simulating and quantifying multiple natural subsea co2 seeps at panarea island (aeolian islands, italy) as a proxy for potential leakage from subseabed carbon storage sites. *Environmental science & technology*, 53 (17):10258–10268, 2019.

J. Gros, , J. S. Arey, S. A. Socolofsky, and A. L. Dissanayake. Dynamics of live oil droplets and natural gas bubbles in deep water. *Environmental science & technology*, xx:xx, 2020.

J. M. Guinotte and V. J. Fabry. Ocean acidification and its potential effects on marine ecosystems. *Annals of the New York Academy of Sciences*, 1134(1):320–342, 2008.

T. Gutierrez and M. D. Aitken. Role of methylotrophs in the degradation of hydrocarbons during the deepwater horizon oil spill. *The ISME journal*, 8(12):2543–2545, 2014.

J. M. Hall-Spencer, R. Rodolfo-Metalpa, S. Martin, E. Ransome, M. Fine, S. M. Turner, S. J. Rowley, D. Tedesco, and M.-C. Buia. Volcanic carbon dioxide vents show ecosystem effects of ocean acidification. *Nature*, 454(7200):96–99, 2008.

J. D. Happell, J. P. Chanton, and W. J. Showers. Methane transfer across the water-air interface in stagnant wooded swamps of florida: Evaluation of mass-transfer coefficients and isotropic fractionation. *Limnology and Oceanography*, 40(2):290–298, 1995.

M. F. Haroon, S. Hu, Y. Shi, M. Imelfort, J. Keller, P. Hugenholtz, Z. Yuan, and G. W. Tyson. Anaerobic oxidation of methane coupled to nitrate reduction in a novel archaeal lineage. *Nature*, 500(7464):567–570, 2013.

J. I. Hedges et al. Global biogeochemical cycles: progress and problems. *Mar. Chem*, 39(1-3):67–93, 1992.

J. Houghton, Y. Ding, D. Griggs, M. Noguer, P. van der Linden, X. Dai, J. Maskell, and C. Johnson, editors. *Climate Change 2001: The Scientific Basis. Contribution of Working Group I to the Third Assessment Report of the Intergovernmental Panel on Climate Change*. Cambridge University Press, Cambridge, UK and New York, USA, 2001. `https://core.ac.uk/download/pdf/299301644.pdf`.

M. Hovland. Do carbonate reefs form due to fluid seepage? *Terra Nova*, 2(1):8–18, 1990a.

M. Hovland. Suspected gas-associated clay diapirism on the seabed off mid norway. *Marine and petroleum geology*, 7(3):267–276, 1990b.

M. Hovland. On the self-sealing nature of marine seeps. *Continental Shelf Research*, 22(16):2387–2394, 2002.

M. Hovland and A. G. Judd. *Seabed pockmarks and seepages: impact on geology, biology and the marine environment*. Graham & Trotman, 1988.

M. Hovland and A. G. Judd. The global production of methane from shallow submarine sources. *Continental Shelf Research*, 12(10):1231–1238, 1992.

M. Hovland and J. H. Sommerville. Characteristics of two natural gas seepages in the north sea. *Marine and Petroleum Geology*, 2(4):319–326, 1985.

M. Hovland, A. G. Judd, and R. Burke Jr. The global flux of methane from shallow submarine sediments. *Chemosphere*, 26(1-4):559–578, 1993.

W. Hundsdorfer and J. G. Verwer. *Numerical solution of time-dependent advection-diffusion-reaction equations*. Springer Verlag, Berlin Heidelberg New York, 2003.

R. H. James, P. Bousquet, I. Bussmann, M. Haeckel, R. Kipfer, I. Leifer, H. Niemann, I. Ostrovsky, J. Piskozub, G. Rehder, et al. Effects of climate change on methane emissions from seafloor sediments in the arctic ocean: A review. *Limnology and Oceanography*, 61(S1):S283–S299, 2016.

P. Jansson, J. Triest, R. Grilli, B. Ferré, A. Silyakova, J. Mienert, and J. Chappellaz. High-resolution underwater laser spectrometer sensing provides new insights into methane distribution at an arctic seepage site. 2019.

Ø. Johansen. Development and verification of deep-water blowout models. *Marine Pollution Bulletin*, 47(9-12): 360–368, 2003.

A. Johnson, F. Besik, and A. Hamielec. Mass transfer from a single rising bubble. *The Canadian Journal of Chemical Engineering*, 47(6):559–564, 1969.

A. Judd and M. Hovland. The evidence of shallow gas in marine sediments. *Continental Shelf Research*, 12 (10):1081–1095, 1992.

A. G. Judd. The global importance and context of methane escape from the seabed. *Geo-Marine Letters*, 23 (3-4):147–154, 2003.

A. G. Judd. Natural seabed gas seeps as sources of atmospheric methane. *Environmental Geology*, 46(8): 988–996, 2004.

I. O. Jun. *A numerical model for hydrocarbon bubbles from natural seeps within hydrate stability zone*. PhD thesis, 2018.

M. Kang, C. M. Kanno, M. C. Reid, X. Zhang, D. L. Mauzerall, M. A. Celia, Y. Chen, and T. C. Onstott. Direct measurements of methane emissions from abandoned oil and gas wells in pennsylvania. *Proceedings of the National Academy of Sciences*, 111(51):18173–18177, 2014.

M. C. Kennicutt. Oil and gas seeps in the gulf of mexico. In *Habitats and biota of the Gulf of Mexico: Before the deepwater horizon oil spill*, pages 275–358. Springer, 2017.

P. Kerrison, J. M. Hall-Spencer, D. J. Suggett, L. J. Hepburn, and M. Steinke. Assessment of ph variability at a coastal co2 vent for ocean acidification studies. *Estuarine, Coastal and Shelf Science*, 94(2):129–137, 2011.

J. D. Kessler, D. L. Valentine, M. C. Redmond, M. Du, E. W. Chan, S. D. Mendes, E. W. Quiroz, C. J. Villanueva, S. S. Shusta, L. M. Werra, et al. A persistent oxygen anomaly reveals the fate of spilled methane in the deep gulf of mexico. *Science*, 331(6015):312–315, 2011.

M. King and P. Danckwerts. *Phase equilibrium in mixtures*. Pergamon Press, 1969.

K. Kohnert, A. Serafimovich, S. Metzger, J. Hartmann, and T. Sachs. Strong geologic methane emissions from discontinuous terrestrial permafrost in the mackenzie delta, canada. *Scientific Reports*, 7(1):1–6, 2017.

K. Krämer, P. Holler, G. Herbst, A. Bratek, S. Ahmerkamp, A. Neumann, A. Bartholomä, J. E. van Beusekom, M. Holtappels, and C. Winter. Abrupt emergence of a large pockmark field in the german bight, southeastern north sea. *Scientific reports*, 7(1):1–8, 2017.

I. Krichevsky and J. Kasarnovsky. Thermodynamical calculations of solubilities of nitrogen and hydrogen in water at high pressures. *Journal of the American Chemical Society*, 57(11):2168–2171, 1935.

K. Kroeger, R. di Primio, and B. Horsfield. Atmospheric methane from organic carbon mobilization in sedimentary basins—the sleeping giant? *Earth-Science Reviews*, 107(3-4):423–442, 2011.

A. Kumar and S. Hartland. Correlations for prediction of mass transfer coefficients in single drop systems and liquid–liquid extraction columns. *Chemical Engineering Research and Design*, 77(5):372–384, 1999.

K. A. Kvenvolden, T. D. Lorenson, and W. S. Reeburgh. Attention turns to naturally occurring methane seepage. *Eos, Transactions American Geophysical Union*, 82(40):457–457, 2001.

I. Leifer and A. Judd. Oceanic methane layers: the hydrocarbon seep bubble deposition hypothesis. *Terra Nova*, 14(6):417–424, 2002.

I. Leifer and I. MacDonald. Dynamics of the gas flux from shallow gas hydrate deposits: interaction between oily hydrate bubbles and the oceanic environment. *Earth and Planetary Science Letters*, 210(3-4):411–424, 2003.

I. Leifer and R. K. Patro. The bubble mechanism for methane transport from the shallow sea bed to the surface: A review and sensitivity study. *Continental Shelf Research*, 22(16):2409–2428, 2002.

I. Leifer, J. F. Clark, and R. F. Chen. Modifications of the local environment by natural marine hydrocarbon seeps. *Geophysical Research Letters*, 27(22):3711–3714, 2000.

M. Leonte, J. D. Kessler, M. Y. Kellermann, E. C. Arrington, D. L. Valentine, and S. P. Sylva. Rapid rates of aerobic methane oxidation at the feather edge of gas hydrate stability in the waters of hudson canyon, us atlantic margin. *Geochimica et Cosmochimica Acta*, 204:375–387, 2017.

M. Leonte, B. Wang, S. Socolofsky, S. Mau, J. Breier, and J. Kessler. Using carbon isotope fractionation to constrain the extent of methane dissolution into the water column surrounding a natural hydrocarbon gas seep in the northern gulf of mexico. *Geochemistry, Geophysics, Geosystems*, 19(11):4459–4475, 2018.

Y. Li, L. Zhan, J. Zhang, L. Chen, J. Chen, and Y. Zhuang. A significant methane source over the chukchi sea shelf and its sources. *Continental Shelf Research*, 148:150–158, 2017.

M. Liira, R. Noormets, H. Sepp, O. Kekišev, M. Maddison, and S. Olaussen. Sediment geochemical study of hydrocarbon seeps in isfjorden and mohnbukta: a comparison between western and eastern spitsbergen, svalbard. *arktos*, 5(1):49–62, 2019.

H. Lin and Y.-Y. Duan. Empirical correction to the peng–robinson equation of state for the saturated region. *Fluid phase equilibria*, 233(2):194–203, 2005.

T. D. Lorenson, J. Greinert, and R. B. Coffin. Dissolved methane in the beaufort sea and the arctic ocean, 1992–2009; sources and atmospheric flux. *Limnology and Oceanography*, 61(S1):S300–S323, 2016.

F. A. Luesken, B. Zhu, T. A. van Alen, M. K. Butler, M. R. Diaz, B. Song, H. J. O. den Camp, M. S. Jetten, and K. F. Ettwig. pmoa primers for detection of anaerobic methanotrophs. *Applied and environmental microbiology*, 77(11):3877–3880, 2011.

R. Mahdi, B. Wang, D. A. Samira, A. M. Thurnherr, et al. Variability of a natural hydrocarbon seep and its connection to the ocean surface. *Scientific Reports (Nature Publisher Group)*, 10(1), 2020.

S. Mau, J. Blees, E. Helmke, H. Niemann, and E. Damm. Vertical distribution of methane oxidation and methanotrophic response to elevated methane concentrations in stratified waters of the arctic fjord storfjorden (svalbard, norway). *Biogeosciences*, 10:6267–6278, 2013.

S. Mau, T. Gentz, J.-H. Körber, M. E. Torres, M. Römer, H. Sahling, P. Wintersteller, R. Martinez, M. Schlüter, and E. Helmke. Seasonal methane accumulation and release from a gas emission site in the central north sea. *Biogeosciences*, 12(18), 2015.

S. Mau, M. Römer, M. E. Torres, I. Bussmann, T. Pape, E. Damm, P. Geprägs, P. Wintersteller, C.-W. Hsu, M. Loher, et al. Widespread methane seepage along the continental margin off svalbard-from bjørnøya to kongsfjorden. *Scientific reports*, 7:42997, 2017.

W. D. McCain. *The Properties of Petroleum Fluids*. PennWell Books, 1990.

I. R. McDonald and J. C. Murrell. The particulate methane monooxygenase gene pmoa and its use as a functional gene probe for methanotrophs. *FEMS microbiology letters*, 156(2):205–210, 1997.

D. McGinnis, J. Greinert, Y. Artemov, S. Beaubien, and A. Wüest. Fate of rising methane bubbles in stratified waters: How much methane reaches the atmosphere? *Journal of Geophysical Research: Oceans (1978–2012)*, 111(C9), 2006a.

D. F. McGinnis, J. Greinert, Y. Artemov, S. Beaubien, and A. Wüest. Fate of rising methane bubbles in stratified waters: How much methane reaches the atmosphere? *Journal of Geophysical Research: Oceans*, 111(C9), 2006b.

M. Michelsen and J. Mollerup. Thermodynamic models: fundamentals & computational aspects, 2004.

J. I. Miller, S. Techtmann, J. Fortney, N. Mahmoudi, D. Joyner, J. Liu, S. Olesen, E. Alm, A. Fernandez, P. Gardinali, et al. Oil hydrocarbon degradation by caspian sea microbial communities. *Frontiers in microbiology*, 10:995, 2019.

F. Millero and A. Poisson. International one-atmosphere equation of state of seawater. *Deep Sea Research Part A, Oceanographic Research Papers*, 28(6):625–629, 1981.

F. Moeinikia, E. P. Ford, H. P. Lohne, O. Arild, M. Mansouri Majoumerd, K. K. Fjelde, et al. Leakage calculator for plugged-and-abandoned wells. *SPE Production & Operations*, 33(04):790–801, 2018.

A. Mucci. The solubility of calcite and aragonite in seawater at various salinities, temperatures, and one atmosphere total pressure. *American Journal of Science*, 283(7):780–799, 1983.

W. H. Munk. Abyssal recipes. *Deep-Sea Research*, 13:707–730, 1966.

C. L. Myhre, B. Ferré, S. M. Platt, A. Silyakova, O. Hermansen, G. Allen, I. Pisso, N. Schmidbauer, A. Stohl, J. Pitt, et al. Extensive release of methane from arctic seabed west of svalbard during summer 2014 does not influence the atmosphere. *Geophysical Research Letters*, 43(9):4624–4631, 2016.

R. Najjar and J. Orr. Design of ocmip-2 simulations of chlorofluorocarbons, the solubility pump and common biogeochemistry. *Internal OCMIP Report, LSCE/CEA Saclay, Gif-sur-Yvette, France*, 1998. URL `http://www.cgd.ucar.edu/oce/klindsay/OCMIP/design.pdf`.

K. Nauhaus, T. Treude, A. Boetius, and M. Krüger. Environmental regulation of the anaerobic oxidation of methane: a comparison of anme-i and anme-ii communities. *Environmental microbiology*, 7(1):98–106, 2005.

C. Niewöhner, C. Hensen, S. Kasten, M. Zabel, and H. Schulz. Deep sulfate reduction completely mediated by anaerobic methane oxidation in sediments of the upwelling area off namibia. *Geochimica et cosmochimica acta*, 62(3):455–464, 1998.

T. Nordam, S. Lofthus, and O. G. Brakstad. Modelling biodegradation of crude oil components at low temperatures. *Chemosphere*, page 126836, 2020.

OECD. Test no. 306: Biodegradability in seawater. In *OCED Guidelines for the Testing of Chemicals*. OCED Publishing, Paris, 1992. https://doi.org/https://doi.org/10.1787/9789264070486-en.

J. E. Olsen, D. Dunnebier, E. Davies, P. Skjetne, and J. Morud. Mass transfer between bubbles and seawater. *Chemical Engineering Science*, 161:308–315, 2017.

J. E. Olsen, D. F. Krause, E. J. Davies, and P. Skjetne. Observations of rising methane bubbles in trondheimsfjord and its implications to gas dissolution. *Journal of Geophysical Research: Oceans*, 124(3):1399–1409, 2019.

J. C. Orr, V. J. Fabry, O. Aumont, L. Bopp, S. C. Doney, R. A. Feely, A. Gnanadesikan, N. Gruber, A. Ishida, F. Joos, et al. Anthropogenic ocean acidification over the twenty-first century and its impact on calcifying organisms. *Nature*, 437(7059):681–686, 2005.

K. G. Osadetz and Z. Chen. A re-evaluation of beaufort sea-mackenzie delta basin gas hydrate resource potential: petroleum system approaches to non-conventional gas resource appraisal and geologically-sourced methane flux. *Bulletin of Canadian Petroleum Geology*, 58(1):56–71, 2010.

M. A. Pack, M. B. Heintz, W. S. Reeburgh, S. E. Trumbore, D. L. Valentine, X. Xu, and E. R. Druffel. Methane oxidation in the eastern tropical north pacific ocean water column. *Journal of Geophysical Research: Biogeosciences*, 120(6):1078–1092, 2015.

G. Panieri, S. Bünz, D. J. Fornari, J. Escartin, P. Serov, P. Jansson, M. E. Torres, J. E. Johnson, W. Hong, S. Sauer, et al. An integrated view of the methane system in the pockmarks at vestnesa ridge, 79 n. *Marine Geology*, 390:282–300, 2017.

A. Péneloux, E. Rauzy, and R. Fréze. A consistent correction for redlich-kwong-soave volumes. *Fluid phase equilibria*, 8(1):7–23, 1982.

D.-Y. Peng and D. B. Robinson. A new two-constant equation of state. *Ind. Eng. Chem. Fundam*, 15(1):59–64, 1976.

B. J. Phrampus, M. J. Hornbach, C. D. Ruppel, and P. E. Hart. Widespread gas hydrate instability on the upper us beaufort margin. *Journal of Geophysical Research: Solid Earth*, 119(12):8594–8609, 2014.

I. Pisso, C. L. Myhre, S. M. Platt, S. Eckhardt, O. Hermansen, N. Schmidbauer, J. Mienert, S. Vadakkepuliyambatta, S. Bauguitte, J. Pitt, et al. Constraints on oceanic methane emissions west of svalbard from atmospheric in situ measurements and lagrangian transport modeling. *Journal of Geophysical Research: Atmospheres*, 121(23):14–188, 2016.

J. W. Pohlman, J. E. Bauer, W. F. Waite, C. L. Osburn, and N. R. Chapman. Methane hydrate-bearing seeps as a source of aged dissolved organic carbon to the oceans. *Nature Geoscience*, 4(1):37–41, 2011.

J. W. Pohlman, M. Riedel, J. E. Bauer, E. A. Canuel, C. K. Paull, L. Lapham, K. S. Grabowski, R. B. Coffin, and G. D. Spence. Anaerobic methane oxidation in low-organic content methane seep sediments. *Geochimica et Cosmochimica Acta*, 108:184–201, 2013.

J. W. Pohlman, J. Greinert, C. Ruppel, A. Silyakova, L. Vielstädte, M. Casso, J. Mienert, and S. Bünz. Enhanced co2 uptake at a shallow arctic ocean seep field overwhelms the positive warming potential of emitted methane. *Proceedings of the National Academy of Sciences*, 114(21):5355–5360, 2017.

H.-O. Pörtner. Ecosystem effects of ocean acidification in times of ocean warming: a physiologist's view. *Marine Ecology Progress Series*, 373:203–217, 2008.

W. S. Reeburgh. Oceanic methane biogeochemistry. *Chemical reviews*, 107(2):486–513, 2007.

G. Rehder, R. S. Keir, E. Suess, and T. Pohlmann. The multiple sources and patterns of methane innorth sea waters. *Aquatic Geochemistry*, 4(3-4):403–427, 1998.

G. Rehder, P. W. Brewer, E. T. Peltzer, and G. Friederich. Enhanced lifetime of methane bubble streams within the deep ocean. *Geophysical research letters*, 29(15):21–1, 2002.

G. Rehder, I. Leifer, P. G. Brewer, G. Friederich, and E. T. Peltzer. Controls on methane bubble dissolution inside and outside the hydrate stability field from open ocean field experiments and numerical modeling. *Marine Chemistry*, 114(1-2):19–30, 2009.

M. Römer, S. Wenau, S. Mau, M. Veloso, J. Greinert, M. Schlüter, and G. Bohrmann. Assessing marine gas emission activity and contribution to the atmospheric methane inventory: A multidisciplinary approach from the d utch d ogger b ank seep area (n orth s ea). *Geochemistry, Geophysics, Geosystems*, 18(7):2617–2633, 2017.

M. Römer, C.-W. Hsu, M. Loher, I. MacDonald, C. dos Santos Ferreira, T. Pape, S. Mau, G. Bohrmann, and H. Sahling. Amount and fate of gas and oil discharged at 3400 m water depth from a natural seep site in the southern gulf of mexico. *Frontiers in Marine Science*, 6:700, 2019.

S. Roy, K. Senger, M. Hovland, M. Römer, and A. Braathen. Geological controls on shallow gas distribution and seafloor seepage in an arctic fjord of spitsbergen, norway. *Marine and Petroleum Geology*, 107:237–254, 2019.

C. D. Ruppel and J. D. Kessler. The interaction of climate change and methane hydrates. *Reviews of Geophysics*, 55(1):126–168, 2017.

C. D. Rye, M.-J. Messias, J. R. Ledwell, A. J. Watson, A. Brousseau, and B. A. King. Diapycnal diffusivities from a tracer release experiment in the deep sea, integrated over 13 years. *Geophysical research letters*, 39 (4), 2012.

C. L. Sabine, R. A. Feely, N. Gruber, R. M. Key, K. Lee, J. L. Bullister, R. Wanninkhof, C. Wong, D. W. Wallace, B. Tilbrook, et al. The oceanic sink for anthropogenic co2. *science*, 305(5682):367–371, 2004.

H. Sahling, M. Römer, T. Pape, B. Bergès, C. dos Santos Fereirra, J. Boelmann, P. Geprägs, M. Tomczyk, N. Nowald, W. Dimmler, et al. Gas emissions at the continental margin west of svalbard: mapping, sampling, and quantification. *Biogeosciences*, 11(21), 2014.

F. J. Sansone and C. S. Martens. Methane oxidation in cape lookout bight, north carolina 1. *Limnology and Oceanography*, 23(2):349–355, 1978.

S. Sauer, A. Crémière, J. Knies, A. Lepland, D. Sahy, T. Martma, S. R. Noble, J. Schönenberger, M. Klug, and C. J. Schubert. U-th chronology and formation controls of methane-derived authigenic carbonates from the hola trough seep area, northern norway. *Chemical Geology*, 470:164–179, 2017.

E. J. Sauter, S. I. Muyakshin, J.-L. Charlou, M. Schlüter, A. Boetius, K. Jerosch, E. Damm, J.-P. Foucher, and M. Klages. Methane discharge from a deep-sea submarine mud volcano into the upper water column by gas hydrate-coated methane bubbles. *Earth and Planetary Science Letters*, 243(3-4):354–365, 2006.

N. Shakhova, I. Semiletov, A. Salyuk, V. Yusupov, D. Kosmach, and Ö. Gustafsson. Extensive methane venting to the atmosphere from sediments of the east siberian arctic shelf. *Science*, 327(5970):1246–1250, 2010.

R. B. Shakirov, S. Mau, G. I. Mishukova, A. I. Obzhirov, M. V. Shakirova, and O. V. Mishukova. The features of methane fluxes in the western and eastern arctic: A review. part i. *Geosystems of Transition Zones*, 4(1): 4–25, 2020. doi: 10.30730/2541-8912.2020.4.1.004-025.

S. A. Socolofsky, A. L. Dissanayake, I. Jun, J. Gros, J. S. Arey, and C. M. Reddy. Texas a&m oilspill calculator (tamoc): Modeling suite for subsea spills. In *Proceedings of the Thirty-Eighth AMOP Technical Seminar*, pages 153–168. Environment Canada Ottawa, 2015.

S. Solomon, D. Qin, M. Manning, Z. Chen, M. Marquis, K. Avery, M. Tignor, and H. Miller, editors. *Climate Change 2007: The Physical Science Basis. Contribution of the Working Group I to the Fourth Assessment Report of the Intergovernmental Panel on Climate Change*. Cambridge University Press, Cambridge, UK and New York, USA, 2007.

L. Steinle, M. Schmidt, L. Bryant, M. Haeckel, P. Linke, S. Sommer, J. Zopfi, M. F. Lehmann, T. Treude, and H. Niemannn. Linked sediment and water-column methanotrophy at a man-made gas blowout in the North Sea: Implications for methane budgeting in seasonally stratified shallow seas. *Limnology and Oceanography*, 61(S1):S367–S386, 2016.

N. Sultan, A. Plaza-Faverola, S. Vadakkepuliyambatta, S. Buenz, and J. Knies. Impact of tides and sea-level on deep-sea Arctic methane emissions. *Nature communications*, 11(1):1–10, 2020.

B. F. Thornton, M. C. Geibel, P. M. Crill, C. Humborg, and C.-M. Mörth. Methane fluxes from the sea to the atmosphere across the siberian shelf seas. *Geophysical Research Letters*, 43(11):5869–5877, 2016.

S. A. Thorpe. *The turbulent ocean*. Cambridge University Press, Cambridge, UK, 2005.

A. Townsend-Small, T. W. Ferrara, D. R. Lyon, A. E. Fries, and B. K. Lamb. Emissions of coalbed and natural gas methane from abandoned oil and gas wells in the united states. *Geophysical Research Letters*, 43(5): 2283–2290, 2016.

M. R. Tveit, M. Khalifeh, T. Nordam, and A. Saasen. Fate of hydrocarbon leaks from plugged and abandoned wells compared to natural seepages. In *ASME 2019 38th International Conference on Ocean, Offshore and Arctic Engineering*. American Society of Mechanical Engineers Digital Collection, 2019.

C. Uhlig, J. B. Kirkpatrick, S. D'Hondt, and B. Loose. Methane-oxidizing seawater microbial communities from an arctic shelf. *Biogeosciences*, 15:3311–3329, 2018.

L. Umlauf, H. Burchard, and K. Hutter. Extending the k–ω turbulence model towards oceanic applications. *Ocean Modelling*, 5(3):195–218, 2003.

D. L. Valentine, D. C. Blanton, W. S. Reeburgh, and M. Kastner. Water column methane oxidation adjacent to an area of active hydrate dissociation, eel river basin. *Geochimica et Cosmochimica Acta*, 65(16):2633–2640, 2001.

D. L. Valentine, J. D. Kessler, M. C. Redmond, S. D. Mendes, M. B. Heintz, C. Farwell, L. Hu, F. S. Kinnaman, S. Yvon-Lewis, M. Du, et al. Propane respiration jump-starts microbial response to a deep oil spill. *Science*, 330(6001):208–211, 2010.

L. Vielstädte, J. Karstens, M. Haeckel, M. Schmidt, P. Linke, S. Reimann, V. Liebetrau, D. F. McGinnis, and K. Wallmann. Quantification of methane emissions at abandoned gas wells in the central north sea. *Marine and Petroleum Geology*, 68:848–860, 2015.

L. Vielstädte, M. Haeckel, J. Karstens, P. Linke, M. Schmidt, L. Steinle, and K. Wallmann. Shallow gas migration along hydrocarbon wells–an unconsidered, anthropogenic source of biogenic methane in the north sea. *Environmental Science & Technology*, 51(17):10262–10268, 2017.

P. Virtanen, R. Gommers, T. E. Oliphant, M. Haberland, T. Reddy, D. Cournapeau, E. Burovski, P. Peterson, W. Weckesser, J. Bright, S. J. van der Walt, M. Brett, J. Wilson, K. J. Millman, N. Mayorov, A. R. J. Nelson, E. Jones, R. Kern, E. Larson, C. J. Carey, İ. Polat, Y. Feng, E. W. Moore, J. VanderPlas, D. Laxalde, J. Perktold, R. Cimrman, I. Henriksen, E. A. Quintero, C. R. Harris, A. M. Archibald, A. H. Ribeiro, F. Pedregosa, P. van Mulbregt, and SciPy 1.0 Contributors. SciPy 1.0: Fundamental Algorithms for Scientific Computing in Python. *Nature Methods*, 17:261–272, 2020. doi: 10.1038/s41592-019-0686-2.

J. S. Von Deimling, J. Greinert, N. Chapman, W. Rabbel, and P. Linke. Acoustic imaging of natural gas seepage in the north sea: Sensing bubbles controlled by variable currents. *Limnology and Oceanography: Methods*, 8(5):155–171, 2010.

J. S. von Deimling, G. Rehder, J. Greinert, D. McGinnnis, A. Boetius, and P. Linke. Quantification of seep-related methane gas emissions at tommeliten, north sea. *Continental Shelf Research*, 31(7-8):867–878, 2011.

J. S. von Deimling, P. Linke, M. Schmidt, and G. Rehder. Ongoing methane discharge at well site 22/4b (North Sea) and discovery of a spiral vortex bubble plume motion. *Marine and Petroleum Geology*, 68:718–730, 2015.

S. G. Wakeham, R. Amann, K. H. Freeman, E. C. Hopmans, B. B. Jørgensen, I. F. Putnam, S. Schouten, J. S. S. Damsté, H. M. Talbot, and D. Woebken. Microbial ecology of the stratified water column of the black sea as revealed by a comprehensive biomarker study. *Organic Geochemistry*, 38(12):2070–2097, 2007.

R. B. Wallace, H. Baumann, J. S. Grear, R. C. Aller, and C. J. Gobler. Coastal ocean acidification: The other eutrophication problem. *Estuarine, Coastal and Shelf Science*, 148:1–13, 2014.

B. Wang, S. A. Socolofsky, J. A. Breier, and J. S. Seewald. Observations of bubbles in natural seep flares at mc 118 and gc 600 using in situ quantitative imaging. *Journal of Geophysical Research: Oceans*, 121(4): 2203–2230, 2016.

B. Wang, C. C. Lai, and S. A. Socolofsky. Mean velocity, spreading and entrainment characteristics of weak bubble plumes in unstratified and stationary water. *Journal of Fluid Mechanics*, 874:102–130, 2019.

B. Wang, I. Jun, S. A. Socolofsky, S. F. DiMarco, and J. Kessler. Dynamics of gas bubbles from a submarine hydrocarbon seep within the hydrate stability zone. *Geophysical Research Letters*, 47(18), 2020. doi: 10.1029/2020GL089256.

R. Wanninkhof. Relationship between wind speed and gas exchange over the ocean. *Journal of Geophysical Research: Oceans*, 97(C5):7373–7382, 1992.

R. Wanninkhof, W. E. Asher, D. T. Ho, C. Sweeney, and W. R. McGillis. Advances in quantifying air-sea gas exchange and environmental forcing. *Annual Review of Marine Science*, 1:213–244, 2009.

B. Ward, K. Kilpatrick, A. Wopat, E. Minnich, and M. Lidstrom. Methane oxidation in saanich inlet during summer stratification. *Continental Shelf Research*, 9(1):65–75, 1989.

R. P. Warzinski, R. Lynn, I. Haljasmaa, I. Leifer, F. Shaffer, B. J. Anderson, and J. S. Levine. Dynamic morphology of gas hydrate on a methane bubble in water: Observations and new insights for hydrate film models. *Geophysical Research Letters*, 41(19):6841–6847, 2014.

A. Weinstein, L. Navarrete, C. Ruppel, T. C. Weber, M. Leonte, M. Y. Kellermann, E. C. Arrington, D. L. Valentine, M. I. Scranton, and J. D. Kessler. Determining the flux of methane into h udson c anyon at the edge of methane clathrate hydrate stability. *Geochemistry, Geophysics, Geosystems*, 17(10):3882–3892, 2016.

M. Wilpshaar, de Bruin G., and N. Versteijlen. *TNO Report: TNO2019 R11562- Inventory of wells through shallow gas layers in the Dutch North Sea*. 1.3 edition, 2019.

L. Zheng and P. D. Yapa. Buoyant velocity of spherical and nonspherical bubbles/droplets. *Journal of Hydraulic Engineering*, 126(11):852–854, 2000.

L. Zheng and P. D. Yapa. Modeling gas dissolution in deepwater oil/gas spills. *Journal of Marine Systems*, 31 (4):299–309, 2002.

Technology for a better society

www.sintef.no